

Experimental study for determining the mass
transfer coefficient under two-phase flow boiling
condition

by

Chen Shen

A thesis submitted in partial fulfillment of the requirements for the degree of

Doctor of Philosophy

in

Chemical Engineering

Department of Chemical and Materials Engineering

University of Alberta

© Chen Shen, 2015

Abstract

The mass transfer is an important phenomenon associated with a wide range of problems in the nuclear industry, such as materials degradation of components and fouling of heat exchangers and steam generators. However, mass transfer under a two-phase flow boiling condition has not been successfully investigated using direct experimental approach due to experimental difficulties. To fulfill the knowledge gap in this area, the objective of this project is to develop a novel experimental device and measurement technique to investigate mass transfer rate under the flow boiling condition. Because of the challenges associated with research in this area, the current study has been divided into three phases: (I) a bulk boiling condition, (II) a pool boiling condition and (III) a two-phase flow boiling condition.

In Phase I, a rotating cylinder electrode system was employed to mimic the flow condition, and the electrolyte was heated to obtain the bulk boiling condition. The mass transfer behavior of oxygen and ferricyanide were determined from room temperature to just below the boiling point (i.e. 99 °C) for rotating speeds between 100 and 3300 rpm. A correlation was successfully developed to predict the mass transfer behavior for the dissolved oxygen reduction and ferricyanide reaction below the boiling condition. However, the experimental data obtained under bulk boiling conditions was on the average 38% higher than the predicted data due to the generation and rupture of boiling bubbles in the bulk solution.

In Phase II, a novel pool boiling setup was designed and constructed to study the mass transfer behavior on a nucleate boiling surface at atmospheric pressure. This study made a valuable contribution to the existing knowledge of mass transfer study on nucleate boiling surface because it is the first successfully attempt according to the open literature. Potassium ferricyanide and hydrogen peroxide were used as the non-volatile and volatile reaction species, respectively. It was found that under subcooled nucleate boiling and fully developed nucleate boiling conditions, the mass transfer coefficient increases with the increasing electrolyte temperature and heat flux for both species. The increase for hydrogen peroxide was faster than that for potassium ferricyanide due to the transfer of hydrogen peroxide ions through both the liquid and vapor phases during the reaction. In addition, an empirical correlation was proposed to include the bubble induced micro-mixing and macro-mixing effects, which occurred during boiling and was proven to agree well with our experimental data.

In Phase III, a novel high temperature and pressure experimental flow loop and measuring technique were developed to determine the mass transfer rate under the flow boiling condition. The experimental setup and measuring technique enabled us to study the mass transfer behavior under the flow boiling condition to a level that no one else has been achieved according to open literature. The mass transfer coefficients were determined experimentally for the first time using this flow loop. An empirical correlation was proposed to represents our experimental data within 10% error. This work will provide a good base for further flow boiling mass transfer studies.

Preface

Chapter 1 is the introduction, which contains literature review related to the presented research works.

Chapter 2 of the thesis has been published as: C. Shen, A. Afacan, J.-L. Luo, and S.J. Klimas, *Mass transfer of dissolved oxygen using rotating cylinder electrode under bulk boiling conditions*. International Journal of Heat and Mass Transfer, 2014. **70**(0): pp. 162-168.

Chapter 3 of the thesis has been published as C. Shen, A. Afacan, J.-L. Luo, A. Siddiqui, and S.J. Klimas, *Mass transfer on nucleate boiling surfaces using the electrochemical method*. International Journal of Heat and Mass Transfer, 2014. **78**(0): pp. 289-293 and C. Shen, A. Afacan, J.-L. Luo, A. Siddiqui, and S.J. Klimas, *Mass Transfer of Diluted Volatile and Non-Volatile Components to a Nucleate Boiling Electrode*. Corrosion, 2015. 71(8): pp. 1003-1011.

Chapter 4 of the thesis was written as a paper manuscript as "A study of flow boiling mass transfer using a novel electrochemical flow loop" and will be submitted for a publication.

Appendix C of the thesis was written as a paper manuscript as "Effect of Boiling Bubbles on Passivation Degradation of Alloy 800 in Thiosulphate-containing Aqueous Solution" and will be submitted for a publication.

For all of the above work, the coauthor, Artin Afacan helped to design and construct the experimental setup as well as help with preparing manuscripts, conference presentations and the

thesis. The coauthors, Stan Klimas and Ali Siddiqui helped to revise the experimental plan and the analysis. Dr. Jing-li Luo, my supervisor, provided valuable discussions and feedbacks on construction of experimental devices, experimental plan and results. She also gave me extremely valuable suggestions and helped in writing, revising and preparing conference presentations, manuscripts and the thesis work. The rest of the research works, such as all the experiments, data collection, analysis, modeling work and interpretation as well as writing the manuscripts and this thesis are my contribution.

The present thesis includes a research project done in collaboration with Canadian Nuclear Laboratories (CNL) in Chalk River.

Dedication

To my beloved wife Qingqing GAO

My little boy, Tony SHEN

and my parents

Acknowledgements

I would like to take this opportunity to express my gratitude to all the people who provide great help for my Ph.D. studies.

Firstly, I would like to express my most sincere gratitude to my supervisor, Dr. Jing-li Luo, for her supervision, advice and encouragement throughout the whole Ph.D. program. Not only have I gained extensive knowledge and brilliant problems solving skills from her, but also her enthusiasm and hospitality for scientific research set an excellent example for me. Dr. Jing-li Luo made me a much better researcher and engineer.

My deepest gratitude goes to Mr. Artin Afacan for who guide me as my co-supervisor though the whole project. He also helped me in writing and revising the manuscripts and my thesis work.

My deep appreciation also goes to my supervisor committee members, Dr. Robert E. Hayes, Dr. John Nychka and Dr. Natalia Semagina for their stimulating and helpful suggestion during the progress of this research. Every time I met with them I gained knowledge about my field as well as their attitude toward research.

I also extend my special thanks to Stan Klimas and Dr. Yuchen Lu for providing me with invaluable advice on the progress of the research. From them, I learned an attitude toward work and research that will benefit me for a lifetime.

My great thanks to all the postdocs in our group, Dr Ming Li, Dr Dahai Xia, Dr. Hongqiang Fan, Dr. Hong Luo, Dr Bin Hua and Dr Qingying Wang. Their encouragement has helped me overcome the hardships that arose during this work. Every time I talked with them, I always learned more than I expected.

I sincerely thank the group members in our group, Ali Siddiqui, Dr. Jaganathan Ulaganathan, Yashar Behnamian, Xueyuan Chen, Zeynab Shirband, Xianzong Wang, Yifei Sun, Tong Gao, Subiao Liu and Yaqian Zhang. For their help, friendship, and contributions towards a wonderful research environment.

I also wish to thank the undergraduate students worked in our lab, Yuel Lai, Haonan Feng, Haobo Wang, Minkang Liu, Yichuan Wang, Yanwen Yu and Jiechen Gao. For their help with the experimental work. My special thanks also go to the machine and instrument shop staff Mr. Bob Smith, Mr. Walter Boddez and Mr. Les Dean for their help and technical expertise.

Finally, I acknowledge and appreciate Canadian Nuclear Laboratories (CNL) for their support and cooperation of the project.

Table of Contents

Chapter 1	Introduction.....	1
1.1	Background	1
1.2	Methods for mass transfer measurement	2
1.2.1	Dissolution method.....	3
1.2.2	Electrochemical method	3
1.3	Mass transfer study under different flow conditions	9
1.3.1	Mass transfer study under a natural convection condition	9
1.3.2	Mass transfer study under a simulated flow condition.....	10
1.3.3	Mass transfer study in multi-phase flow conditions.....	11
1.4	Mass transfer study under other special conditions	13
1.4.1	Mass transfer study under a non-isothermal condition.....	13
1.4.2	Mass transfer study under a boiling condition	16
1.5	Background of mass transport correlations	19
1.5.1	Mechanism of mass transport under forced convection.....	19
1.5.2	Mechanism of boiling phenomenon	21
1.5.3	Examining the similarity of a gas evolution electrode and a boiling electrode.....	23
1.6	Summary of present research status	26
1.7	Objectives and structure of thesis	26
1.8	References.....	27
Chapter 2	Phase I – bulk boiling condition.....	35
2.1	Introduction.....	35
2.2	Experimental setup.....	37
2.3	Experimental procedure	38
2.4	Results and discussion	41
2.4.1	Mass transfer behavior of dissolved oxygen under the below boiling condition	41
2.4.2	Mass transfer behavior of dissolved oxygen under bulk boiling condition.....	48
2.4.3	Mass transfer behavior of ferricyanide under below boiling condition	51
2.4.4	Mass transfer behavior of ferricyanide under bulk boiling condition	53
2.5	Conclusions.....	56

2.6	References.....	57
Chapter 3	Phase II -- pool boiling condition.....	61
3.1	Introduction.....	61
3.2	Experimental	64
3.2.1	Experimental set-up	64
3.2.2	Experimental procedure.....	65
3.2.3	Uncertainty Analysis	66
3.3	Background	68
3.4	Results and discussion	71
3.4.1	Stability of hydrogen peroxide reaction	71
3.4.2	Mass transfer under natural convection condition.....	73
3.4.3	Mass transfer rate under subcooled boiling condition (Onset of nucleate boiling) ...	75
3.4.4	Mass transfer under fully developed boiling condition.....	79
3.4.5	Effect of surface roughness under fully developed nucleate boiling condition	82
3.4.6	Mechanism and difference between ferricyanide and hydrogen peroxide reactions	83
3.4.7	Empirical correlation for mass transfer under pool boiling condition	87
3.5	Conclusions.....	91
3.6	References.....	92
Chapter 4	Phase III -- flow boiling conditions.....	95
4.1	Introduction.....	95
4.2	Experimental setup.....	97
4.3	Experimental procedure	100
4.4	Results and discussion	101
4.4.1	Effect of temperature on mass transfer rate.....	101
4.4.2	Effect of the flow rate on the mass transfer rate.....	103
4.4.3	Effect of the operating pressure on the mass transfer rate.....	104
4.4.4	Mass transfer measurement under the flow boiling condition	108
4.4.5	Empirical correlation for mass transfer behavior under the flow boiling condition	112
4.5	Conclusions.....	115
4.6	References.....	117
Chapter 5	Conclusions	120

Chapter 6 Recommendations and future work	122
Bibliography.....	124
Appendix A Experimental data.....	147
A.1.1 Data for Phase I	147
A.1.2 Data for Phase II	152
A.1.3 Data for Phase II	156
Appendix B Calculations	158
B.1 Sample calculation.....	158
B.1.1 Calculation of dissolved oxygen concentration.	158
B.1.2 Sample mass transfer coefficient calculation.....	160
B.2 Calculation for design of phase III.....	162
B.2.1 Solution tank	162
B.2.2 Pre heater	162
B.2.3 Entrance length	163
B.3 References.....	165
Appendix C Effect of Boiling Bubbles on Passivation Degradation of Alloy 800 in Thiosulphate-containing Aqueous Solution.....	166
C.1 Introduction	166
C.2 Experimental.....	167
C.2.1 Experimental set up.....	167
C.2.2 Experimental procedure	169
C.3 Results and discussion.....	173
C.3.1 Corrosion potential.....	173
C.3.2 Anodic polarization.....	174
C.3.3 Electrochemical impedance spectroscopy (EIS).....	176
C.3.4 X-ray photoelectron spectroscopy (XPS)	178
C.3.5 Secondary ion mass spectrometry (SIMS).....	183
C.3.6 Effect of boiling bubbles on passivation degradation.....	190
C.4 Conclusions	194
C.5 References	195

List of Figures

Figure 1-1. Typical cathodic polarization curve with a limiting current plateau.....	4
Figure 1-2. Cell assembly F1 and F2 are working electrode halves. CE is the counter electrode, OAl and OA2 are current-followers and Tr is the transformer [68].	14
Figure 1-3. Temperature and concentration contours for a wire surface temperature of 80 °C [70].	15
Figure 1-4. Current-potential curves at different temperatures (a) without nucleate boiling and (b) with nucleate boiling. A bulk temperature is 11 °C [72].	17
Figure 1-5. Typical Boiling Curve [80]	21
Figure 1-6. Diagram of heat transfer mechanisms in boiling. (a) Bubble agitation model; (b) Vapour-liquid exchange mechanism; (c) Evaporative mechanism [81].	22
Figure 1-7. Comparison of the processes of bubble generation in nucleate boiling (upper part) and generation of gas in an electrochemical process (lower part) [85].	24
Figure 1-8. Bubble heat transfer mechanisms [86].	25
Figure 2-1. The experimental set-up	38
Figure 2-2. The typical cathodic polarization curves (a) and mass transfer coefficient for various rotating speeds (b) at 20 °C and dissolved oxygen concentration 8.83 ppm.	43
Figure 2-3. Limiting current density vs. dissolved oxygen concentrations at 20 °C (a) and 60 °C (b) at the different rotating speeds, respectively.	45
Figure 2-4. Calculated mass transfer coefficient vs. dissolved oxygen concentrations at 20 °C (a) and 60 °C (b) at the different rotating speeds, respectively.	46
Figure 2-5. Comparison of experimental and predicted <i>Sherwood</i> numbers for dissolved oxygen mass transfer at temperatures below boiling.	47
Figure 2-6. Photograph of rotating cylinder electrode system under bulk boiling electrolyte condition. (a) The electrochemical cell and (b) the cylinder electrode.	48
Figure 2-7. Polarization curves obtained in bulk boiling electrolyte (99.8 °C) for the different inlet oxygen/argon ratios at constant rotating speed of 500 rpm.	49
Figure 2-8. Polarization curves obtained in boiling electrolyte (99.8 °C) with the inlet oxygen/argon ratio of 5 % and at the different rotating speeds.	51
Figure 2-9. Mass transfer coefficient vs. temperature at the different rotating speeds for ferricyanide ions.....	53

Figure 2-10. Cathodic polarization curves (a) and mass transfer coefficient (b) for reduction of ferricyanide reaction obtained in bulk boiling electrolyte at different rotating speeds.	54
Figure 2-11 Comparison of the experimentally determined and predicted <i>Sherwood, Sh</i> numbers obtained using ferricyanide reactions.	56
Figure 3-1. Schematic diagram of the nucleate boiling experimental setup.	65
Figure 3-2. Factors (a) micromixing (b) macromixing (c) non-isothermal convection influence mass transfer under boiling condition.	71
Figure 3-3. Current density as a function time for Alloy 800 in the hydrogen peroxide at various electrolyte temperatures.	73
Figures 3-4. Cathodic polarization curves for ferri-/ferrocyanide (a) and hydrogen peroxide (b) reactions for different electrolyte temperatures under natural convection condition	75
Figures 3-5. Potentiostatic test for (a) ferri-/ferrocyanide and (b) hydrogen peroxide reactions at subcooled nucleate boiling condition.	77
Figures 3-6. Mass transfer coefficients for (a) ferri-/ferrocyanide and (b) hydrogen peroxide reactions under natural convection, subcooled nucleate boiling and fully developed nucleate boiling conditions.	78
Figures 3-7. Cathodic polarization curves for (a) ferri-/ferrocyanide and (b) hydrogen peroxide reactions under fully developed nucleate boiling condition.	80
Figures 3-8. The mass transfer coefficients for ferri-/ferrocyanide (a) and hydrogen peroxide (b) reactions as a function of heat flux under fully developed nucleate boiling condition	82
Figure 3-9. Polarization curves for various surface roughness under pool boiling condition.	83
Figures 3-10. The Sherwood number of ferri-/ferrocyanide and hydrogen peroxide as a function of electrolyte temperature or heat flux for (a) natural convection, (b) subcooled nucleate boiling condition and (c) fully developed nucleate boiling conditions, respectively.	85
Figures 3-11. The proposed mass transfer mechanisms of ferricyanide ion and hydrogen peroxide in the presence of bubbles under boiling condition.	87
Figures 3-12. Mass and heat transfer coefficient (a) and comparison of the experimentally determined and predicted <i>Sherwood</i> numbers (b) under pool boiling conditions.	90
Figure 4-1. Schematic diagram of flow loop	98
Figure 4-2. Schematic diagram of electrochemical flow cell	99
Figure 4-3. Schematic diagram of the experimental part.	99

Figures 4-4. (a) Cathodic polarization curves (Electrolyte flow rate 17.0 kg/m ² s; Operating pressure 445 kPa) and (b) the calculated mass transfer coefficient for the flow loop system at various electrolyte temperatures (Electrolyte flow rate 17.0 kg/m ² s; Operating pressure 445 kPa).	102
Figures 4-5. (a) Cathodic polarization curves (Electrolyte temperature 22 °C; Operating pressure 445 kPa) and (b) the calculated mass transfer coefficient as a function electrolyte flow rate for various electrolyte temperatures (Operating pressure 445 kPa).	104
Figures 4-6. (a) Cathodic polarization curves (Electrolyte temperature 22 °C; Electrolyte flow rate 17.0 kg/m ² s) and (b) the calculated mass transfer coefficient as a function of operating pressure and for various electrolyte temperatures (Electrolyte flow rate 17.0 kg/m ² s).	106
Figures 4-7. Comparison between the experimentally determined present studies Sherwood numbers and predicted Sherwood numbers.	107
Figures 4-8. Potentiostatic tests for increasing oil temperatures (Operating pressure 100 kPa; Electrolyte flow rate 17.0 kg/m ² s).	109
Figure 4-9. Cathodic polarization curves for single-phase and flow boiling conditions. (Operating pressure 100 kPa; Electrolyte flow rate 17.0 kg/m ² s).	110
Figures 4-10. Cathodic polarization curves under the flow boiling condition (Operating pressure 100 kPa).	111
Figure 4-11. Comparison between the experimentally determined and predicted mass transfer coefficient under the flow boiling condition	115
Figure B-1. Calculation results of dissolved O ₂ concentration.....	160
Figure C-1. Rotating electrode electrochemical experimental set-up.....	169
Figure C-2. Corrosion potentials for Alloy 800 in deaerated testing electrolyte at various temperatures.....	174
Figure C-3. Anodic potentiodynamic polarization curves for Alloy 800 in deaerated testing electrolyte at various temperatures.	175
Figure C-4. EIS for Alloy 800 in deaerated testing electrolyte at various temperatures.	178
Figure C-5. XPS analysis of S in the Alloy 800 specimen after immersion in the test solution at various temperatures.	181

Figure C-6. XPS analyses of Fe, Ni and Cr in the Alloy 800 specimen after immersion in the test solution at various temperatures. 182

Figure C-7. SIMS analyses of O and S after immersion of the specimen in the test solution at various temperatures. 188

Figure C-8. SIMS analyses of Fe, Ni and Cr after immersion of the specimen in the test solution at various temperatures. 189

Figure C-9. Effect of boiling bubble on the degradation of anodic film on Alloy 800 after immersion in the test solution at various temperatures..... 193

List of Tables

Table 1-1. Electrochemical systems used in mass transfer studies.....	7
Table 2-1. Viscosity, density and dissolved oxygen diffusivity in 0.1 M NaOH aqueous for solution temperatures range between 20 – 80 °C [21, 22]......	39
Table 3-1. Diffusivities of potassium ferricyanide and hydrogen peroxide at various temperatures.	66
Table A-1. Experimental data for oxygen reaction conducted under temperature of 20 °C.....	147
Table A-2. Experimental data for oxygen reaction conducted under temperature of 40 °C.....	148
Table A-3. Experimental data for oxygen reaction conducted under temperature of 60 °C.....	149
Table A-4. Experimental data for oxygen reaction conducted under temperature of 80 °C.....	150
Table A-5. Experimental data for ferricyanide reaction under the concentration of 0.01 mol/L	151
Table A-6. Experimental data for ferricyanide reaction under pool boiling condition with the concentration of 0.01 mol/L.....	152
Table A-7. Experimental data for ferricyanide reaction under subcooled boiling condition with the concentration of 0.01 mol/L.....	154
Table A-8. Experimental data for hydrogen peroxide reaction under pool boiling condition with the concentration of 0.00195 mol/L.....	155
Table A-9. Experimental data for hydrogen peroxide reaction under single-phase condition with the concentration of 0.002 mol/L.....	156
Table A-10. Experimental data for hydrogen peroxide reaction under flow boiling condition with the concentration of 0.002 mol/L.....	157
Table B-1. Dimensions of the flow loop and electrochemical flow cell as well as the operating range.....	164
Table C-1. Composition of testing electrolyte.....	168
Table C-2. Binding energies of XPS peaks	172
Table C-3. Constants of the EEC model.....	176
Table C-4. Atomic ratio of different S components over all S components at different temperatures.....	183

Nomenclature

a, b, c, e	empirical factors, dimensionless
a_s	mass transfer area per unit column volume, m^2/m^3 or $1/\text{m}$
A	surface area, m^2
Bo	boiling number, dimensionless
C	concentration, mol/m^3
C_0	ion concentration at the electrode interface, mol/m^3
C_b	bulk ion concentration, mol/m^3
C_{in}	inlet ion concentration, mol/m^3
C_{out}	outlet ion concentration, mol/m^3
C_p	liquid specific heat, $\text{J}/(\text{kg}\cdot\text{K})$
C_{sat}	saturation ion concentration, mol/m^3
d	diameter, m
d_c	hydraulic diameter, m
d_b	break off diameter of the gas bubble, m
D	diffusivity, m^2/s
E_1	suppression factor, dimensionless
E_2	enhancement factor, dimensionless
F	Faraday constant, $96485 \text{ C}/\text{mole}$
F_1, F_2	empirical factors, dimensionless
g	gravity of Earth, m/s^2
Gr	Grashof number, dimensionless
i	current density, A/m^2

i_L	limiting current density, A/ m ²
k	mass transfer coefficient, m/s
k_{fb}	mass transfer coefficient under the flow boiling condition, m/s
k_{pool}	mass transfer coefficient under the pool boiling condition, m/s
k_{sp}	mass transfer coefficient for single-phase flow, m/s
h	heat transfer coefficient, W/(m ² ·K)
h_{sp}	heat transfer coefficient for single-phase, W/(m ² ·K)
h_{pool}	heat transfer coefficient under the pooling boiling condition, W/(m ² ·K)
h_{fb}	heat transfer coefficient under the flow boiling condition, W/(m ² ·K)
H	Henry's law constant, MPa
J	molar flux, mol/ m ² s
J_L	the power of latent heat, W
L	characteristic length, m
L_e	electrode length, m
\dot{m}	mass flow rate, kg/s
M	molecular weight, g/mol
n	numbers of electrons transferred per reaction
N	mass flux per unit area, kg/m ² s
$N(t)$	concentration as a function of time, mol/m ³
Nu	Nusselt number for heat transfer hL/λ , dimensionless
pr	reduced pressure, MPa
Pr	Prandtl number for heat transfer $\mu C_p/\lambda$, dimensionless
q	heat flux, kW/m ²

Q	volumetric liquid flow rate, m^3/s
Ras	surface roughness, μm
Ra	Rayleigh number $PrGr$, dimensionless
Re	Reynolds number VL/ν , dimensionless
Re_G	gas evolution Reynolds number
Sc	Schmidt number ν/D , dimensionless
Sh	Sherwood number kL/D , dimensionless
Sh_{conv}	Sherwood number caused by non-isothermal convection
Sh_{macro}	Sherwood number caused by macro mixing
Sh_{micro}	Sherwood number caused by micro mixing
t	time, s
$t_{0.5}$	half-life, s
T	temperature, K
T_{in}	inlet temperature, K
T_{out}	outlet temperature, K
T_s	temperature of the surface, K
u	electrophoretic mobility of particles, $\text{m}^2/(\text{V s})$
V	velocity of the electrolyte, m/s
V_M	molar volume, m^3/mol
V_G	gas evolution rate, m^3/s
X_{tt}	Martinelli parameter, dimensionless
z	length of the test section, m

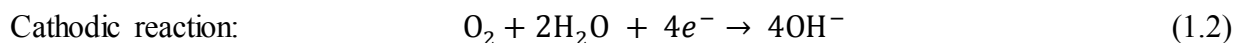
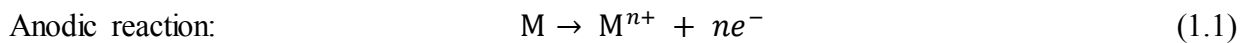
Greek

β	volumetric thermal expansion coefficient, dimensionless
ε_{∞}	thermoelectric coefficient under steady heat flux and no convection (“thermal EMF”), V/°C
λ	thermal conductivity, W/m k
λ_L	latent heat of evaporation, J/kg
μ	dynamic viscosity, Pa s
ν	kinematic viscosity μ/ρ , m ² /s
θ	contact angle, °
ρ	density, kg/m ³
ρ_G	density of gas, kg/m ³
ρ_L	density of liquid, kg/m ³
σ	standard deviation
σ_s	surface tension, N/m
φ	electrical potential, V
ω	experimental or calculated error

Chapter 1 Introduction

1.1 Background

Systems operating under a flow boiling condition that has two phases are commonly encountered in the nuclear industry. Flow boiling is a complex condition, which includes a high temperature (above 100 °C), vapor generation (gas bubbling at the solid surface) and a gas-liquid two-phase flow [1-3]. It is important to study mass transfer in this condition, as it is associated with a wide range of problems in the nuclear industry, such as materials degradation of components, and the fouling of heat exchangers and steam generators [4, 5]. For example, when oxygen reduction is the primary cathodic reaction, the mass transfer rate of dissolved oxygen under boiling may be related to the rate of corrosion in steam generators under operating conditions. The electrochemical reactions of the corrosion in a neutral aqueous solution containing dissolved oxygen can be written as [6]:



To understand how the mass transport of oxygen affects stress corrosion cracking rates under the operating condition of a steam generator, it is necessary, for the following reasons, to quantify the mass transfer rate of dissolved oxygen to the wall under flow boiling:

- (1) The electrochemical corrosion potential (ECP) which is one of the most important factors affecting stress corrosion cracking rates is a function of oxygen concentration at the

metal surface. The dissolved oxygen concentration on the surface can be predicted from the bulk concentrations only if the mass transfer rate of oxygen is known.

- (2) The degradation of the tubing materials of the steam generators under boiling and flow conditions is often diffusion controlled, i.e., the rate-determining step is the mass transport of dissolved oxygen to the corroding metal surface [7-9].

Another example to show the importance of quantifying mass transfer under the flowing boiling condition is the mass transfer rate of dilute foulant, such as dissolved iron corrosion products. The mass transfer rate is very important for predicting the precipitation fouling rate on nuclear fuel.

The mass transfer behavior has been widely investigated for stationary single-phase [10-13], single-phase flow [14-16] and multiple-phase flow conditions [17-19]. However, no experimental studies have been reported in the open literature on mass transfer under the two-phase flow boiling condition. The lack of experimental data can be attributed to experimental difficulties because there is no commercially available facility that can be used for the measurements under two-phase flow boiling. It is more challenging to interpret data for two-phase flow boiling than for single-phase flow condition.

1.2 Methods for mass transfer measurement

The two most frequently used methods to measure the liquid-solid mass transfer coefficient are the dissolution method and electrochemical method [20, 21].

1.2.1 Dissolution method

The dissolution method employs a soluble solid material inside the liquid phase and measures the concentration difference of the dissolved material between the inlet and outlet liquid flows. The liquid-solid mass transfer value can then be calculated [22]. The mass transfer coefficient can be calculated using the following equation [23]:

$$k a_s = \frac{Q}{z A} \ln \left[\frac{C_{sat} - C_{in}}{C_{sat} - C_{out}} \right] \quad (1.3)$$

where k is the mass transfer coefficient; a_s is the mass transfer area per unit column volume; Q is the volumetric liquid flow rate; z is the length of the test section; A is the area for mass transfer test section, and C_{sat} , C_{in} and C_{out} represent the saturation, inlet and outlet concentrations of the dissolved testing material, respectively.

1.2.2 Electrochemical method

The other widely used method for mass transfer measurement is the electrochemical method or so-called limiting current method [24]. This method involves measuring the value of the limiting current plateau on a current-voltage chart when the electrode reactions proceed at the highest possible rate [13]. The electrochemical method includes potential dynamic measurement, which changes the potential of the working electrode and records the current signal. This measured current presents the rate of electrochemical reaction on the working electrode surface. Figure 1-1 shows a typical relationship of the measured current and voltage drop. This figure is also called

the polarization curve, and it shows how the reaction rate changes with the change of potential of the working electrode. The electrode reactions involve two steps: movement of ions from the bulk solution to the electrode surface, and the electrochemical reaction occurring at the surface of the electrode [25]. When the reaction rate at the interface becomes faster, the ion movement becomes the rate-determining step and the ions at the interface are almost completely depleted. This is where the limiting current plateau appears and the electrode reactions proceed at the highest possible rate. Further increase in potential will not change the current density until the equilibrium potential of hydrogen is reached.

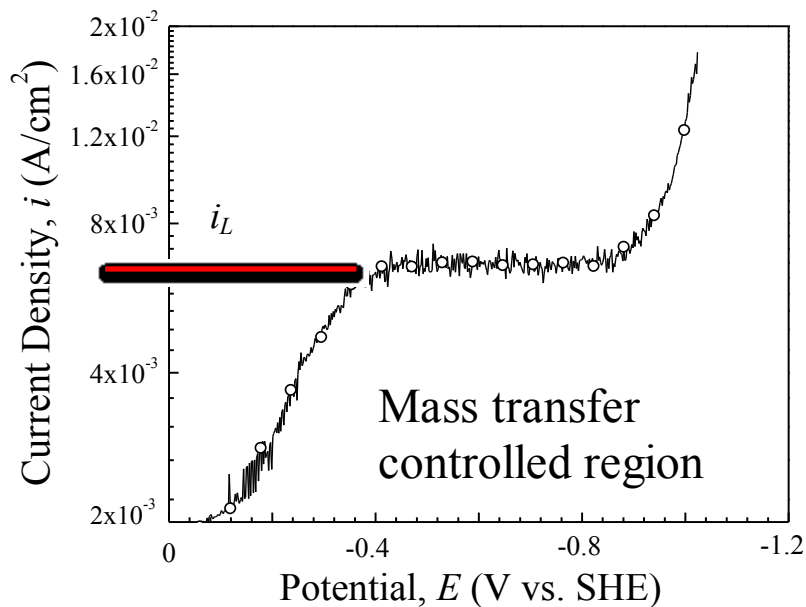


Figure 1-1. Typical cathodic polarization curve with a limiting current plateau

The mass flux of the ions to the electrode can be related to the measured limiting current density using the following relationship [26]:

$$J = - \frac{i_L}{nF} \quad (1.4)$$

where J is the molar flux; i_L is the limiting current density; F is the Faraday constant, 96490 C/mol and n is the number of electrons transferred per ion [27]. By the definition of the overall mass transfer coefficient, k , can be expressed as:

$$k = \frac{J}{(C_0 - C_b)} \quad (1.5)$$

where C_0 is the reactant concentration at the interface and C_b is the concentration in the bulk electrolyte. The value of the interface concentration, C_0 , equals zero during our experiment since there is no reactant in the interface in the mass transfer controlled reaction region.

In the mass transfer controlled reaction region, the concentration of reacting ion at the electrode becomes negligible. Therefore, one only need to consider the bulk concentration [28]. Combining equations (1.4) and (1.5) and using the measured limiting current density, i_L , the overall mass transfer coefficient can be expressed as:

$$k = \frac{i_L}{nFC_b} \quad (1.6)$$

Dang-Vu et al. [29] expressed their results in terms of the dimensionless group using the following equation:

$$Sh = a \times Re^b Sc^c \quad (1.7)$$

where a , b and c are constants and often determined using the experimental data. Sh is the Sherwood number, Re is the Reynolds number, Sc is the dimensionless Schmidt number as defined below:

$$Sh = \frac{kL}{D} \quad (1.8)$$

$$Sc = \frac{\nu}{D} \quad (1.9)$$

$$Re = \frac{VL}{\nu} \quad (1.10)$$

where L is the characteristic length, D is the diffusivity of the reactant, V is the velocity of the electrolyte and ν is the kinematic viscosity.

However, such relationship Eq. (1.7) may not be valid in the present study since the equation does not contain any heat transfer parameter which could vastly affect the mass transfer in the flow boiling regime.

The dissolution method is often used to determine an average volumetric liquid-solid mass transfer at a certain time period, while the electrochemical method is used to obtain in situ mass transfer rates of the electrode specimen based on the ion exchange limit [30]. For the dissolution method, the dissolution of copper in an acidic solution is often used to study the liquid-solid mass transfer behavior [31]. However, this method may not be able to determine the effect of different materials on the mass transfer at the interface because most of the metal materials are

not suitable for the dissolution experiment. On the other hand, the electrochemical method could allow researchers to investigate the mass transfer behavior as long as the solids are electrically conductive. The electrochemical method has become widely accepted for mass-transfer measurement in the past several decades [32, 33]. Therefore, for the present study, the electrochemical method is being used to measure limiting current under two-phase and boiling conditions.

Only limited compounds can be used because the compound requires being chemically stable and the suitable electrode potential where a well-defined limiting current plateau appears. One of the most important steps in the electrochemical method is to choose an appropriate electrochemical system to study mass transfer behavior [12, 34, 35]. Table 1-1 shows some of the systems that are often used in the electrochemical method.

Table 1-1. Electrochemical systems used in mass transfer studies

Electrochemical reactions	Potential (V vs SHE)	Supporting electrolyte	Ref.
$O_2 + 2H_2O + 4e^- \rightarrow 4OH^-$	+0.401	NaOH	[36]
$Cu^{2+} + 2e^- \rightarrow Cu$	+0.337	H ₂ SO ₄	[37]
$Fe(CN)_6^{3-} + e^- \rightarrow Fe(CN)_6^{4-}$	+0.360	NaOH	[38]
$I_3^- + 2e^- \rightarrow 3I^-$	+0.536	KI	[39]
$Ag^+ + e^- \rightarrow Ag$	+0.799	HClO ₄	[40]
$Ce^{4+} + e^- \rightarrow Ce^{3+}$	+1.61	H ₂ SO ₄	[41]
$H_2O_2 + 2e^- \rightarrow 2OH^-$	-	Na ₂ SO ₄	[42]

The top three are the most popular ones: (1) Reduction of dissolved oxygen from a neutral or basic solution; (2) Deposition of copper from an acidified copper sulfate solution; (3) Reduction of ferricyanide/ferrocyanide from solutions containing an excess of sodium hydroxide or potassium hydroxide as the supporting electrolyte. Even these compounds are not exact the same compare with the real operating condition. But they can provide good reference for the concerned compounds.

The deposition of Cu and Ag are not suitable for this work since it would change the surface roughness of the specimen. The oxygen reaction is most suitable for our study since it represents the main cathodic reaction in the corrosion process. However, since the concentration of oxygen is not likely to be stable under boiling conditions, other stable agents are needed in our study. The reaction of potassium ferricyanide/ferrocyanide does not change the electrolyte chemistry during the measurement. Potassium ferricyanide/ferrocyanide is one of the best agents to conduct mass transfer measurement under boiling conditions. However, because potassium ferricyanide/ferrocyanide is a non-volatile compound, the results may not be applicable to the volatile compound under boiling conditions. Hydrogen peroxide is a volatile compound that has significant interactions with metal surfaces [43-45] and is considered to be corrosive in a supercritical water-cooled reactor (SWCR) [46]. Nickchi and Alfantazi [47] measured the limiting current for the reduction reaction of hydrogen peroxide up to 200 °C in autoclaves, but boiling is not likely to take place continuously in autoclaves. According to the authors' best knowledge, the mass transfer behavior from a bulk electrolyte to a boiling surface was still unclear for different compounds.

1.3 Mass transfer study under different flow conditions

1.3.1 Mass transfer study under a natural convection condition

The mass transfer mechanism has been extensively investigated in the last several decades under various conditions [15, 48-50]. Selman and Tobias [13] stated that the liquid-solid mass transfer had been well studied beginning in 1950s. Fenech and Tobias [10] measured the limiting current on the horizontal rectangular cathodes facing upward in CuSO_4 and H_2SO_4 solutions in an unstirred cell. They examined the influence of the electrolyte concentration, the distance of the electrode to the ceramic diaphragm, and the size of the electrode on the mass transfer. For an electrode with a width larger than 20 mm, they proposed a mass transfer equation which includes the effect of liquid properties and electrode sizes. Their equation shows that the mass transfer coefficient increased with the increasing size of the specimen. Wragg [11] did similar work and pointed out some deficiencies of the Fenech and Tobias study [24]. Wragg argued that the rectangular-shaped electrode and its position relative to the rectangular cell affected the symmetry of the system's geometry and boundary layer formation. Wragg's work showed that using the distance from the electrode to the diaphragm as the characteristic dimension is not appropriate since it has been shown to have no effect on the mass-transfer rates. Wragg et al. [11] performed experiments that investigated the free convection mass transfer behavior of upward-facing horizontal surfaces using the electrochemical technique involving the measurement of limiting currents for the deposition of copper on copper electrodes. Wragg et al. gave a comprehensive quantitative account of the horizontal surface and free convection ionic mass transfer and also provided good correlations for the experimental data.

Smith and Wragg [12] employed a limiting current electrolytic technique to measure the rate of solid-liquid mass transfer between the electrolyte and vertical arrays of cylinder cathodes. Their findings were consistent with the study done by Schultz [51] regarding mass transfer behavior for single cylinders. In addition, they found that depending on the geometry and the magnitude of the density gradients, either the concentration is the dominating cause in decreasing the mass transfer or the enhanced velocity is the dominating cause for increasing the mass transfer.

1.3.2 Mass transfer study under a simulated flow condition

Among many possible experimental methods of simulating flow conditions, the rotating electrode is noteworthy, not only because it affords experimental reproducibility, but it makes it possible to use hydrodynamic and mass momentum transfer analogy methods to interpret and correlate data [52-55].

Brunner [56] was the first to study the effect of rotating speed on the rate of mass transfer. He found that the diffusion layer thickness decreases with the $2/3$ power of the rotational speed. Eisenberg et al. [52] claimed that Brunner's work did not consider neither the rotor diameter nor the physical properties affected the mass transfer study. Therefore, they investigated the rates of ionic mass transfer at nickel electrodes rotating about their axes in the center of stationary electrodes using a ferricyanide/ferrocyanide couple in alkaline solutions. They developed a general mass transfer equation, which takes into account the system's physical properties as well as its geometric and hydrodynamic factors. This equation also allows the prediction of mass transfer under a wide range of operating conditions.

Other researchers have investigated the effect of an electrode's shape on mass transfer behavior. Cobo et al. [57] worked on the experimental study of the ionic mass transport on rotating electrodes whose electrochemically active part is an axially placed one-base spherical segment. They used the reduction of ferricyanide ions and the electro deposition of copper ions. Based on their data, they obtained an equation to express the mass transfer rate as a function of a spherical segment electrode with an angle up to 40° and angular velocity of the rotating electrode. Filinovsky et al. [58] developed a mathematical approach for the mass transfer behavior of platinum and copper double ring electrode systems. The results of their experimental measurements of diffusion currents were in accordance with their mathematical calculations. Despic et al. [59] studied the mass transfer properties on a rotating disc with a rectangular patch electrode. Janssen and Barendrecht [60] characterized the rate of mass transfer to a rotating cone and ring electrode. Ives et al. [61] studied the cathodic electrode processes which may occur during the metallic corrosion in chlorine-treated and untreated seawaters using a rotating gold disc electrode system. The overall reduction of free chlorine was controlled by a mass transport process.

1.3.3 Mass transfer study in multi-phase flow conditions

Delaunay et al. [17] used the electrochemical technique to measure the overall mass transfer coefficients in an upward co-current gas-liquid flow under bubbles flow and surging flow conditions. They compared the limiting current of two typical current-potential curves obtained with the cathodic reduction of the potassium ferricyanide ions with and without a gas flow.

Delaunay et al. observed that the gas phase does not greatly modify the shape of the diffusion plateau. The significant decrease of the average conductivity of the solution did not have sufficient enough effect on the potential distribution in the solution to explain why the current plateau was not observed. Thus, Delaunay et al. concluded that the electrochemical technique, which was frequently used for a single-phase flow, was still applicable for a two-phase flow with a large range of gas and liquid flow rates.

Latifi et al. [19] investigated the overall liquid-solid mass transfer in a gas-organic liquid flow through a packed bed under trickle-flow and liquid-filled column conditions using the electrochemical method. They extended the electrochemical technique to measure liquid-solid mass transfer rates in an organic medium at a high Schmidt number. Bartelmus [62] measured the local solid-liquid mass transfer coefficient in a three-phase fixed bed reactor using the limiting current technique. Mass transfer equations for the single phase of a liquid flow, gas continuous flow, and pulsed flow regime (with non-continuous gas flow) were obtained.

Wen et al. [18] conducted extensive experimental studies on solid-liquid mass transfer in gas-liquid-solid three-phase reversed flow jet-loop reactors using the electrochemical method. The effects of the liquid jet-flow rate, gas jet-flow rate, particle size, particle density, and nozzle diameter on the solid-liquid mass transfer coefficient were evaluated. The results showed that the solid-liquid mass transfer coefficients were found to increase when the particle density and gas jet-flow rate increased. The mass transfer coefficients were independent of the liquid jet-flow rate and particle size, but were slightly dependent on the nozzle diameter.

1.4 Mass transfer study under other special conditions

1.4.1 Mass transfer study under a non-isothermal condition

In addition to normal flow conditions, mass transfer behaviors have been investigated under other special conditions such as non-isothermal [63], electric field [64], magnetic field [65, 66], and boiling conditions. Grundler et al. [67] designed an electrode capable of performing electro-analytical experiments in which a platinum wire electrode inside an aqueous electrolyte solution was continuously joule-heated during dc polarization. The proposed symmetrical electrode arrangement allowed the measurement of low magnitude electrochemical signals even when a high magnitude audio frequency current was used for heating. The schematic diagram of the experimental electrode design is shown in Figure 1-2. The two halves of the wire electrode (F1 and F2) were soldered and the contacts were sealed with molten paraffin wax. Grundler et al. claimed that during heating, a thin layer of melting wax reliably prevented the contact between the aqueous solution and electrical connections. A current follower with capacitive feedback was connected between the working electrode and the potentiostat to selectively filter the small ac component that might still exist. This so-called “hot wire electrochemistry” performed the high temperature electrochemical studies that were accessible using the described simple arrangement together with standard electrochemical instrumentation. Beckmann et al. [68] used the above experimental set-up to perform electro-analytical measurements at elevated temperatures. A thin platinum wire with a diameter of 25 μm was directly heated using ac current. The electrochemical signal at this wire was measured simultaneously. The limiting currents were measured using a cylindrical electrode that was continuously heated due to thermal convection. Beckmann et al. found that the limiting currents were independent of the scan rate for the same

temperatures. This was in contrast to isothermal conditions where the pseudo-limiting current, after changing from a peak to a sigmoidal shape, was never independent of the scan rate at a cylindrical electrode [69]. Furthermore, Beckmann et al. [68] have shown that the temperature-dependence of the limiting currents at heated wire electrodes demonstrated an Arrhenius-type behavior, as was expected based on the temperature-dependence of the diffusion coefficient.

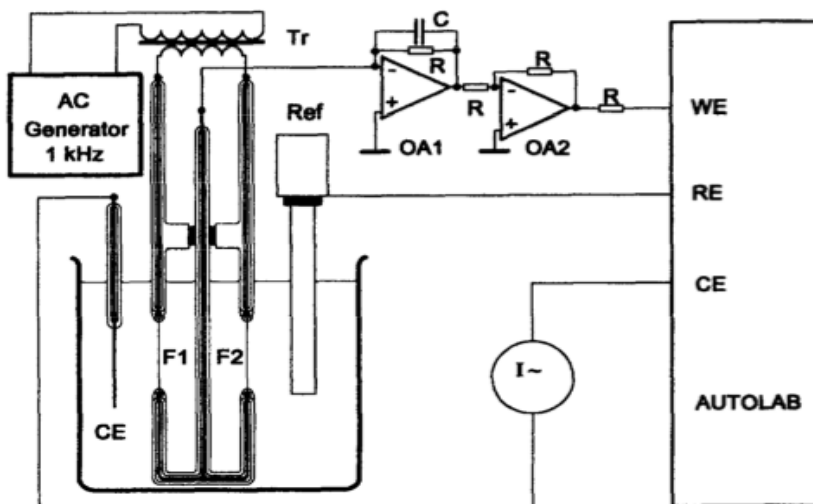


Figure 1-2. Cell assembly F1 and F2 are working electrode halves. CE is the counter electrode, OA1 and OA2 are current-followers and Tr is the transformer [68].

Beckmann et al. [70] used directly heated wire electrodes to analyze the temperature-dependence of electrochemical reactions. A microelectrode platinum wire with a diameter of 25 μm was heated directly in situ using an electric current-generated mass as well as heat energy transport phenomena. With continuous heating, a steady-state surface temperature was established as a result of thermally promoted convection. Figure 1-3 shows the temperature and concentration contours for a wire surface temperature of 80 $^{\circ}\text{C}$ (i.e., no boiling is anticipated). Beckmann et al. found that the temperature profile expanded into solution much further than any concentration profile that could be generated by electrochemical processes. Most of the compounds diffusion was taking place within a fairly limited range of temperatures, on the order of 10 $^{\circ}\text{C}$. Beckmann

et al. found that the Nernst diffusion layer approaches a constant thickness if the temperature difference between the bulk and electrode surfaces exceeds 30 °C. As a result, diffusion-limited current values of cyclic voltammetry and chronoamperometry were evaluated directly. These results appear to be specific to the natural convection at the microelectrode, and are not directly relevant to the topic at hand. Since the “hot wire method” used a Pt wire with a diameter of 25 μm as an electrode, the convection and diffusion behavior may not be applicable to a larger scale (diameter around 10 cm), which is not the case in the present study.

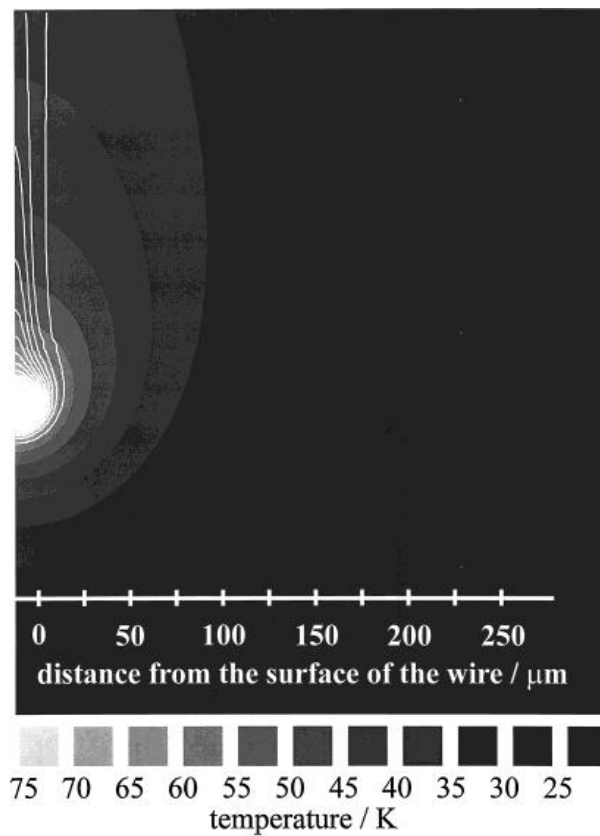


Figure 1-3. Temperature and concentration contours for a wire surface temperature of 80 °C [70].

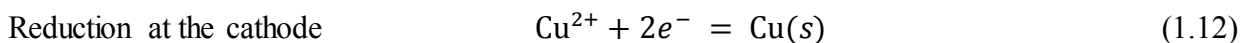
1.4.2 Mass transfer study under a boiling condition

Brusakov [71] studied the deposition of materials onto heat-transfer surfaces due to thermoelectric effects. He stated that thermoelectric effects occur in a temperature gradient-generated electric field with systems containing charged colloidal particles. He managed to create an electric field caused by positively charged particles to deposit on heated surfaces. In his study, thermoelectric coefficients for the systems of interest ranged from 0.2×10^{-3} to 1.5×10^{-3} V/°C. He concluded that thermoelectric effects could affect both transport and attachment and proposed the following equation to transport particles, which takes into account the thermoelectric effects:

$$J = \frac{\varepsilon_{\infty} u C_p}{\lambda} \quad (1.11)$$

where ε_{∞} is the thermoelectric coefficient under steady heat flux and no convection; u is the electrophoretic mobility of particles; C_p is the specific heat and λ is the thermal conductivity.

Wragg and Nasiruddin [72] published a relevant work on mass transfer rate under boiling conditions. They measured mass transfer on heated surfaces using the electrochemical method. Surface temperatures ranged from 11°C to 125°C at atmospheric pressure. The experiments were carried out using copper disc electrodes with diameters between 2 and 51 mm and a copper sulphate solution with concentrations ranging from 0.005 to 0.15 mol/L. The supporting electrolyte was 1.5 mol/L sulphuric acid. The electrochemical reaction studied was:



Oxidation at the anode

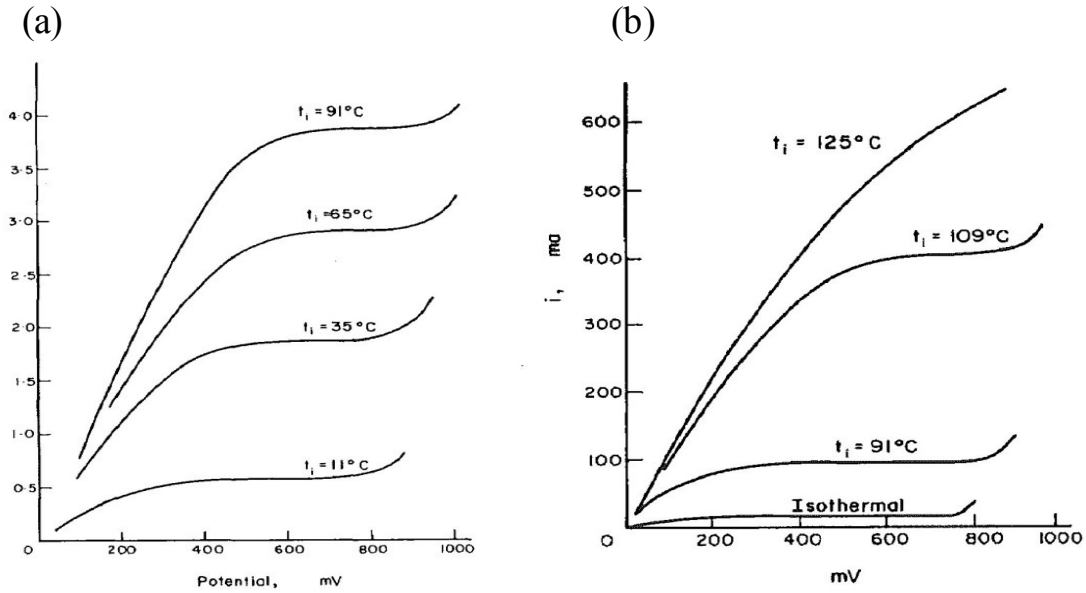


Figure 1-4. Current-potential curves at different temperatures (a) without nucleate boiling and (b) with nucleate boiling. A bulk temperature is 11°C [72].

There was no flow or mixing of the solution and the cathode was heated using an epoxy-coated resistance wire. The bulk temperature was adjusted to 11°C and controlled using a cooling coil. The limiting current was measured for different temperature gradients, electrode diameters, and solution concentrations. The limiting current plateaus at temperatures below the onset of the nucleate boiling on the surface are shown in Figures 1-4 (a) and (b). It can be seen that for temperatures where nucleate boiling occurred, a limiting current plateau was not observed at 125°C .

For each current-potential curve, the temperature was taken at the electrode surface. It was concluded that the mass-transfer rate under boiling conditions could not be measured using this experimental technique due to the intense local turbulence at the electrode-solution interface caused by bubble nucleation, growth, movement, and collapse. The paper did not explore the possibility that it might be necessary to employ mass transfer rates under a boiling condition with different types or concentrations of the electro-active compounds. Also, this paper did not discuss the possible error of electrochemical measurement generated by the electrical heating method.

Sarac and Wragg [73] later constructed another set-up to investigate the mass transfer in the presence of simultaneous subcooled boiling conditions. A vertical nickel rod with a thermocouple inserted into its center and an electrical connection screwed into it was used as the working electrode. The boiling was obtained by quickly and fully immersing the preheated nickel rod in a static pool of ferri-/ferrocyanide NaOH solution. The experiments were carried out for the combination of the subcooling temperature and electrolyte concentration. Sarac and Wragg found that in the nucleate boiling regime, the variation of the mass transfer coefficient with a temperature difference between the electrode and electrolyte showed similar trends to the variation of heat transfer with a temperature difference. However, Sarac and Wragg only took measurements in a limited time period (within 10s), and the temperature of the rod was changing even within this short period. The experimental data would have been more reliable if the experimental conditions had been stable.

1.5 Background of mass transport correlations

1.5.1 Mechanism of mass transport under forced convection

There have been extensive studies on determining the heat and mass transfer rates in pipe flow. Many correlations have been developed for forced convection, turbulent, liquid-only flow conditions [16, 48, 74]. Many mass transfer correlations are developed using the heat transfer correlation because of the similarity between the heat and mass boundary layers [75]. For a Reynolds number higher than 10000 and a Prandtl number between 0.7 and 160, the Nusselt number can be calculated using the following Dittus-Boelter equation [76]:

$$Nu = 0.023Re^{0.8}Pr^{0.4} \quad (1.14)$$

Where the Nusselt number, Nu , and Prandtl number, Pr can be defined as [77]:

$$Nu = \frac{hL}{\lambda} \quad (1.15)$$

$$Pr = \frac{\mu C_p}{\lambda} \quad (1.16)$$

where h is the heat transfer coefficient and μ is the dynamic viscosity.

The heat transfer coefficient, h , can be calculated using the following equation [77]:

$$h = \frac{Nu \lambda}{L} \quad (1.17)$$

The heat transfer calculations can then be related to mass transfer calculations using the Chilton-Colburn analogy where the Prandlt number is replaced with the Schmidt number to calculate the Sherwood number. However, the following assumptions must be made before the analogy can be applied [77]:

- The variation of the fluid physical properties with concentrations in the mass-transfer system must be equivalent to the variation of the physical properties with temperatures in the heat-transfer system.
- The mass flux of the solute must be small enough that the fluid velocities induced by the mass-transfer itself are negligible compared to the externally imposed velocities.
- The kinetic energy of the flow must be negligible compared with the enthalpy differences within the flow.
- The flow velocity must be lower compared to the speed of sound; otherwise temperature gradients will occur where there are changes in pressure.
- Boundary conditions must be equivalent for both heat and mass transfer systems.
- Heat transfer by nucleate boiling must be excluded.

Once these assumptions are made, the Sherwood number can be calculated using the same form used in Equation 1.7, as the following relationships show [77]:

$$Sh = 0.023Re^{0.8}Sc^{1/3} \quad (1.18)$$

The mass transfer coefficient can then be calculated using Eq. (1.8).

1.5.2 Mechanism of boiling phenomenon

The physical boiling phenomenon is already well developed and the heat transfer behavior for different boiling regions has been well studied [9, 78, 79]. Rohsenow [80] studied the transport of heat under boiling conditions. Figure 1-5 shows the heat flux as a function of temperature for different regimes of boiling. The boiling curve was divided into six regions. Regions 2 and 3 are in the scope of the current investigation because nucleate boiling occurs in these two regions. A mass transfer under boiling is likewise expected to depend on the boiling regime (i.e., the position on the boiling curve below).

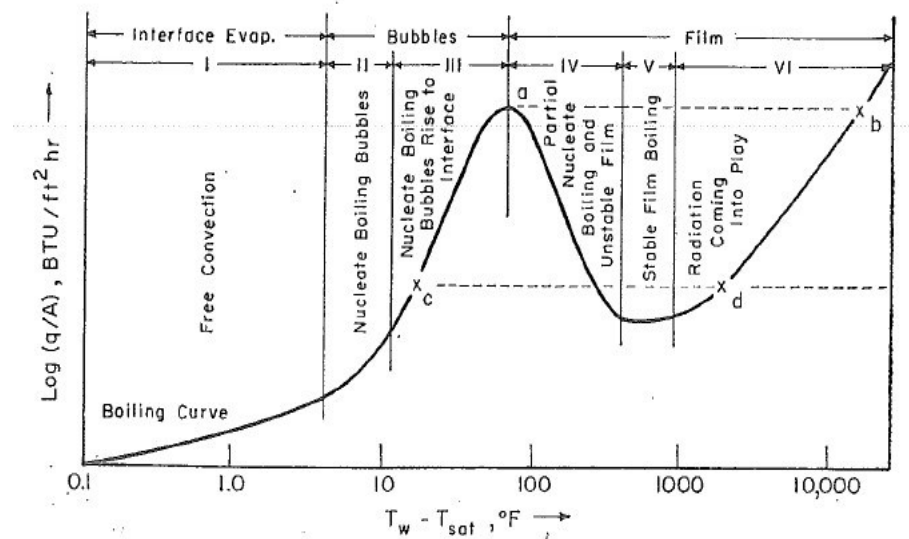


Figure 1-5. Typical Pool Boiling Curve [80]

Hsu and Graham [81] examined three basic modes of boiling: nucleate boiling, transition boiling and film boiling. Nucleate boiling was characterized by the formation of bubbles at nucleation centres where the vapour phase developed with less free energy required than that in the bulk.

Three models of nucleate boiling were discussed, with each model having a dominant heat-transfer mechanism. The mechanisms proposed were bubble agitation, vapour-liquid exchange, and evaporative. A schematic of each mechanism is shown in Figure 1-6. Hsu and Graham hypothesized that heat transfer during nucleate boiling is composed of all the mechanisms with each mechanism dominating in a certain area fraction and/or time fraction.

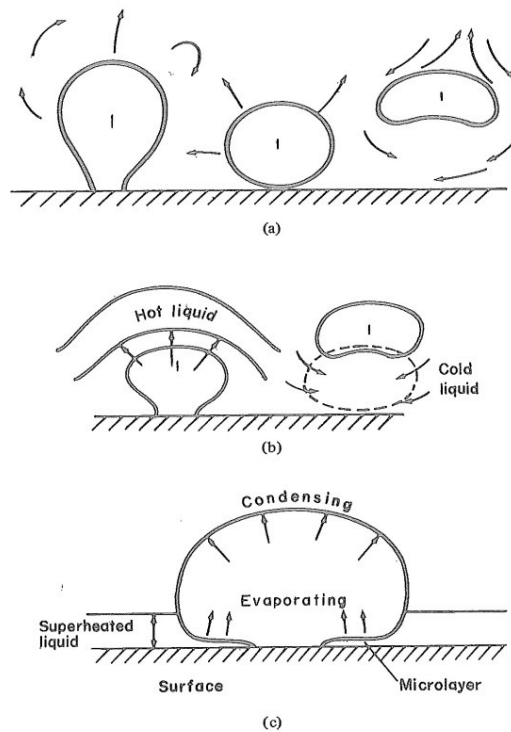


Figure 1-6. Diagram of heat transfer mechanisms in boiling. (a) Bubble agitation model; (b) Vapour-liquid exchange mechanism; (c) Evaporative mechanism [81].

1.5.3 Examining the similarity of a gas evolution electrode and a boiling electrode

The mass transfer behaviour for the gas evolution electrode was investigated [82-84] and it was proven that there were similarities between the gas evolution electrode and the boiling electrode. Voght et al. [85] examined the analogy between the gas evolution during electrolysis and boiling at a solid surface. They noted that the two processes fell into different scientific and technological fields and, therefore, the analogy was not recognized. The analogy was found to be rational and beneficial because more data were available for boiling than for electrolytic gas evolution. Figure 1-7 shows a schematic of the Voght et al. proposed comparison of the two processes. They stated that in an electrolytic process, at least two mass transfer processes are interconnected, namely that of the reaction substrate(s) transport to the electrode surface and the reaction product(s) transport away from the surface. The analogy was limited because of the different physical nature of the two processes. The gas evolution in electrolytic processes was found to begin at volumetric (or molar) gas fluxes approximately six orders of magnitude lower than those at the nucleate boiling. In electrolysis, the bubble break-off diameter strongly depends on surface wettability and fluid surface tension, both of which depend strongly on surface charges and the electrode potential. The upper limit for bubble generation in electrolysis (about 0.05 m/s for hydrogen evolution from 25°C water at atmospheric pressure) was found to be only about 5% of the corresponding value of the critical heat flux. Voght et al. assumed that the process that would be analogous to post-dry-out film boiling does not exist in electrolysis. In boiling, microconvection tended to be the prevailing mode of heat transfer over the region of steam bubble generation. In electrolysis, microconvection was the dominant mode of mass transfer only in the upper practical range of application.

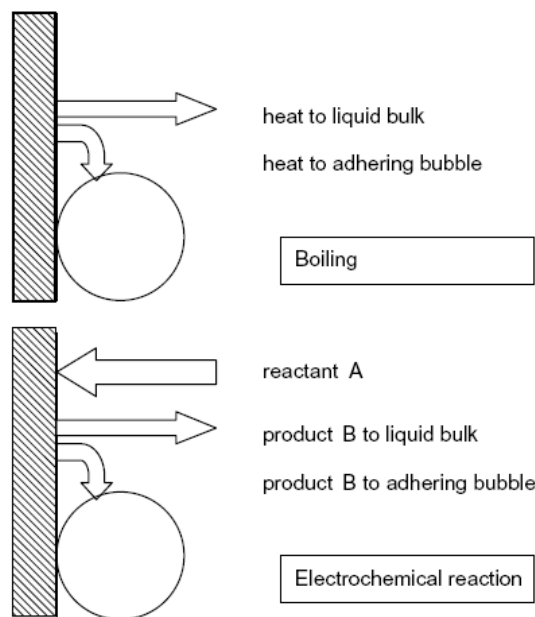


Figure 1-7. Comparison of the processes of bubble generation in nucleate boiling (upper part) and generation of gas in an electrochemical process (lower part) [85].

Kim [86] presented a review of recent experimental, analytical, and numerical work for the single bubble heat transfer. The proposed mechanisms of heat transfer during boiling were enhanced convection, transient conduction, microlayer evaporation, and contact line heat transfer. In this study, boiling was described as a process in which mass, momentum, and energy transfer (single and two-phase) involving a solid wall, liquid, and vapour were tightly coupled. The mechanisms through which energy was transferred from the wall are shown in Figure 1-8. The heat transfer models reviewed were the transient conduction model, micro-layer heat transfer model, and contact line heat transfer model. The experiments reviewed included micro-heater array data, micro heat flux sensor data, liquid crystal data, and infrared camera data. It was concluded that the dominant mechanism by which heat was transferred by isolated bubbles

during boiling was transient conduction and/or microconvection, and that heat transfer through micro-layer evaporation and contact line heat transfer did not account for more than approximately 25% of the overall heat transfer.

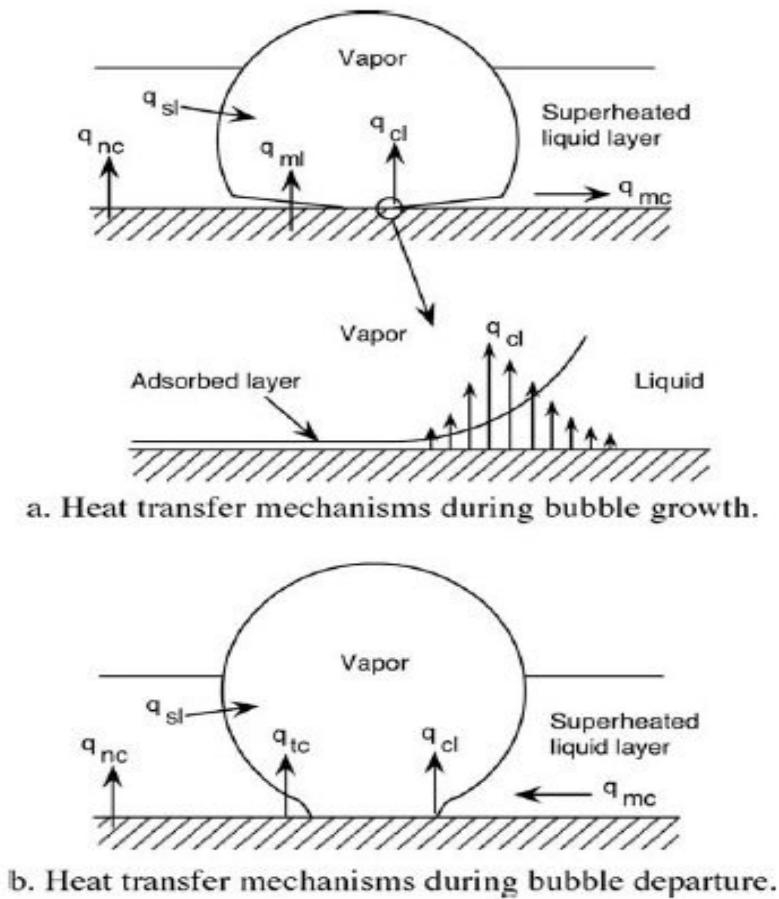


Figure 1-8. Bubble heat transfer mechanisms [86].

1.6 Summary of present research status

This chapter mainly discussed the current status of both experimental and theoretical mass transfer studies under different experimental conditions. Mass transfer behavior was widely studied under various operating conditions for different applications. Results showed that the mass transfer is an important issue for all different processes, such as chemical reactions, fouling, corrosion, and material degradation. However, the experimental study of mass transfer on a boiling surface under a flow boiling condition has not been reported due to experimental difficulties and the lack of an experimental measurement facility.

Analogies such as the Chilton-Colburn analogy exist between mass transfer and heat transfer theories based on the boundary layer similarities. However, the boundary layer breaks down during bubble nucleation and departure. Therefore, the Chilton-Colburn analogy does not work for mass transfer behavior under boiling conditions. Furthermore, researchers have tried to connect boiling with the gas evolution electrode, but the result has not been quite satisfactory. Therefore, there is still a knowledge gap both theoretically and experimentally for the mass transfer on boiling surfaces under flow boiling conditions.

1.7 Objectives and structure of thesis

In order to improve the understanding of the fundamental phenomenon of mass transfer under flow boiling condition, the objectives of this study are to experimentally determine the mass transfer coefficient and to investigate the effect of bubbles under boiling conditions on the mass

transfer of concerned compounds in a two-phase flow under boiling conditions. To fulfill this objective, it is necessary to design and construct a novel experimental device that could allow direct electrochemical measurements on the boiling surface under flow boiling conditions.

Due to the challenges of the project, the mass transfer behavior will be studied in three phases: Phase I, the mass transfer rate, will be measured under bulk boiling conditions using an existing rotating cylinder electrode system; Phase II, the pool boiling condition, will use a homemade pool boiling setup; and Phase III, the two-phase flow boiling condition, will use a novel flow boiling loop device. The structure of this thesis is arranged according to the above order: Introduction (Chapter 1), Phase I (Chapter 2), Phase II (Chapter 3), Phase III (Chapter 4), and Conclusion and future works (Chapter 5).

1.8 References

- [1] Dedov, A.V., A.T. Komov, A.N. Varava and V.V. Yagov, "Hydrodynamics and heat transfer in swirl flow under conditions of one-side heating. Part 2: Boiling heat transfer. Critical heat fluxes," *International Journal of Heat and Mass Transfer*, 53 (2010): pp. 4966-4975.
- [2] Wang, Y. and K. Sefiane, "Effects of heat flux, vapour quality, channel hydraulic diameter on flow boiling heat transfer in variable aspect ratio micro-channels using transparent heating," *International Journal of Heat and Mass Transfer*, 55 (2012): pp. 2235-2243.
- [3] Abraham, J.P., E.M. Sparrow and W.J. Minkowycz, "Internal-flow Nusselt numbers for the low-Reynolds-number end of the laminar-to-turbulent transition regime," *International Journal of Heat and Mass Transfer*, 54 (2011): pp. 584-588.
- [4] Turner, C.W. and S.J. Klimas, "Deposition of magnetite particles from flowing suspensions under flow-boiling and single-phase forced-convective heat transfer," *The Canadian Journal of Chemical Engineering*, 78 (2000): pp. 1065-1075.

- [5] Diercks, D., W. Shack and J. Muscara, "Overview of steam generator tube degradation and integrity issues," *Nuclear engineering and design*, 194 (1999): pp. 19-30.
- [6] Mahato, B.K., S.K. Voora and L.W. Shemilt, "Steel pipe corrosion under flow conditions-I. An isothermal correlation for a mass transfer model," *Corrosion Science*, 8 (1968): pp. 173-193.
- [7] Lu, Y., G. Goszczynski and S. Ramamurthy, "Degradation of alloy 800 under steam generator secondary side crevice conditions," *17th International Conference on Nuclear Engineering*, (2009): pp. 1-9.
- [8] Vogt, H., "Heat transfer in boiling and mass transfer in gas evolution at electrodes - The analogy and its limits," *International Journal of Heat and Mass Transfer*, 59 (2013): pp. 191-197.
- [9] Qi, S.L., P. Zhang, R.Z. Wang and L.X. Xu, "Flow boiling of liquid nitrogen in micro-tubes: Part I – The onset of nucleate boiling, two-phase flow instability and two-phase flow pressure drop," *International Journal of Heat and Mass Transfer*, 50 (2007): pp. 4999-5016.
- [10] Fenech, E.J. and C.W. Tobias, "Mass transfer by free convection at horizontal electrodes," *Electrochimica Acta*, 2 (1960): pp. 311-325.
- [11] Wragg, A.A., "Free convection mass transfer at horizontal electrodes," *Electrochimica Acta*, 13 (1968): pp. 2159-2165.
- [12] Smith, A.F.J. and A.A. Wragg, "An electrochemical study of mass transfer in free convection at vertical arrays of horizontal cylinders," *Journal of Applied Electrochemistry*, 4 (1974): pp. 219-228.
- [13] Selman, J.R. and C.W. Tobias, "Mass transfer measurements by the limiting current technique," *Advances in Chemical Engineering*, 10 (1978): pp. 211-318.
- [14] Teng, J.T., R. Greif, I. Cornet and R.N. Smith, "Study of heat and mass transfer in pipe flows with non-newtonian fluids," *International Journal of Heat and Mass Transfer*, 22 (1979): pp. 493-498.
- [15] Mahinpey, N., M. Ojha and O. Trass, "Transient mass and heat transfer in a smooth pipe," *International Journal of Heat and Mass Transfer*, 44 (2001): pp. 3919-3930.
- [16] Lolja, S.A., "Momentum and mass transfer on sandpaper-roughened surfaces in pipe flow," *International Journal of Heat and Mass Transfer*, 48 (2005): pp. 2209-2218.
- [17] Delaunay, G., A. Storck, A. Laurent and J.-C. Charpentier, "Electrochemical study of liquid-solid mass transfer in packed beds with upward cocurrent gas-liquid flow,"

- Industrial & Engineering Chemistry Process Design and Development, 19 (1980): pp. 514-521.
- [18] Jianping, W., H. Lin, Z. Yong, L. Chao and C. Yunlin, "Solid-liquid mass transfer in a gas-liquid-solid three-phase reversed flow jet loop reactor," Chemical Engineering Journal, 78 (2000): pp. 231-235.
- [19] Latifi, M.A., A. Laurent and A. Storck, "Liquid-solid mass transfer in a packed bed with downward cocurrent gas-liquid flow: An organic liquid phase with high Schmidt number," The Chemical Engineering Journal, 38 (1988): pp. 47-56.
- [20] Reiss, L.P. and T.J. Hanratty, "Measurement of instantaneous rates of mass transfer to a small sink on a wall," AIChE Journal, 8 (1962): pp. 245-247.
- [21] Miller, C.T., M.M. Poirier, McNeil and A.S. Mayer, "Dissolution of trapped nonaqueous phase liquids: Mass transfer characteristics," Water Resources Research, 26 (1990): pp. 2783-2796.
- [22] Tan, C.-S., S.-K. Liang and D.-C. Liou, "Fluid-solid mass transfer in a supercritical fluid extractor," The Chemical Engineering Journal, 38 (1988): pp. 17-22.
- [23] Speccia, V., G. Baldi and A. Gianetto, "Solid-liquid mass transfer in concurrent two-phase flow through packed beds," Industrial & Engineering Chemistry Process Design and Development, 17 (1978): pp. 362-367.
- [24] Ross, T.K. and A.A. Wragg, "Electrochemical mass transfer studies in annuli," Electrochimica Acta, 10 (1965): pp. 1093-1106.
- [25] Lin, C.S., E.B. Denton, H.S. Gaskill and G.L. Putnam, "Diffusion-Controlled Electrode Reactions," Industrial & Engineering Chemistry, 43 (1951): pp. 2136-2143.
- [26] Highfill, W. and M. Al-Dahhan, "Liquid-Solid Mass Transfer Coefficient in High Pressure Trickle Bed Reactors," Chemical Engineering Research and Design, 79 (2001): pp. 631-640.
- [27] Burns, J.R. and R.J.J. Jachuck, "Determination of liquid-solid mass transfer coefficients for a spinning disc reactor using a limiting current technique," International Journal of Heat and Mass Transfer, 48 (2005): pp. 2540-2547.
- [28] Tobias, C.W., M. Eisenberg and C.R. Wilke, "Fiftieth Anniversary: Diffusion and Convection in Electrolysis---A Theoretical Review," Journal of The Electrochemical Society, 99 (1952): pp. 359C-365C.
- [29] Dang-Vu, T., H.D. Doan and A. Lohi, "Local Mass Transfer in a Packed Bed: Experiments and Model," Industrial & Engineering Chemistry Research, 45 (2005): pp. 1097-1104.

- [30] Al-Dahhan, M., W. HighFill and B.T. Ong, "Drawbacks of the Dissolution Method for Measurement of the Liquid-Solid Mass-Transfer Coefficients in Two-Phase Flow Packed-Bed Reactors Operated at Low and High Pressures," *Industrial & Engineering Chemistry Research*, 39 (2000): pp. 3102-3107.
- [31] Gregory, D.P. and A.C. Riddiford, "Dissolution of copper in sulfuric acid solutions," *Journal of The Electrochemical Society*, 107 (1960): pp. 950–956.
- [32] Berger, F.P. and K.F.F.L. Hau, "Mass transfer in turbulent pipe flow measured by the electrochemical method," *International Journal of Heat and Mass Transfer*, 20 (1977): pp. 1185-1194.
- [33] Maceiras, R., X.R. Novoa, E. A lvarez and M.A. Cancela, "Local mass transfer measurements in a bubble column using an electrochemical technique," *Chemical Engineering and Processing: Process Intensification*, 46 (2007): pp. 1006-1011.
- [34] Jolls, K.R. and T.J. Hanratty, "Use of electrochemical techniques to study mass transfer rates and local skin friction to a sphere in a dumped bed," *AIChE Journal*, 15 (1969): pp. 199-205.
- [35] Madden, A.J. and D.G. Nelson, "A novel technique for determining mass transfer coefficients in agitated solid-liquid systems," *AIChE Journal*, 10 (1964): pp. 415-430.
- [36] Cornet, I., R. Greif, J.T. Teng and F. Roehler, "Mass transfer to rotating rods and plates," *International Journal of Heat and Mass Transfer*, 23 (1980): pp. 805-811.
- [37] Benzina, M., D. Mowla and G. Lacoste, "Mass transfer studies in porous electrodes: Application of the limiting current technique," *The Chemical Engineering Journal*, 27 (1983): pp. 1-7.
- [38] Pao C, C., "Local liquid-solid mass transfer measurement in a trickle film flow model using an electrochemical technique," *International Journal of Heat and Mass Transfer*, 30 (1987): pp. 2305-2317.
- [39] Daguinet, M., "Etude du transport de matiere en solution, a l'aide des electrodes a disque et a anneau tournants," *International Journal of Heat and Mass Transfer*, 11 (1968): pp. 1581-1596.
- [40] Rousar, I., J. Hostomsky, V. Cezner and B. Stverak, "Limiting Local Current Densities for Electrodes Located on the Walls of a Rectangular Channel with Laminar Flow; Asymptotic Solution and Experimental Verification," *Journal of The Electrochemical Society*, 118 (1971): pp. 881-884.
- [41] Janssen, L.J.J. and J.G. Hoogland, "The effect of electrolytically evolved gas bubbles on the thickness of the diffusion layer," *Electrochimica Acta*, 15 (1970): pp. 1013-1023.

- [42] Nickchi, T. and A. Alfantazi, "Electrochemical corrosion behaviour of Incoloy 800 in sulphate solutions containing hydrogen peroxide," *Corrosion Science*, 52 (2010): pp. 4035-4045.
- [43] Stewart, K.L. and A.A. Gewirth, "Mechanism of electrochemical reduction of hydrogen peroxide on copper in acidic sulfate solutions," *Langmuir*, 23 (2007): pp. 9911-9918.
- [44] Hall, S.B., E.A. Khudaish and A.L. Hart, "Electrochemical oxidation of hydrogen peroxide at platinum electrodes. Part V: inhibition by chloride," *Electrochimica Acta*, 45 (2000): pp. 3573-3579.
- [45] Hall, S.B., E.A. Khudaish and A.L. Hart, "Electrochemical oxidation of hydrogen peroxide at platinum electrodes. Part IV: phosphate buffer dependence," *Electrochimica Acta*, 44 (1999): pp. 4573-4582.
- [46] Nickchi, T. and A. Alfantazi, "Kinetics of passive film growth on Alloy 800 in the presence of hydrogen peroxide," *Electrochimica Acta*, 58 (2011): pp. 743-749.
- [47] Nickchi, T. and A. Alfantazi, "Corrosion characteristics of alloy 800 in aqueous solutions up to 200 C," *Journal of The Electrochemical Society*, 160 (2013): pp. C64-C76.
- [48] Ratkovich, N., P.R. Berube and I. Nopens, "Assessment of mass transfer coefficients in coalescing slug flow in vertical pipes and applications to tubular airlift membrane bioreactors," *Chemical Engineering Science*, 66 (2011): pp. 1254-1268.
- [49] Thomas, F.I.M. and M.J. Atkinson, "Ammonium uptake by coral reefs: Effects of water velocity and surface roughness on mass transfer," *Limnology and Oceanography*, 42 (1997): pp. 81-88.
- [50] Dawson, D.A. and O. Trass, "Mass transfer at rough surfaces," *International Journal of Heat and Mass Transfer*, 15 (1972): pp. 1317-1336.
- [51] Schutz, G., "Natural convection mass-transfer measurements on spheres and horizontal cylinders by an electrochemical method," *International Journal of Heat and Mass Transfer*, 6 (1963): pp. 873-879.
- [52] Eisenberg, M., C.W. Tobias and C.R. Wilke, "Ionic mass transfer and concentration polarization at rotating electrodes," *Journal of The Electrochemical Society*, 101 (1954): pp. 306-320.
- [53] Ma, H., D. Du, J. Sun, Y. Zhang and N. Deng, "Convective mass transfer from a horizontal rotating cylinder in a slot air jet flow," *International Journal of Heat and Mass Transfer*, 54 (2011): pp. 186-193.

- [54] Parys, H.V., E. Tourwe, T. Breugelmans, M. Depauw, J. Deconinck and A. Hubin, "Modeling of mass and charge transfer in an inverted rotating disk electrode (IRDE) reactor," *Journal of Electroanalytical Chemistry*, 622 (2008): pp. 44-50.
- [55] Lee, J. and J.B. Talbot, "A model of electrocodeposition on a rotating cylinder electrode," *Journal of The Electrochemical Society*, 154 (2007): pp. D70-D77.
- [56] Brunner, E., *Z. physik. Chem.*, 47 (1904).
- [57] Cobo, O.A., S.L. Marchiano and A.J. Arvia, "Ionic mass transfer at rotating electrodes formed by solids of revolution. Rotating one-base spherical segment electrodes," *Electrochimica Acta*, 17 (1972): pp. 503-509.
- [58] Filinovsky, V.J., I.V. Kadija, B. Nikolic and M.B. Nakic, "Mass transfer on the rotating double ring electrodes: Reactions without gas evolution," *Journal of Electroanalytical Chemistry and Interfacial Electrochemistry*, 54 (1974): pp. 39-46.
- [59] Despic, A.R., M.V. Mitrovic, B.Z. Nikolic and S.D. Cvijovic, "Mass transfer at a rotating disc with rectangular patch electrodes," *Journal of Electroanalytical Chemistry and Interfacial Electrochemistry*, 60 (1975): pp. 141-149.
- [60] Janssen, L.J.J. and E. Barendrecht, "Mass transfer at a rotating ring-cone electrode and its use to determine supersaturation of gas evolved," *Electrochimica Acta*, 29 (1984): pp. 1207-1212.
- [61] Ives, M.B., Y.C. Lu and J.L. Luo, "Cathodic reactions involved in metallic corrosion in chlorinated saline environments," *Corrosion Science*, 32 (1991): pp. 91-102.
- [62] Bartelmus, G., "Local solid-liquid mass transfer coefficients in a three-phase fixed bed reactor," *Chemical Engineering and Processing: Process Intensification*, 26 (1989): pp. 111-120.
- [63] Sara, H., A.A. Wragg and M.A. Patrick, "Combined heat and mass transfer by natural convection at horizontal cylinder electrodes," *International Communications in Heat and Mass Transfer*, 18 (1991): pp. 853-863.
- [64] Chang, L.S., T.E. Carleson and J.C. Berg, "Heat and mass transfer to a translating drop in an electric field," *International Journal of Heat and Mass Transfer*, 25 (1982): pp. 1023-1030.
- [65] Postelnicu, A., "Influence of a magnetic field on heat and mass transfer by natural convection from vertical surfaces in porous media considering Soret and Dufour effects," *International Journal of Heat and Mass Transfer*, 47 (2004): pp. 1467-1472.

- [66] Takhar, H.S., A.J. Chamkha and G. Nath, "Flow and mass transfer on a stretching sheet with a magnetic field and chemically reactive species," *International Journal of Engineering Science*, 38 (2000): pp. 1303-1314.
- [67] Grundler, P., T. Zerihun, A. Kirbs and H. Grabow, "Simultaneous joule heating and potential cycling of cylindrical microelectrodes," *Analytica Chimica Acta*, 305 (1995): pp. 232-240.
- [68] Beckmann, A., A. Schneider and P. Grundler, "Electrically heated cylindrical microelectrodes. Electrochemical measurements in THF," *Electrochemistry Communications*, 1 (1999): pp. 46-49.
- [69] Aoki, K., K. Honda, K. Tokuda and H. Matsuda, "Voltammetry at microcylinder electrodes: Part I. Linear sweep voltammetry," *Journal of Electroanalytical Chemistry and Interfacial Electrochemistry*, 182 (1985): pp. 267-279.
- [70] Beckmann, A., B.A. Coles, G. Richard, P. Grandler, F. Marken and A. Neudeck, "Modeling hot wire electrochemistry. Coupled heat and mass transport at a directly and continuously heated wire," *The Journal of Physical Chemistry B*, 104 (2000): pp. 764-769.
- [71] Boden, P., "Corrosion of Cu and Cu-base alloys under conditions of boiling heat transfer-I. Corrosion of Cu," *Corrosion Science*, 11 (1971): pp. 353-362.
- [72] Wragg, A.A. and A.K. Nasiruddin, "Ionic mass transfer by free convection with simultaneous heat transfer," *Electrochimica Acta*, 18 (1973): pp. 619-627.
- [73] Sarac, H., A. Wragg and M. Patrick, "An electrochemical mass transfer investigation in the presence of simultaneous subcooled pool boiling," *International Communications in Heat and Mass Transfer*, 30 (2003): pp. 909-920.
- [74] Rivero, E.P., P. Granados, F.F. Rivera, M. Cruz and I. Gonzalez, "Mass transfer modeling and simulation at a rotating cylinder electrode (RCE) reactor under turbulent flow for copper recovery," *Chemical Engineering Science*, 65 (2010): pp. 3042-3049.
- [75] Chin, D.-T. and K.-L. Hsueh, "An analysis using the Chilton-Colburn analogy for mass transfer to a flat surface from an unsubmerged impinging jet," *Electrochimica Acta*, 31 (1986): pp. 561-564.
- [76] Baehr, H. and K. Stephan, "Heat and Mass Transfer, Springer, Berlin, 1998."
- [77] Coney, M., *Erosion-corrosion: the Calculation of Mass-transfer Coefficients* 1981: CEGB.

- [78] Warriar, G.R. and V.K. Dhir, "Heat Transfer and Wall Heat Flux Partitioning During Subcooled Flow Nucleate Boiling---A Review," *Journal of Heat Transfer*, 128 (2006): pp. 1243-1256.
- [79] Basu, N., G.R. Warriar and V.K. Dhir, "Onset of nucleate boiling and active nucleation site density during subcooled flow boiling," *Journal of Heat Transfer*, 124 (2002): pp. 717-728.
- [80] Rohsenow, W.M. and H.Y. Choi, *Heat, mass, and momentum transfer* 1961: Prentice-Hall New Jersey.
- [81] Hsu, Y.Y. and R.W. Graham, "Transport processes in boiling and two-phase systems, including near-critical fluids," Washington, DC, Hemisphere Publishing Corp.; New York, McGraw-Hill Book Co., 1976. 559 p., 1 (1976).
- [82] Vogt, H., "On the gas-evolution efficiency of electrodes I-Theoretical," *Electrochimica Acta*, 56 (2011): pp. 1409-1416.
- [83] Vogt, H., "On the gas-evolution efficiency of electrodes. II-Numerical analysis," *Electrochimica Acta*, 56 (2011): pp. 2404-2410.
- [84] Vogt, H., "Mechanisms of mass transfer of dissolved gas from a gas-evolving electrode and their effect on mass transfer coefficient and concentration overpotential," *Journal of Applied Electrochemistry*, 19 (1989): pp. 713-719.
- [85] Vogt, H., O. Aras and R.J. Balzer, "The limits of the analogy between boiling and gas evolution at electrodes," *International Journal of Heat and Mass Transfer*, 47 (2004): pp. 787-795.
- [86] Kim, J., "Review of nucleate pool boiling bubble heat transfer mechanisms," *International Journal of Multiphase Flow*, 35 (2009): pp. 1067-1076.

Chapter 2 Phase I -- bulk boiling condition

2.1 Introduction

One of the most successful methods for measuring the mass transfer is the electrochemical method (the limiting current technique) which makes use of limiting current plateau at a voltage-current chart when the electrode reactions proceed at the highest possible rate [1-3]. This technique has been employed more frequently in the last several decades due to its fast data acquisition as well as the capability of quantifying both local and average mass transfer coefficients [1, 4]. The electrochemical method has been successfully used to investigate mass transfer behavior under conditions with no forced flow [5-7], single-phase flow [8-10] and multi-phase flow [11-13]. However, there are very limited experimental studies to examine mass transfer behavior at boiling condition using electrochemical method. Wragg and Nasiruddin [14] investigated the mass transfer behavior of cathodic deposition of copper from cupric sulphate solutions using electrochemical method under pool boiling condition. The electrode was heated from room temperature to 125 °C at which the mass transfer behavior at the nucleate boiling regime was examined. However, they found that under the boiling condition, the limiting current value could not be quantified due to the intense local turbulence at the electrode-solution interface caused by bubble nucleation, growth, movement and collapse. One of the reason could be the electric heating method they used effect the electrochemical measurement, this problem have been solved in the present study by the oil heating method.

Among many possible experimental techniques for generating flow condition, the rotating electrode is notable because of its high reproducibility and imitation of the hydrodynamic conditions as well as mass transfer analogy for the interpretation and correlating to the experimental data [15-17]. Eisenberg et al. [15] investigated the rates of ionic mass transfer at nickel rotating electrode using the ferri- and ferrocyanide redox couple in alkaline solutions. All experiments were conducted at 25 °C. They proved that ferri- and ferrocyanide couple could be used to study mass transfer and such electrode reactions could be considered to remain predominantly mass transfer control for the Reynolds number of $Re \leq 11,000$. Abdel-Aziz et al. [18] studied the rates of mass transfer using an electrochemical method of the square cylinder rotating electrode. They used 0.01 M $K_3Fe(CN)_6$ + 0.1 M $K_4Fe(CN)_6$ redox couple in 1 M, 2 M, and 3 M NaOH solutions. The electrolyte temperature for all their experiments was kept constant at 25 °C. The rate of mass transfer at the square-rotating electrode was found to be higher than that at the traditional circular rotating electrode by an amount ranging from 47% to 200%.

Limited information is available in the literature regarding the experimental work on mass transfer controlled materials degradation under the conditions of pool boiling and flow boiling. The lack of experimental data may be attributed to the fact that performing the preferred measurements under flow boiling is difficult. In addition, the interpretation of the limited data may be complex and challenging compared to the single-phase data.

The objectives of this chapter are to determine the mass transfer rates of dissolved oxygen using rotating cylinder electrode and to investigate the effects of rotating speed and dissolved oxygen concentration on the mass transfer behavior for the approaching to boiling and bulk boiling

conditions. Additionally, the mass transfer rates will also be measured for the reduction of ferricyanide ion to ferrocyanide under above conditions to confirm the mass transfer rates of dissolved oxygen.

2.2 Experimental setup

The schematic of the experimental set-up is shown in Figure 2-1. A Modulated Speed Rotator (Pine Instrument Co.) is used to vary the rotating speed (from 100 rpm to 3300 rpm). A cylinder (external diameter 12 mm, inside diameter 6 mm, height 8 mm) made of 304 stainless steel (C < 0.08%, Cr 17.5-20%, Ni 8-11%, Mn < 2%, Si < 1%, P < 0.045%, S < 0.03%) is used as the rotating specimen. A platinum coil (the circle diameter is 60 mm) around the specimen is used as the counter electrode. An Ag/AgCl reference electrode (Fisher Scientific) with operating temperature range from -5 °C to +110 °C is utilized to provide stable reference potential. The reference electrode potential was converted to Standard Hydrogen Potential (SHE) by the Eq. C.1 and C.2. The temperature of the electrolyte is controlled using external oil circulating bath (Cole-Parmer PolyStat Co.), in the temperature range of 20 °C to boiling point (99.8 °C). A condenser is used to condensing the evaporated water back to the electrolyte. This setup allows us to simulate the flow condition and to examine enhanced mass transfer under the flow and bulk boiling conditions.

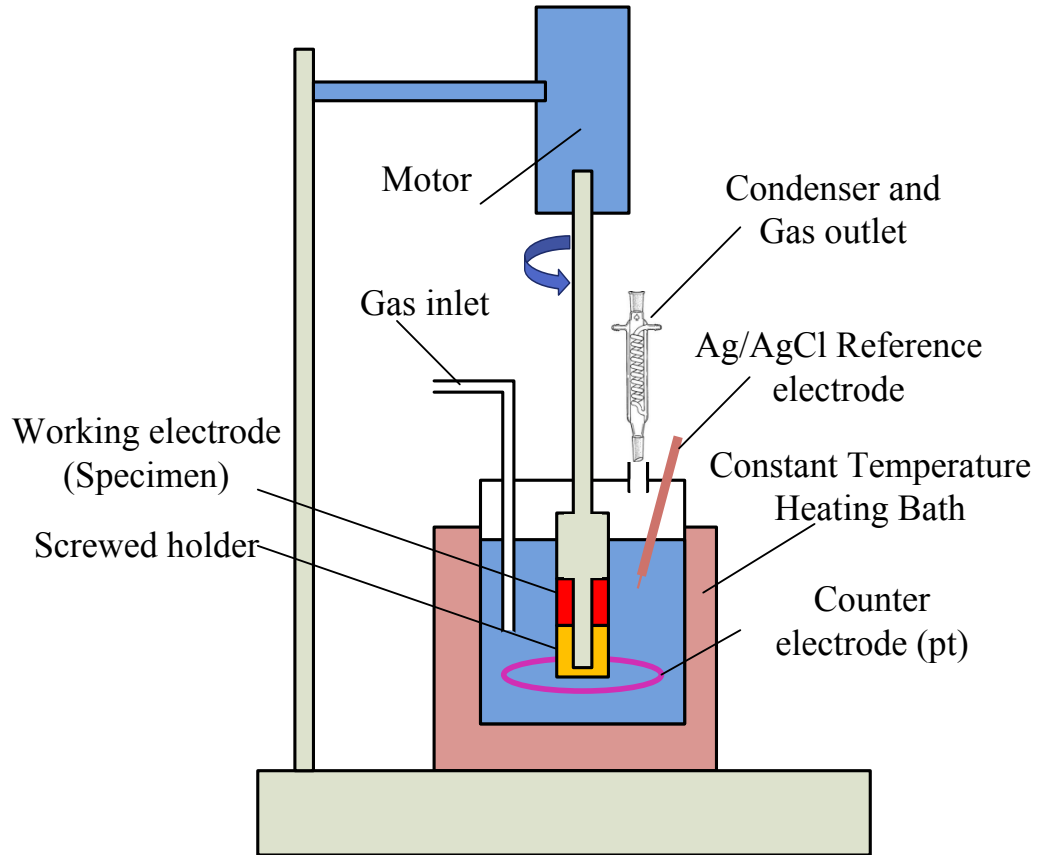


Figure 2-1. The experimental set-up.

2.3 Experimental procedure

Before each test, the specimens were polished using grit 600#, 800# and 1200# sand papers and rinsed with distilled water followed by ethanol, then air dried in a fume hood. The specimens were treated by cathodic polarization in the test solution for 20 min at -0.80 mV vs. standard hydrogen electrode (SHE) before each polarization measurement at various temperatures. The test solution, which behaves as a supporting electrolyte was prepared using distilled water and analytical grade NaOH. The solution pH is 12.5 at room temperature. The electrolyte solution

was continuously purged with ultra-high purity gas mixture containing 1%, 5%, 10% and 20% by volume oxygen to maintain a constant dissolved oxygen concentration in the test solution. Since it is difficult to measure the dissolved oxygen concentration under elevated temperatures. The dissolved oxygen concentration in the electrolyte was determined using Henry's law [19, 20]. It was essential that the partial pressure of water was included in calculations of the dissolved oxygen concentration in the electrolyte solution. The physical properties of the supporting electrolyte as a function of temperatures are given in Table 2-1. [21, 22].

Table 2-1. Viscosity, density and dissolved oxygen diffusivity in 0.1 M NaOH aqueous for solution temperatures range between 20 – 80 °C [21, 22].

Temperature (°C)	Viscosity (m ² /s)	Density (kg/L)	Diffusivity (m ² /s)
20	9.9712×10 ⁻⁷	1.0029	1.7601×10 ⁻⁹
40	6.7198×10 ⁻⁷	0.9971	2.7923×10 ⁻⁹
60	4.7570×10 ⁻⁷	0.9880	4.0010×10 ⁻⁹
80	3.6873×10 ⁻⁷	0.9763	5.3079×10 ⁻⁹

For the measurements of the reduction of ferricyanide ion to ferrocyanide, the concentrations of the potassium ferro- and ferricyanide electrolyte were both 10 mM. The supporting electrolyte was the same as that of the dissolved oxygen reaction. The electrolyte solution was continuously purged with ultra high purity Argon for 1 h to eliminate dissolved oxygen in the test solution. For the electrolyte temperature range of 20 - 100 °C, the diffusivities of ferricyanide were found to be in the range of 6.45×10⁻¹⁰ to 2.83×10⁻⁹ m²/s [23].

A SI 1287 Electrochemical Interface (Solartron Analytical Co.) was used as a potentiostat to conduct the electrochemical measurements. The potential scanning rate was selected to be 2 mV/s for the cathodic polarization measurements.

The mass transfer coefficient of the reactant species, k , and the *Sherwood* number, Sh , were calculated using the Eq. (1.6) and Eq. (1.8):

The uncertainty in the experimentally determined mass transfer coefficient was calculated using the method described by Coleman and Steel [24] and Holman [25]. The uncertainty in the experimentally determined mass transfer coefficient based on experimental errors in the measured limiting current density, ω_{i_L} , and bulk ion concentration, ω_{C_b} , was calculated by

$$\omega_k = \pm \left[\left(\frac{\partial k}{\partial i_L} \omega_{i_L} \right)^2 + \left(\frac{\partial k}{\partial C_b} \omega_{C_b} \right)^2 \right]^{0.5} \quad (2.1)$$

where ω_{i_L} is the total error in the measured limiting current density. The value of ω_{i_L} was calculated from the sum of the systematic (accuracy) and random (precision) errors of the data. The accuracy error comes from the maximum error in the measuring device. The limiting current measurements have error of $\pm 0.3\%$. The precision error was obtained directly from the standard deviation, σ , of the measured values. To determine the precision error, Coleman and Steel [24] stated that when the number of data points for one time series is equal to or greater than 10, two times the standard deviation gave a good approximation for the $\pm 95\%$ confidence interval. Therefore, the total error in the measured limiting current was calculated by

$$\omega_{i_L} = \pm(0.003i_L + 2\sigma_{i_L}) \quad (2.2)$$

Similarly, the total error in the bulk ion concentration, ω_{C_b} , was assumed to be only due to error in the preparation of electrolyte solution, which was assumed to be 4 %. Therefore, the total error in the bulk ion concentration was obtained by

$$\omega_{C_b} = \pm(0.04C_b) \quad (2.3)$$

2.4 Results and discussion

2.4.1 Mass transfer behavior of dissolved oxygen under the below boiling condition

Figures 2-2 (a) and (b) show the typical polarization curves and the experimentally obtained mass transfer coefficients for 0.1 M NaOH electrolyte containing 8.83 ppm of dissolved oxygen at a constant temperature of 20 °C. The calculated dissolved oxygen value is confirmed by the measurement in room temperature. The rotational speed was varied from 100 rpm to 3300 rpm. The mass transfer coefficient was calculated using the measured value of i_L obtained from the plateau part of Figure 2-2 (a). In this system, the first reaction involved is the reduction reaction of dissolved oxygen. It can be observed from Figure 2-2 (a) that there is a clear current plateau for all rotating speeds between potentials of -0.85 and -1.10 V (SHE) where the reaction rate is controlled by the mass transport of dissolved oxygen from bulk solution to the solution/electrode interface. The other reduction reaction taking place is the hydrogen evolution which is dominant at potentials below -1.20 V (SHE):



The hydrogen reduction reaction shown above is not a mass transfer controlled reaction, since there are always sufficient water molecules available for the reaction [26]. It is clear from Figures 2-2 (a) and (b) that the limiting current density value and the mass transfer coefficient increase with the increasing rotating speed. This indicates that the mass transfer controlled reaction rate increases with rotating speed. According to Nernst-Planck flux equation [27], the mass flux of reactive species can be expressed as:

$$N = CV - D(\nabla C) - \left(\frac{nDF}{RT}\right)C(\nabla\varphi) \quad (2.5)$$

Combining the definition of mass transfer coefficient Eq. (1.5) with Eqs. (1.6) and (2.5), the value of the limiting current density can be expressed as:

$$i_L = nFCV - nFD(\nabla C) - \left(\frac{n^2F^2D}{RT}\right)C(\nabla\varphi) \quad (2.6)$$

As shown in Eq. (2.6), the limiting current density value is a combination of three factors: The first is the convective contribution driven by motion of the electrolyte; the second factor is the diffusion caused by concentration gradient and the third is the electromigration due to the electrical field [27]. When the rotating speed increases, the diffusivity value does not change at

the same temperature. Also, the third factor is eliminated by the supporting electrolyte. Therefore, the first factor which is the convection factor of total mass transfer increases; thus the mass transfer of dissolved oxygen increases. These results shown in Figures 2-2 (a) and (b) are in agreement with those obtained by Gareth et al. [28].

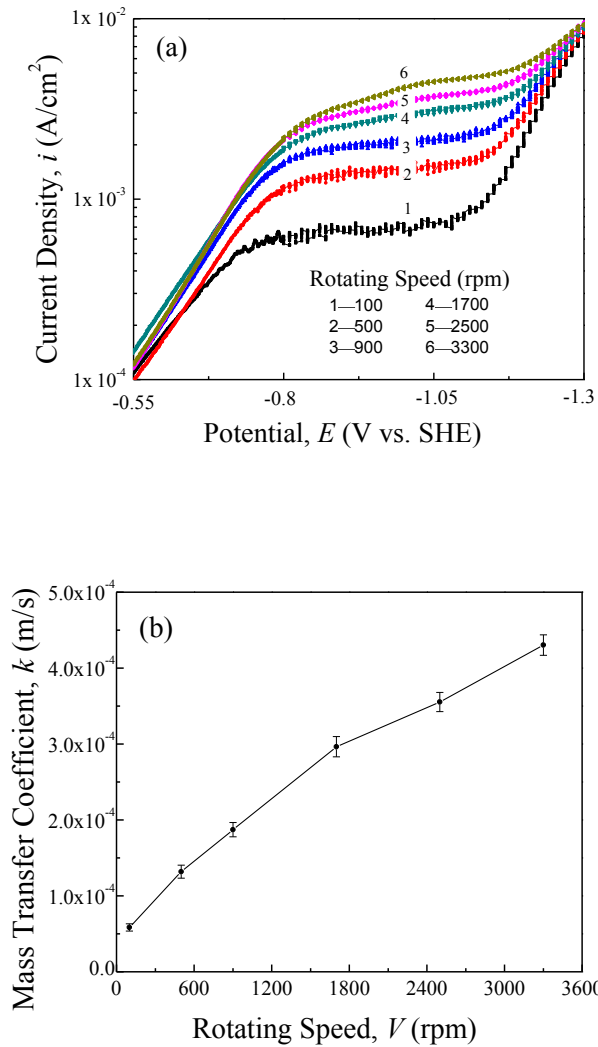
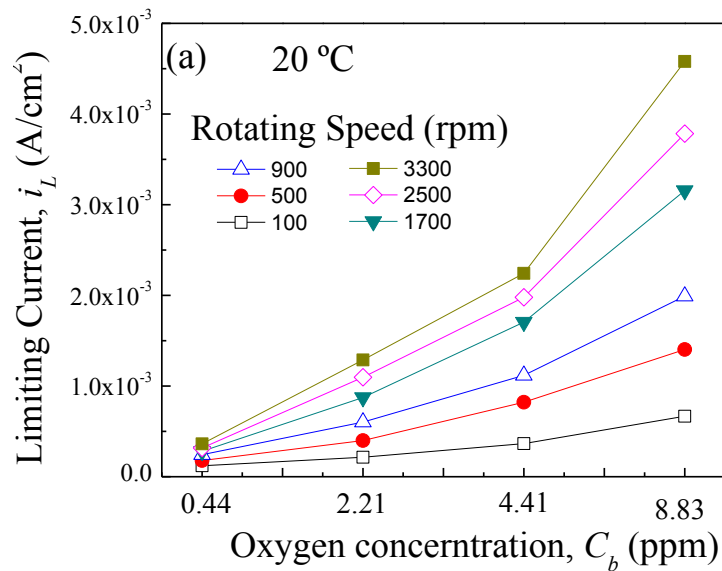


Figure 2-2. The typical cathodic polarization curves (a) and mass transfer coefficient for various rotating speeds (b) at 20 °C and dissolved oxygen concentration 8.83 ppm.

The limiting current densities were also measured for various dissolved oxygen concentrations and electrolyte temperatures. The experiments were conducted for electrolyte temperatures of 20°C and 60°C while the rotating speeds were varied between 100 to 3300 rpm. Figures. 2-3 (a) and (b) show the measured limiting current density as a function of dissolved oxygen concentration for the electrolyte temperatures of 20°C and 60°C, respectively. It can be seen that the limiting current density values decrease with the decreasing dissolved oxygen concentrations at both electrolyte temperatures and all rotational speeds. This was expected because decreasing dissolved oxygen concentration reduced the reaction rate of oxygen reduction.



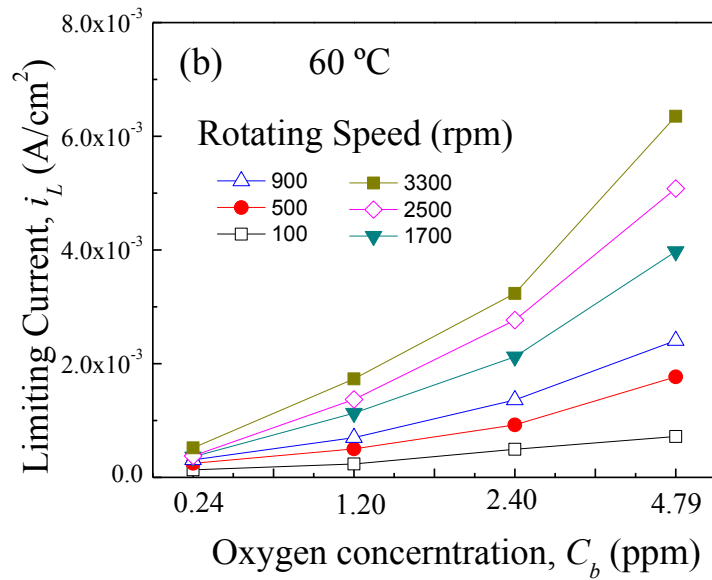


Figure 2-3. Limiting current density vs. dissolved oxygen concentrations at 20 °C (a) and 60 °C (b) at the different rotating speeds, respectively.

Figures 2-4 (a) and (b) show the measured mass transfer coefficients as a function of dissolved oxygen concentrations for electrolyte temperatures of 20 °C and 60 °C, respectively. It can be observed from Figure 2-4 (a) that the mass transfer coefficient remains relatively constant until the dissolved oxygen concentration reaches to 2.21 ppm level. However, the mass transfer coefficient increases when dissolved oxygen concentration decreased below 2.21 ppm level. The reason could be that the diffusivity of dissolved oxygen is independent of its concentration before the concentration reached a critical level where the concentration could start having significant effect on diffusivity after the critical level [29]. This critical level is dependent on the solution temperature. Figure 2-4 (b) confirms the above argument. When the electrolyte solution temperature increased to 60 °C, the mass transfer coefficient still increased at the critical concentration of dissolved oxygen lower than 1 ppm. The mass transfer coefficient increases with the decreasing of dissolved oxygen concentration due to the changes in diffusivity.

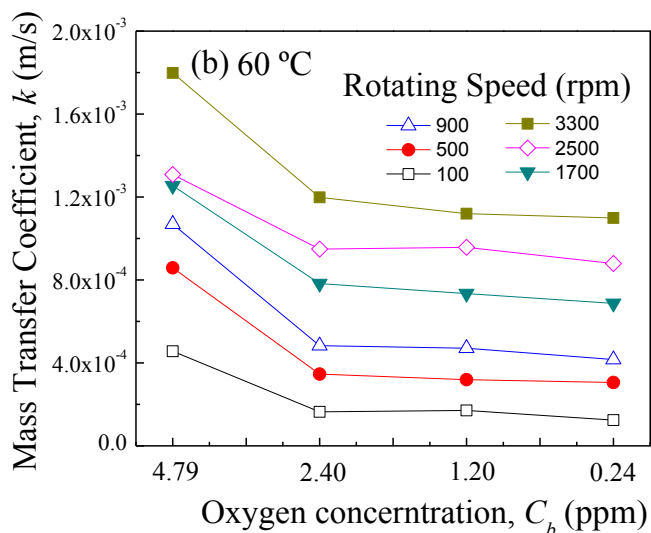
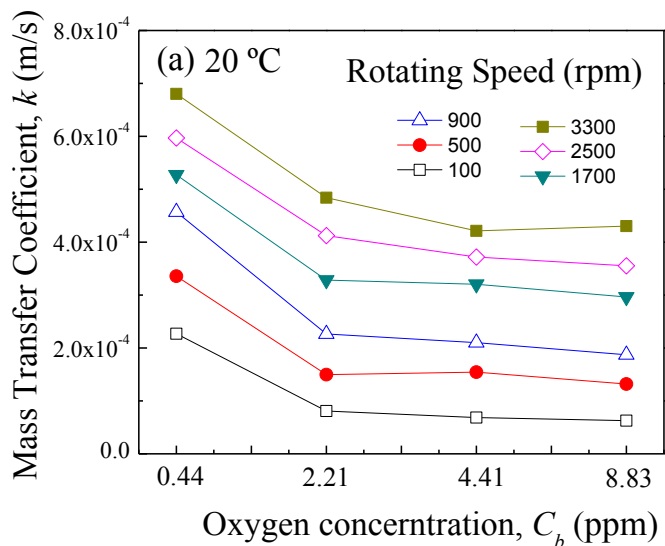


Figure 2-4. Calculated mass transfer coefficient vs. dissolved oxygen concentrations at 20 °C (a) and 60 °C (b) at the different rotating speeds, respectively.

To describe the mass transport behavior of dissolved oxygen for a rotating cylinder system at elevated electrolyte temperature without bulk boiling, the experimental data below boiling point

were expressed in terms of *Sherwood*, Sh , using Eq. (1.8) and was correlated with the product of *Reynolds*, Re and *Schmidt*, Sc numbers. A correlation was developed using a nonlinear regression algorithm in conjunction with the physical properties given in Table 1 in the following form:

$$Sh = 1.1404 Re^{0.583} Sc^{0.33} \quad (2.7)$$

Figure 2-5 shows the comparison of the predicted *Sherwood*, Sh , values obtained using Eq. (2.7) and the values experimentally measured. The figure includes a total of 72 data points and most of the data points are within 15% error. This equation is valid in the ranges of $733.27 < Re < 65435.06$; $69.47 < Sc < 566.51$; $20\text{ }^\circ\text{C} < T < 80\text{ }^\circ\text{C}$ and $C_b > 1\text{ ppm}$ and includes the effects of temperature, the dissolved oxygen concentration and diffusivity of dissolved oxygen.

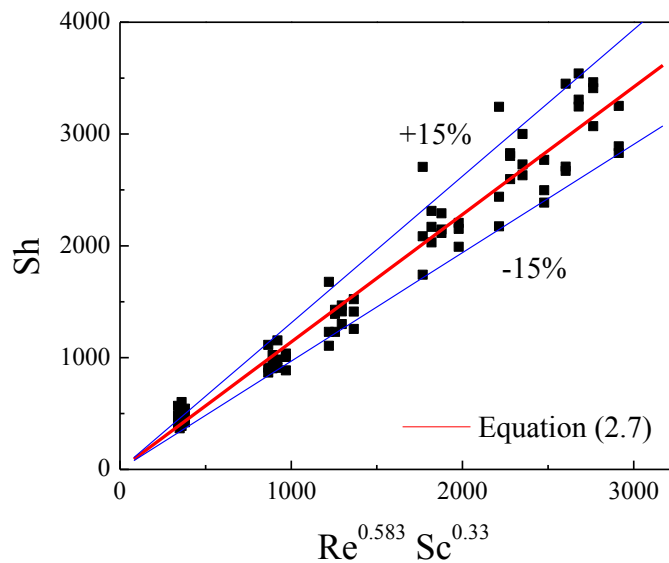


Figure 2-5. Comparison of experimental and predicted *Sherwood* numbers for dissolved oxygen mass transfer at temperatures below boiling.

2.4.2 Mass transfer behavior of dissolved oxygen under bulk boiling condition

For mass transfer rate measurements under the bulk boiling condition, the electrolyte solution was heated using an external oil-heating bath. To reach bulk boiling condition, the circulating oil in the heating bath was heated up to 150 °C. Figures. 2-6 (a) and (b) show photographs of the boiling rotating electrode system. Since the electrolyte solution was heated above the boiling point, the bubbles were generated from any nucleation sites inside the reactor, i.e., on the surface of reactor wall and on the cylinder electrode. A few bubbles were also generated inside the solution.

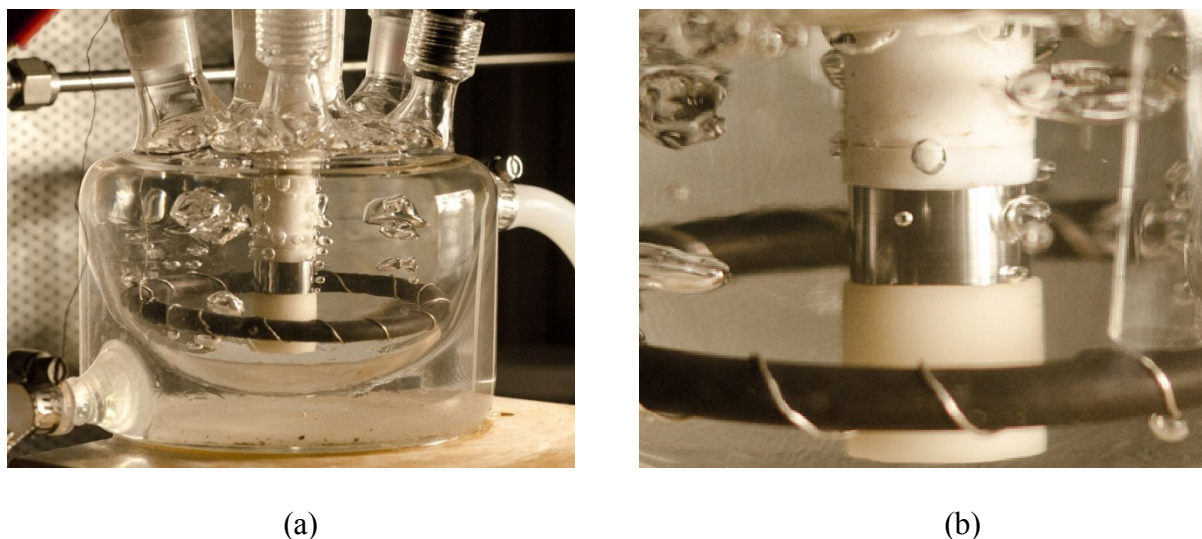


Figure 2-6. Photograph of rotating cylinder electrode system under bulk boiling electrolyte condition. (a) The electrochemical cell and (b) the cylinder electrode.

Figure 2-7 shows the polarization curves for the reduction of dissolved oxygen reaction under boiling conditions for the inlet oxygen to argon ratios up to 20 vol%. It can be observed that even

under boiling conditions, the inlet oxygen to argon ratio still influences the polarization curve. Increasing the oxygen to argon ratio resulted in the increase in the current density values, which corresponded to a higher oxygen reduction reaction rate. This implies that the dissolved oxygen concentration had a distinct impact on the reaction rate under bulk boiling conditions, although there are no clear plateaus as shown in Figure 2-7.

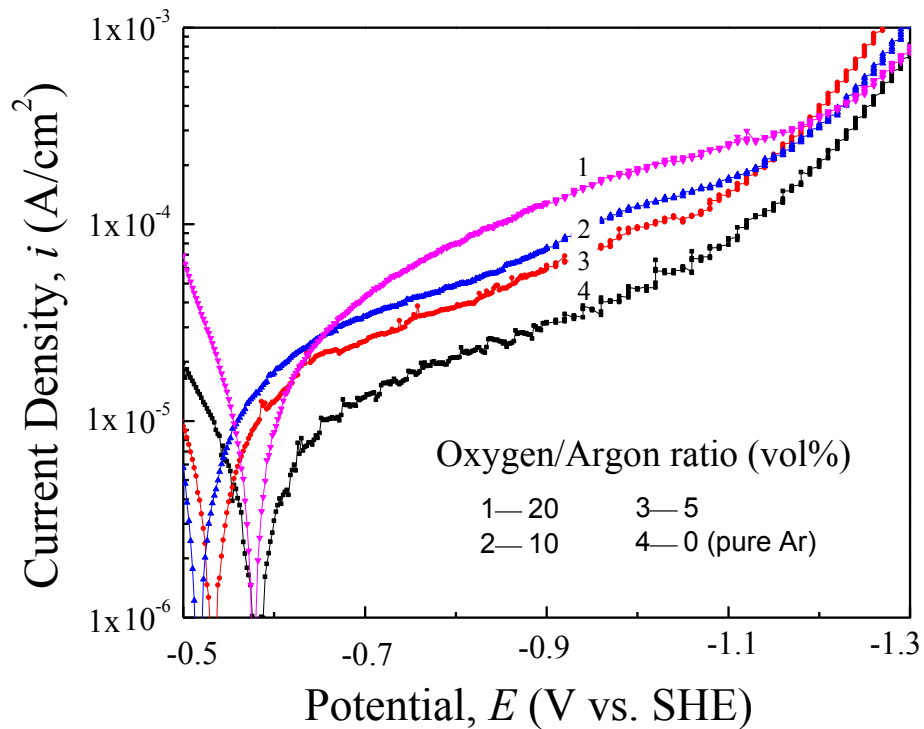


Figure 2-7. Polarization curves obtained in bulk boiling electrolyte (99.8 °C) for the different inlet oxygen/argon ratios at constant rotating speed of 500 rpm.

Figure 2-8 presents the polarization curves obtained under boiling conditions. For these sets of data, the inlet oxygen to argon ratio was kept constant at 5 vol% but the rotating speeds varied

from 100 rpm to 3300 rpm. It can be seen that unlike in previous conditions shown in Figure 2-2 (a), the rotating speed has little effect on polarization curves under these boiling conditions. Therefore, it could be concluded that the oxygen reduction reaction under the boiling electrolyte condition appeared not to be entirely mass transfer controlled. The reason could be that the oxygen concentration was very low (at the ppb level) and unstable due to bubble generation and rupture in the boiling electrolyte solution. Therefore, the current density was relatively low in this condition (in a range of 10^{-4} A/cm²) and the dynamic system fluctuations could also affect the results. Furthermore, under boiling electrolyte condition, the dissolved oxygen in the bulk solution could be carried over to the vapor phase and when the vapor bubbles collapsed on the working electrode, the oxygen could return back to the electrolyte solution, which increased the local oxygen concentration near the electrode and electrolyte interface. Thus, the interface concentration of dissolved oxygen could not reach to zero where the limiting current plateau appeared. Therefore, the regions of activation-controlled reaction extended and the region of mass transfer controlled reaction region could not be reached. From Figures 2-7 and 2-8, it could be concluded that under bulk boiling electrolyte conditions, the mass transfer of dissolved oxygen could not be measured using the limiting current method because of the changes in dissolved oxygen concentrations.

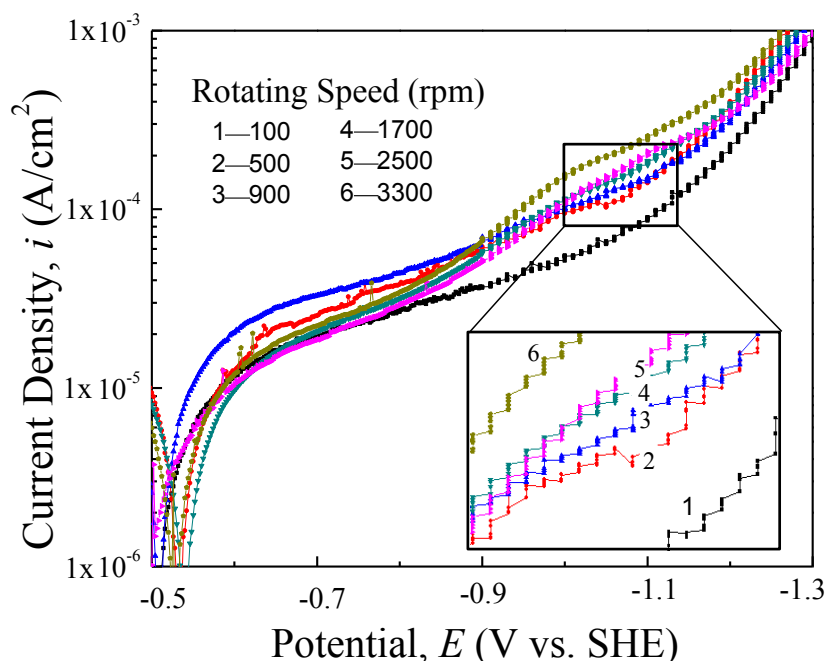
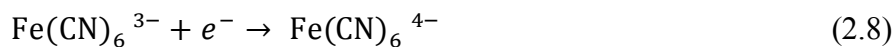


Figure 2-8. Polarization curves obtained in boiling electrolyte (99.8 °C) with the inlet oxygen/argon ratio of 5 % and at the different rotating speeds.

2.4.3 Mass transfer behavior of ferricyanide under below boiling condition

Due to its volatile nature, the concentration of dissolved oxygen changes with changing electrolyte temperature. In order to eliminate this effect, another non-volatile species, ferricyanide, was utilized to investigate mass transfer under the below boiling and the bulk boiling conditions. The electrochemical reaction of ferricyanide is shown below



This electrochemical system is proven to have a good chemical stability which provides long and well defined limiting current plateaus [1]. The anodic reaction of this system is the reverse

reaction of Eq. (2.10). Therefore, the total concentration of reaction species in the electrolyte does not change during the non-boiling experiment. Also, unlike the deposition of Cu, which is another widely used electrochemical system to determine mass transfer [30], the reaction of ferricyanide would not change the condition of the specimen surface during the reaction.

Figure 2-9 shows the experimentally determined mass transfer coefficients as a function of electrolyte temperature for various rotating speeds. The temperature of the electrolyte was varied between 20°C to 80°C and rotating speed range was from 100 to 3300 rpm. It can be observed that for any given electrolyte temperature, the mass transfer coefficient increases with increasing the rotating speed. As the rotating speed increases, the flux of electro active species to the surface of the electrode increases due to convection and hence the mass transfer coefficient increases. These trends are in agreement with those obtained by Kovatcheva et al., [31]. Figure 2-9 also shows that the mass transfer coefficient increases with increasing the electrolyte temperature. This is because the liquid has more internal energy at the higher electrolyte temperature and the molecules move faster. Consequently, the diffusivity of ferricyanide increases with temperature, which leads to an enhanced mass transfer coefficient [32].

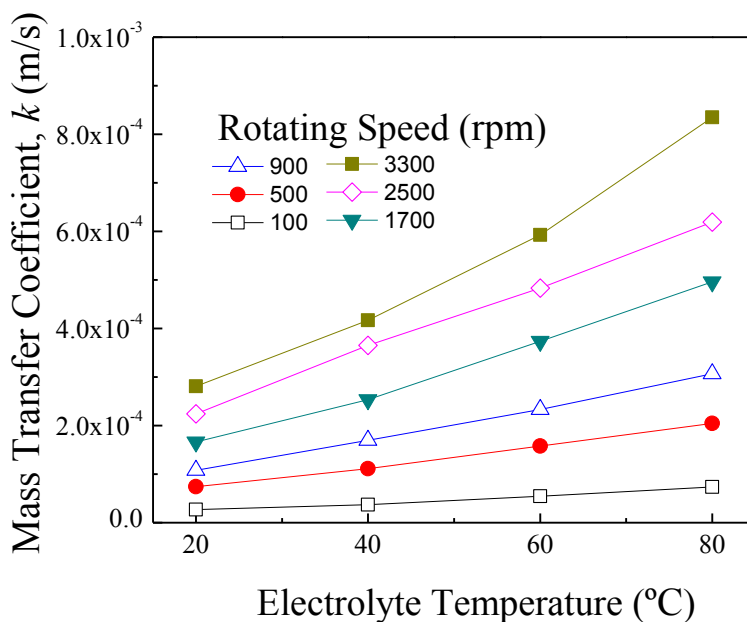


Figure 2-9. Mass transfer coefficient vs. temperature at the different rotating speeds for ferricyanide ions.

2.4.4 Mass transfer behavior of ferricyanide under bulk boiling condition

Due to the unstable concentration of dissolved oxygen, the mass transfer behavior under the bulk boiling condition was investigated using the ferricyanide reaction, which provided a stable concentration of reactant under the bulk boiling condition. The cathodic polarization curves and the experimentally obtained mass transfer coefficients for the reduction reaction of ferricyanide are shown in Figures 2-10 (a) and (b).

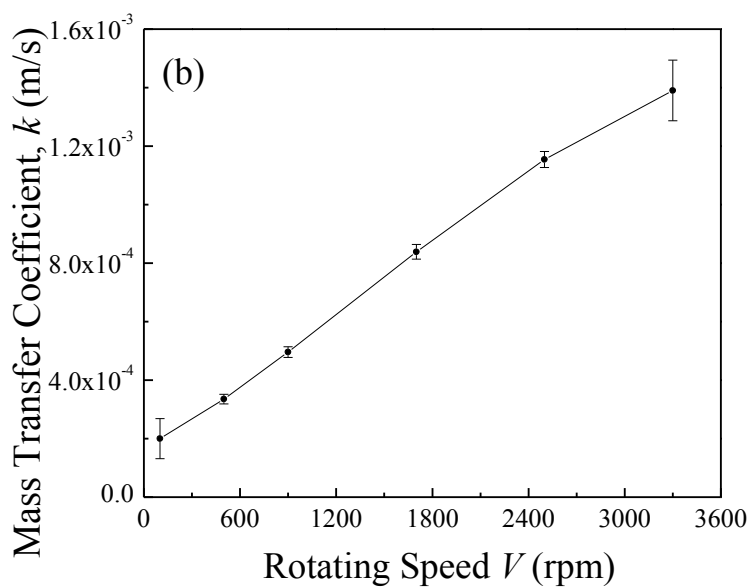
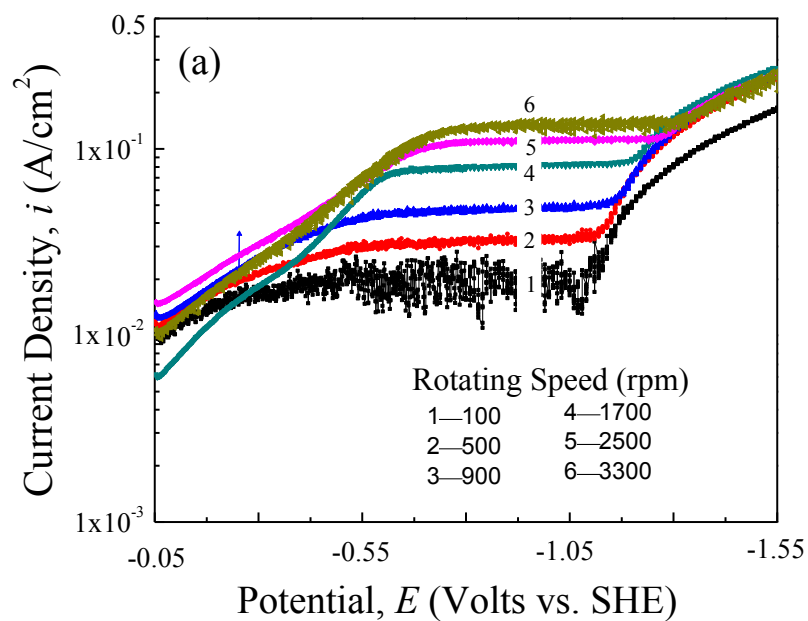


Figure 2-10. Cathodic polarization curves (a) and mass transfer coefficient (b) for reduction of ferricyanide reaction obtained in bulk boiling electrolyte at different rotating speeds.

Figure 2-10 (a) shows that unlike the oxygen reaction as shown Figures 2-7 and 2-8, clear current density plateaus are obtained for this reaction, which indicates that the reaction of ferricyanide could reach the mass transfer controlled region even under the bulk boiling condition. As expected, the measured mass transfer coefficient increases as rotating speed increases as shown in Figure 2-10 (b).

The question might arise of whether ferricyanide could mimic the mass transfer behavior of dissolved oxygen under bulk boiling condition. Figure 2-11 shows a comparison between the predicted values and the experimentally determined mass transfer coefficients, k , obtained using the ferricyanide reactions. The predicted values were calculated using Eq. (2.7) in which only dissolved oxygen reduction data under the solution temperature between 20 °C and 80 °C were considered. It can be seen that Eq. (2.7) not only represented the experimental data obtained for the ferricyanide reaction at temperature between 20 °C and 80 °C but also was able to predict the experimental data at just below the boiling point (99 °C) within an error range of 15 %. Therefore, Eq. (2.7) proves to be suitable for the oxygen reaction and is capable of predicting other non-volatile species, from room temperature up to just below the boiling point. This study also confirms that the ferricyanide reaction could be used to study dissolved oxygen behavior when the dissolved oxygen concentration was not stable such as under a bulk boiling condition. However, Figure 2-11 also shows that the experimental data obtained under boiling condition could not be represented well using Eq. (2.7). The experimentally determined mass transfer coefficients under the boiling condition are, on average, 38 % higher than those obtained just below boiling point due to the generation and rupture of boiling bubbles in bulk solution. This

indicate that the conventional correlations generated from non-boiling condition are not applicable in boiling conditions.

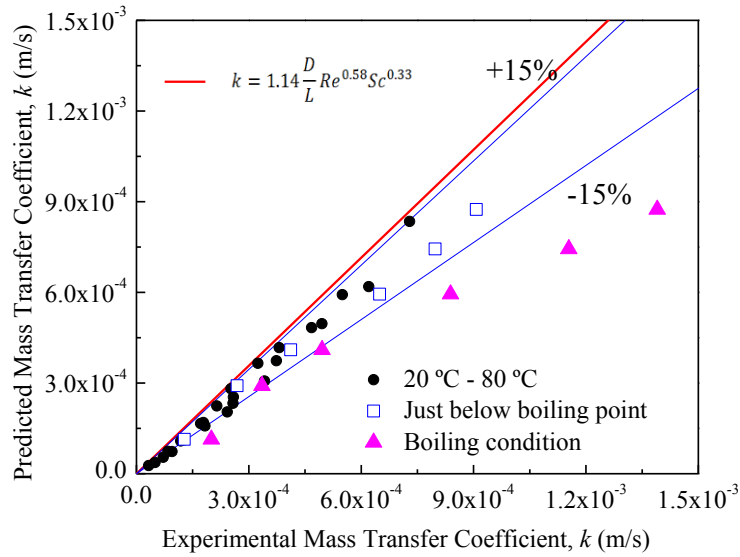


Figure 2-11 Comparison of the experimentally determined and predicted mass transfer coefficient obtained using ferricyanide reactions.

2.5 Conclusions

The mass transfer behaviors of the dissolved oxygen and ferricyanide ions on the rotating cylinder electrode were investigated under the conditions of approaching to boiling and bulk boiling for various dissolved oxygen concentrations and different rotating speeds. The following conclusions were obtained:

- 1) Below boiling electrolyte temperatures, the mass transfer coefficients for both dissolved oxygen reduction and ferricyanide ion were found to increase with the increasing electrolyte bulk temperature and rotating speed.
- 2) After the electrolyte was heated to bulk boiling condition, the limiting current plateau for oxygen reduction reaction was not observed due to the unstable and very low concentration of dissolved oxygen. However, a distinct current plateau was obtained for the reduction reaction of ferricyanide reaction.
- 3) It was found that a mass transfer correlation developed using dissolved oxygen reduction could be used to predict the mass transfer behavior for the ferricyanide reaction from room temperature up to the temperature just below the boiling point. This indicated that the ferricyanide reaction could be used to predict dissolved oxygen reduction at elevated electrolyte temperatures. It was also found that the mass transfer rates obtained under the bulk boiling condition was 38% higher than those obtained just below boiling point due to the generation and rupture of the boiling bubbles.

2.6 References

- [1] Selman, J.R. and C.W. Tobias, "Mass transfer measurements by the limiting current technique," *Advances in Chemical Engineering*, 10 (1978): pp. 211-318.
- [2] Burns, J.R. and R.J.J. Jachuck, "Determination of liquid-solid mass transfer coefficients for a spinning disc reactor using a limiting current technique," *International Journal of Heat and Mass Transfer*, 48 (2005): pp. 2540-2547.
- [3] Kim, D.H., I.H. Kim and H.N. Chang, "Experimental study of mass transfer around a turbulence promoter by the limiting current method," *International Journal of Heat and Mass Transfer*, 26 (1983): pp. 1007-1016.

- [4] Delaunay, G., A. Storck, A. Laurent and J.-C. Charpentier, "Electrochemical study of liquid-solid mass transfer in packed beds with upward cocurrent gas-liquid flow," *Industrial & Engineering Chemistry Process Design and Development*, 19 (1980): pp. 514-521.
- [5] Ross, T.K. and A.A. Wragg, "Electrochemical mass transfer studies in annuli," *Electrochimica Acta*, 10 (1965): pp. 1093-1106.
- [6] Wragg, A.A., "Free convection mass transfer at horizontal electrodes," *Electrochimica Acta*, 13 (1968): pp. 2159-2165.
- [7] Smith, A.F.J. and A.A. Wragg, "An electrochemical study of mass transfer in free convection at vertical arrays of horizontal cylinders," *Journal of Applied Electrochemistry*, 4 (1974): pp. 219-228.
- [8] Berger, F.P. and K.F.F.L. Hau, "Mass transfer in turbulent pipe flow measured by the electrochemical method," *International Journal of Heat and Mass Transfer*, 20 (1977): pp. 1185-1194.
- [9] El-Shazly, Y.M., R.R. Zahran, H.A. Farag and G.H. Sedahmed, "Mass transfer in relation to flow induced corrosion of the bottom of cylindrical agitated vessels," *Chemical Engineering and Processing: Process Intensification*, 43 (2004): pp. 745-751.
- [10] Comet, I., R. Greif, J.T. Teng and F. Roehler, "Mass transfer to rotating rods and plates," *International Journal of Heat and Mass Transfer*, 23 (1980): pp. 805-811.
- [11] Pao C, C., "Local liquid-solid mass transfer measurement in a trickle film flow model using an electrochemical technique," *International Journal of Heat and Mass Transfer*, 30 (1987): pp. 2305-2317.
- [12] Latifi, M.A., A. Laurent and A. Storck, "Liquid-solid mass transfer in a packed bed with downward cocurrent gas-liquid flow: An organic liquid phase with high Schmidt number," *The Chemical Engineering Journal*, 38 (1988): pp. 47-56.
- [13] Bartelmus, G., "Local solid-liquid mass transfer coefficients in a three-phase fixed bed reactor," *Chemical Engineering and Processing: Process Intensification*, 26 (1989): pp. 111-120.
- [14] Wragg, A.A. and A.K. Nasiruddin, "Ionic mass transfer by free convection with simultaneous heat transfer," *Electrochimica Acta*, 18 (1973): pp. 619-627.
- [15] Eisenberg, M., C.W. Tobias and C.R. Wilke, "Ionic mass transfer and concentration polarization at rotating electrodes," *Journal of The Electrochemical Society*, 101 (1954): pp. 306-320.

- [16] Ma, H., S. Hao, M. Wang, G. Yang and F. Wang, "Convective mass transfer from a horizontal rotating large-diameter cylinder," *International Journal of Heat and Mass Transfer*, 55 (2012): pp. 1419-1422.
- [17] Ma, H., D. Du, J. Sun, Y. Zhang and N. Deng, "Convective mass transfer from a horizontal rotating cylinder in a slot air jet flow," *International Journal of Heat and Mass Transfer*, 54 (2011): pp. 186-193.
- [18] Abdel-Aziz, M.S.M., A.H. El-Shazly, H.A. Farag and G.H. Sedahmed, "Mass transfer behavior of rotating square cylinder electrochemical reactor in relation to wastewater treatment," *Energy Conversion and Management*, 52 (2011): pp. 2870-2875.
- [19] Harvey, A.H., "Semiempirical correlation for Henry's constants over large temperature ranges," *AIChE Journal*, 42 (1996): pp. 1491-1494.
- [20] Saul, A. and W. Wagner, "International equations for the saturation properties of ordinary water substance," *Journal of Physical and Chemical Reference Data*, 16 (1987): pp. 893-901.
- [21] Akerlof, G. and G. Kegeles, "The density of aqueous solutions of sodium hydroxide," *Journal of the American Chemical Society*, 61 (1939): pp. 1027-1032.
- [22] Han, P. and D.M. Bartels, "Temperature dependence of oxygen diffusion in H₂O and D₂O," *The Journal of Physical Chemistry*, 100 (1996): pp. 5597-5602.
- [23] Arvia, A.J., S.L. Marchiano and J.J. Podesta, "The diffusion of ferrocyanide and ferricyanide ions in aqueous solutions of potassium hydroxide," *Electrochimica Acta*, 12 (1967): pp. 259-266.
- [24] Coleman, H.W. and W.G. Steele, *Experimentation and uncertainty analysis for engineers* 1999: John Wiley & Sons Incorporated.
- [25] Holman, J.P., *Experimental methods for engineers* 2001: McGraw Hill.
- [26] Ives, M.B., Y.C. Lu and J.L. Luo, "Cathodic reactions involved in metallic corrosion in chlorinated saline environments," *Corrosion Science*, 32 (1991): pp. 91-102.
- [27] Leibovitz, J., "Theorems of electrochemical mass transport in dilute solutions of mixtures of electrolytes, including weak electrolytes and hydrolysis reactions," *Journal of The Electrochemical Society*, 152 (2005): pp. E282-E297.
- [28] Kear, G., K. Bremhorst, S. Coles and S.-H. Huang, "Rates of mass transfer to patch electrodes in disturbed flows using oxygen reduction under limiting current conditions," *Corrosion Science*, 50 (2008): pp. 1789-1795.

- [29] Kovatcheva, N., A. Polyenin and Z. Zapryanov, "The change of the diffusivity with the change of the concentration of the solvent in a solution," *Acta mechanica*, 80 (1989): pp. 259-272.
- [30] Patrick, M.A. and A.A. Wragg, "Optical and electrochemical studies of transient free convection mass transfer at horizontal surfaces," *International Journal of Heat and Mass Transfer*, 18 (1975): pp. 1397-1407.
- [31] Cobo, O.A., S.L. Marchiano and A.J. Arvia, "Ionic mass transfer at rotating electrodes formed by solids of revolution. Rotating one-base spherical segment electrodes," *Electrochimica Acta*, 17 (1972): pp. 503-509.
- [32] Ferrell, R.T. and D.M. Himmelblau, "Diffusion coefficients of nitrogen and oxygen in water," *Journal of Chemical and Engineering Data*, 12 (1967): pp. 111-115.

Chapter 3 Phase II -- pool boiling condition

For Phase II study, a novel pool-boiling device was designed to measure the mass transfer behavior. This device enabled us to conduct direct electrochemical measurement on nucleate boiling surface.

3.1 Introduction

The mass transfer of dilute species on a nucleate boiling surface plays an important role in fouling, corrosion and materials degradation [1]. The mass transfer rate of dissolved oxygen is related to stress corrosion cracking of heat exchange tubing in recirculating steam generators [2, 3]. The mass transfer of some dissolved irons on a nucleate boiling electrode is critical to the fouling problems of thermal power plants [4, 5]. The corrosion control of reboilers is dependent on the mass transfer rate of corrosion inhibitors to the boiling surface [6].

Heat and momentum transfer under boiling conditions has been extensively studied [7, 8], but there is little experimental work for mass transfer of dilute species on nucleate boiling surface due to the experimental difficulties [9]. Wragg and Nasiruddin [10] attempted to investigate the mass transfer behavior of copper ions from the bulk solution to a subcooled boiling surface using the electrochemical method. They found that the measurements could not be done at the electrode-solution interface due to the intense local turbulence caused by bubble nucleation, growth, movement and collapse during boiling. Sarac and Wragg [11] later constructed a setup to investigate mass transfer in the presence of simultaneous subcooled boiling. The boiling

phenomenon of this experiment was obtained by quickly and fully immersing a preheated nickel rod in a static pool of ferricyanide/ferrocyanide NaOH solution. They found that in the nucleate boiling regime, the variation of mass transfer coefficient with temperature difference between electrode and electrolyte showed similar trends to that of heat transfer with temperature difference. However, their measurements were taking place within a limited time period (10 s). Their experimental data showed that the specimen temperature was changing during this short time period. It can be seen that their experimental data would have been more reliable if the experimental conditions were more stable.

A few other researchers attempted to build a relationship between gas evolving surface and nucleate boiling surface [9, 12]. Vogt et al., [13] reviewed the analogies and pointed out that the existing analogy is restricted to the transfer of the dissolved gas due to reaction on the electrode and the transfer of energy caused by heating of the surface. They also concluded that the analogy was difficult to be extended to reactant transferred from the liquid bulk to the electrode.

The electrochemical method used in this study is a cathodic polarization measurement. Also known as the limiting current technique, it is widely used for the mass transfer studies due to the convenient and reliable in-situ measurements [14]. This method is used to measure the reaction rate when the reaction is controlled by the mass transfer rate. Thus, the mass transfer rate can be calculated based on the measured reaction rate. However, a limited number of species can be used for this measurement because the reaction requires chemical stability as well as a suitable electrode reaction potential at which limiting current plateaus appear. The reaction of potassium ferri-/ferrocyanide was suitable for both bulk boiling and fully developed nucleate boiling

conditions [15, 16]. Since potassium ferri-/ferrocyanide is a non-volatile species, the previous results may not be applicable to volatile species under boiling conditions. Hydrogen peroxide is a volatile species that has significant interaction with metal surfaces [17] and is considered to be corrosive in supercritical water cooled reactors [18]. Nickchi and Alfantazi [19] measured the limiting current for the reduction reaction of hydrogen peroxide up to 200 °C in an autoclave. They speculated that nucleation was not likely taking place inside the autoclave. According to the authors' best knowledge, the mass transfer behavior from the bulk electrolyte to the nucleate boiling surface was still unclear for different species.

The present chapter describes a novel pool-boiling device, which allows us to use direct electrochemical measurements on a stable nucleate boiling surface to investigate the mass transfer behavior. Both volatile and non-volatile species will be used to measure the mass transfer rate under natural convection, subcooled nucleate boiling and fully developed nucleate boiling conditions. The effects of heat flux and surface roughness on mass transfer under fully developed nucleate boiling surfaces will also be investigated. Also, the relationship between mass transfer and heat flux with the consideration of surface roughness will be proposed. The findings from this work would be very useful for predicting corrosion potential for heat exchangers, steam generators and reboilers [20].

3.2 Experimental

3.2.1 Experimental set-up

The schematic of the novel nucleate boiling apparatus is shown in Figure 3-1. The specimen used as the working electrode is the Alloy 800 heat exchanger tube with inner diameter of 13.4 mm, outer diameter of 15.8 mm and 30 mm in length. Circulating oil is employed to heat the inner surface of the specimen and the boiling phenomenon takes place on the outer surface of the specimen. The electrochemical measurements are conducted on the outer surface of the specimen where boiling occurs. A platinum coil with a diameter of 60 mm is used as a counter electrode. An Ag/AgCl electrode with saturated KCl solution (Fisher Scientific) for temperatures up to 125 °C is used as the reference electrode. The specimen is heated using an external heating circulating bath (Cole-Parmer PolyStat Co.). The temperature of circulating oil is varied from room temperature to 171 °C. K-type thermocouples are used to measure the temperature of the bulk electrolyte (T_1) and the temperatures of the heating oil before entering and after leaving the specimen (T_3 and T_2). A condenser is used to maintain constant an electrolyte concentration.

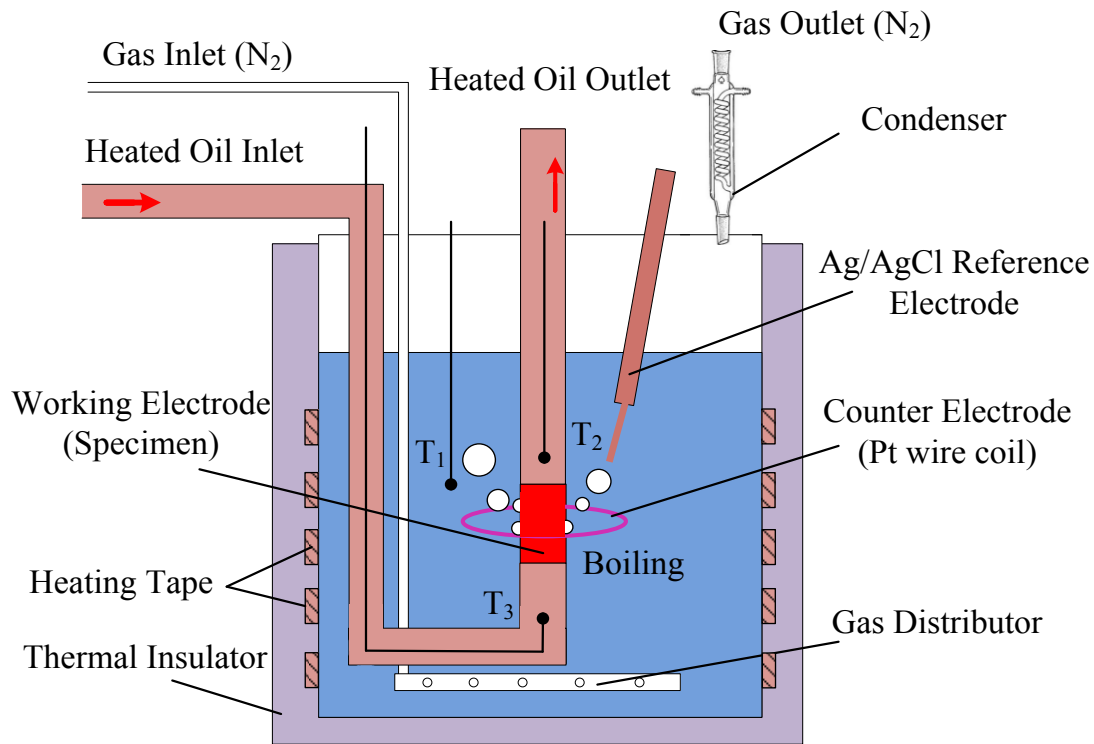


Figure 3-1. Schematic of the nucleate boiling experimental setup.

3.2.2 Experimental procedure

Before each test, the specimens were polished using #60 grit sand paper to obtain an average roughness of $0.95 \mu\text{m}$ so that the roughness was close to the conventional operating condition. The values of roughness were tested using Pocket Surf roughness tester. In this study, two different types of electrolyte were used. The first one was prepared using distilled water and analytical grade NaOH to make 0.1 M NaOH solution as the supporting electrolyte with 0.01 M potassium ferricyanide/ferrocyanide added to the mixture as the reaction species. The second electrolyte contained 0.025 M Na_2SO_4 as the supporting electrolyte and 0.00195 M H_2O_2 solution as the reaction species. The electrolytes were deoxygenated by purging with pure

nitrogen gas for 1 hour before each measurement. The electrochemical measurements were conducted using a SI 1287 electrochemical interface (Solartron Analytical Co.). The potentiodynamic polarizations were conducted from -50 mV vs OCP until the hydrogen evolution reaction clearly shows at a scan rate of 2 mV/s. The diffusivities of the potassium ferricyanide for the temperature range of 20 °C to 100 °C obtained from open literature [21] are shown in Table 3-1. The diffusivity values of hydrogen peroxide are also included in Table 3-1 where the diffusivity at 20 °C was obtained from literature [22] and the values for other temperatures were calculated using the Stokes-Einstein equation [23].

Table 3-1. Diffusivities of potassium ferricyanide and hydrogen peroxide at various temperatures.

Temperature (°C)	20	40	60	80	96
Potassium ferricyanide (m ² /s)	6.45×10 ⁻¹⁰	1.03×10 ⁻⁹	1.56×10 ⁻⁹	2.16×10 ⁻⁹	2.83×10 ⁻⁹
Hydrogen peroxide (m ² /s)	6.60×10 ⁻¹⁰	1.08×10 ⁻⁹	1.59×10 ⁻⁹	2.21×10 ⁻⁹	2.89×10 ⁻⁹

3.2.3 Uncertainty Analysis

For each test, the heat flux on the specimen surface was calculated based on the temperature difference between the two thermocouples using the following equation:

$$q = \frac{\dot{m} C_p (T_{in} - T_{out})}{A} \quad (3.1)$$

where q is the heat flux, \dot{m} is the mass flow rate, C_p is the heat capacity of the heating oil, A is the specimen surface area, T_{in} and T_{out} are the oil temperature at the inlet and outlet of the specimen.

The uncertainty in the experimentally determined heat flux was calculated using the method described by Coleman and Steel [24] and Holman [25]. The uncertainty in the heat flux was estimated based on experimental errors in the measured oil mass flow rate, the inlet and outlet oil temperatures, specific heat capacity and the surface area. The uncertainty can be written as:

$$\omega_q = \pm \left[\left(\frac{\partial q}{\partial \dot{m}} \omega_{\dot{m}} \right)^2 + \left(\frac{\partial q}{\partial c_p} \omega_{c_p} \right)^2 + \left(\frac{\partial q}{\partial T_{in}} \omega_{T_{in}} \right)^2 + \left(\frac{\partial q}{\partial T_{out}} \omega_{T_{out}} \right)^2 + \left(\frac{\partial q}{\partial A} \omega_A \right)^2 \right]^{0.5} \quad (3.2)$$

Evaluating the partial derivatives and simplifying, gave uncertainty in the heat flux as:

$$\omega_q = \pm q \times \left\{ \left(\frac{\omega_{\dot{m}}}{\dot{m}} \right)^2 + \left(\frac{\omega_{c_p}}{c_p} \right)^2 + \left[\frac{\omega_{T_{in}}}{(T_{in} - T_{out})} \right]^2 + \left[\frac{\omega_{T_{out}}}{(T_{in} - T_{out})} \right]^2 + \left(\frac{\omega_A}{A} \right)^2 \right\}^{0.5} \quad (3.3)$$

where ω_q is the uncertainty in heat flux, $\omega_{\dot{m}}$ is the uncertainty in mass flow rate, ω_{c_p} is the uncertainty in specific heat capacity, $\omega_{T_{in}}$ is the uncertainty in inlet temperature, $\omega_{T_{out}}$ is the uncertainty in outlet temperature and ω_A is the uncertainty in surface area.

The mass transfer coefficient of the reactant species, k , the *Sherwood* number, Sh , and the uncertainty in the experimentally determined mass transfer coefficient were calculated using Eq. (1.6) and Eq. (1.8).

3.3 Background

According to Stephan and Vogt [12], gas bubble generation enhances mass transfer due to the convective flow of electrolyte during bubble growth on the electrode surface. They developed a model for mass transfer enhancement by gas bubble evolution. In this model, the authors assumed that the shape of the bubbles was spherical or hemispherical, a specific small area may be attributed to each individual bubble and the flow along the micro-area is laminar. These three assumptions are appropriate for the present study [26]. The other assumption Stephan and Vogt [12] made is that the influence of mass transfer due to the flow induced by the detaching of the bubble is negligible. However, this assumption appears not to be universally accurate according to Fukunaka's study [27]. Stephan and Vogt [12] have described their data with the following correlation which stated that the mass transfer coefficient was proportional to the square root of the gas bubble evolution rate:

$$Sh_{micro} = 0.93Re_G^{0.5}Sc^{0.487} \quad (3.4)$$

where Sh_{micro} is the Sherwood number caused by bubble generation, Sc is the Schmidt number of the solution and Re_G is the gas evolution Reynolds number that is defined as:

$$Re_G = \frac{V_G d_b \rho}{A \mu} \quad (3.5)$$

where V_G is the gas evolution rate, d_b is the break off diameter of the gas bubble, A is the surface area, ρ and μ are the density and viscosity of the solution, respectively.

Alkire and Lu [28] claimed that the micromixing caused by the expansion of the bubble and the macromixing effect caused by the motion of the detached bubble contributed to the mass transfer enhancement. Therefore, they concluded that the total effects could be expressed by summation of the above two factors. Fukunaka et al. [27] proposed the following empirical correlation to include only macromixing effects to the mass transfer equation:

$$Sh_{macro} = 0.0172 Ra^{0.5} \quad (3.6)$$

where Ra is the Rayleigh number and can be calculated using the following equation:

$$Ra = Pr Gr \quad (3.7)$$

where Pr is Prandtl number and Gr is the Grashof number and can be expressed as:

$$Gr = \frac{g\beta(T_s - T_b)L^3}{\left(\frac{\mu}{\rho}\right)^2} \quad (3.8)$$

where g is the gravity of Earth, β is the volumetric thermal expansion coefficient, T_s is the wall temperature of the specimen which can be calculated using Thom correlation [26], T_b is the bulk temperature and L is the characteristic length.

The models obtained by Stephan and Vogt [12] and Fukunaka et al. [27] were developed for the isothermal condition, which means that these models did not consider the mass transfer caused by non-isothermal convection. However, the non-isothermal nature of convection also causes the mass transfer enhancement. Wragg and Nasiruddin [10] investigated the mass transfer of the cathodic deposition of copper ions in non-isothermal conditions on a flat horizontal surface, and summarized their work with the following empirical equation:

$$Sh_{conv} = 0.163 (Sc Gr)^{0.33} \quad (3.9)$$

Figure 3-2 showed all the enhancement effects that caused by the boiling bubble on the mass transfer rate. A correlation which considered the effects of micromixing, macromixing and non-isothermal convection on mass transfer under boiling condition has been proposed as follows:

$$Sh = a Re_G^{0.5} Sc^{0.487} + b Ra^{0.5} + c (Sc Gr)^{0.33} \quad (3.10)$$

where a , b and c are empirical factors could be determined based on the experimental work.

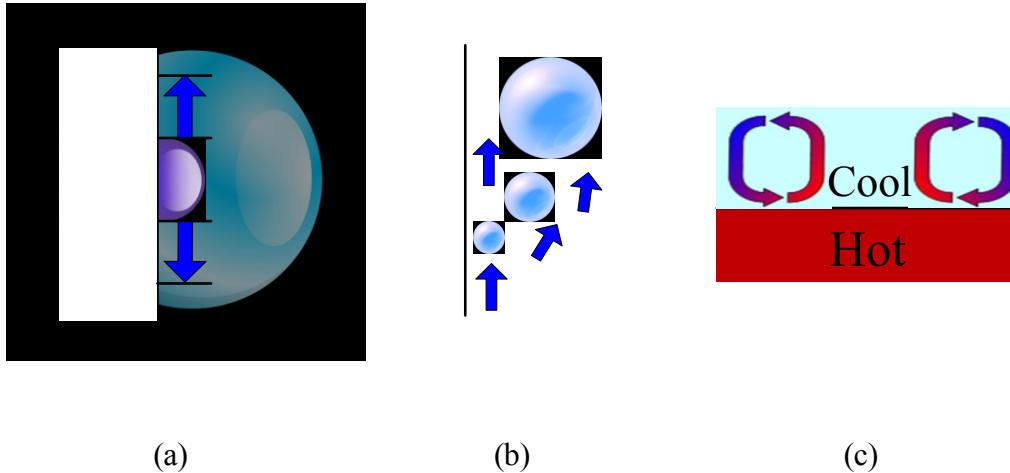


Figure 3-2. Factors (a) micromixing (b) macromixing (c) non-isothermal convection influence mass transfer under boiling condition.

3.4 Results and discussion

3.4.1 Stability of hydrogen peroxide reaction

It is well known that hydrogen peroxide tends to decompose to oxygen and water at elevated temperatures. Also, unlike the reduction of ferricyanide, the reduction reaction of hydrogen peroxide is not reversible at the anode. Therefore, the concentration of hydrogen peroxide would continually decrease as the reaction proceeds. Nickchi and Alfantazi [19] titrated the solution with KMnO_4 in the presence of sulfuric acid before and after their experiments with reduction reaction of hydrogen peroxide in an autoclave. They found that the decrease in hydrogen peroxide concentration was less than 5% before and after their experiments. Their result may not be applicable to the current study, since a half open system was employed in the present study.

Figure 3-3 shows the experimental data for the stability of the hydrogen peroxide concentration at various electrolyte temperatures. The tests were conducted at the cathodic polarization potential of -0.8 V vs. standard hydrogen electrode (SHE). The current density value, which represents the reduction reaction rate of hydrogen peroxide, is proportional to the hydrogen peroxide concentration. As can be observed from Figure 3-3, the current density remained constant at the electrolyte temperature of 20 °C, but the current density continuously decreased at 80 °C and boiling conditions. The decrease indicated that the hydrogen peroxide was decaying during the measurements at 80 °C and boiling conditions. And this decay should follow the exponential decay rules. The following half-life equation [29] was used to fit the decay rate of hydrogen peroxide as shown in Figure 3-3.

$$\ln \frac{N(t)}{N_0} = \frac{t}{t_{0.5}} \ln \left(\frac{1}{2} \right) \quad (3.11)$$

where $N(t)$ is the concentration of hydrogen peroxide at time t , N_0 is the initial concentration and $t_{0.5}$ is the half-life. The regression lines shown in Figure 3-3 indicated that the half-life for electrolyte temperature of 80 °C and for boiling condition were 1300 s and 1000 s, respectively. This decay was incorporated for all the data analysis of hydrogen peroxide experiments. Also, it can be observed that the current density at boiling condition is higher than that of lower temperatures, this would indicate the mass transfer rate of hydrogen peroxide is higher at boiling condition.

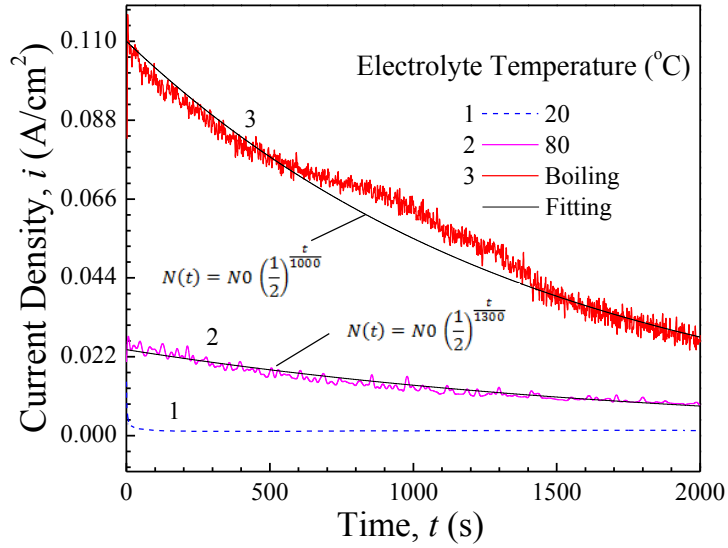


Figure 3-3. Current density as a function time for Alloy 800 in the hydrogen peroxide at various electrolyte temperatures.

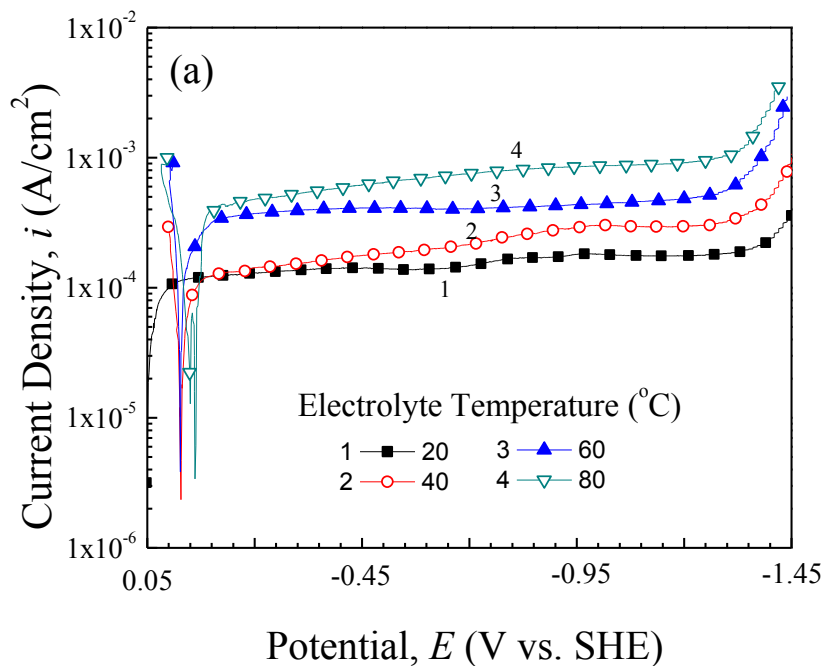
3.4.2 Mass transfer under natural convection condition

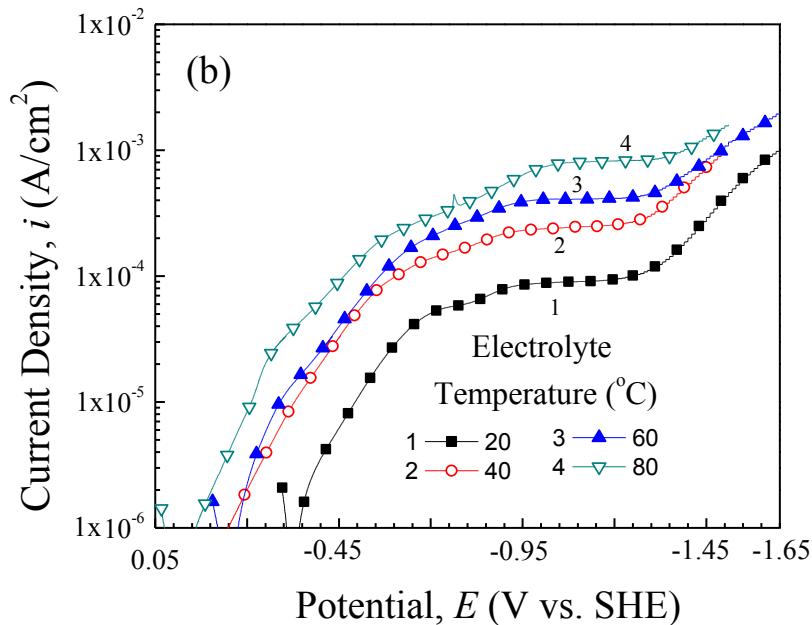
Figures 3-4 (a) and (b) show the typical polarization curves for potassium ferri-/ferrocyanide and hydrogen peroxide electrolytes at the electrolyte temperatures of 20 °C, 40 °C, 60 °C and 80 °C. The reduction reactions of ferricyanide [16] is shown in Eq. (2.10) and hydrogen peroxide [30] is shown below:



Both Figs show that, for all electrolyte temperatures, a clear current plateau can be observed at the potential range between -0.3 and -1.3 V vs. SHE for ferricyanide reaction and -0.15 and $-$

1.35 V vs. SHE for hydrogen peroxide reaction. The current further increased at potentials lower than -1.35 V due to the hydrogen evolution reaction occurring on the electrode. The current plateau indicated that the electrochemical reaction was mass transfer controlled at this region and the value of this limiting current represented the reaction rate of the mass transfer controlled reaction, and therefore the mass transfer rate. Figures 3-4 (a) and (b) show that the mass transfer rate increased with increasing electrolyte temperature, since the liquid had more internal energy at the higher temperatures and the molecules moved faster. As a consequence, the diffusivity of ferricyanide increased with temperature, leading to an enhanced mass transfer rate [31].





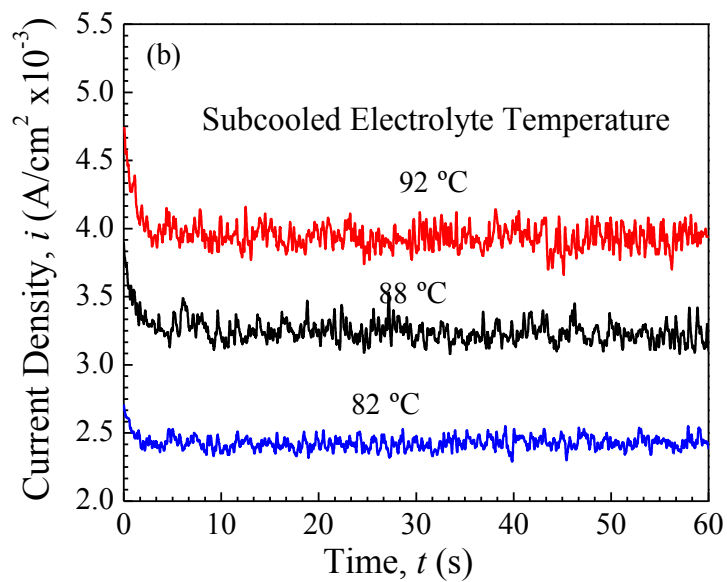
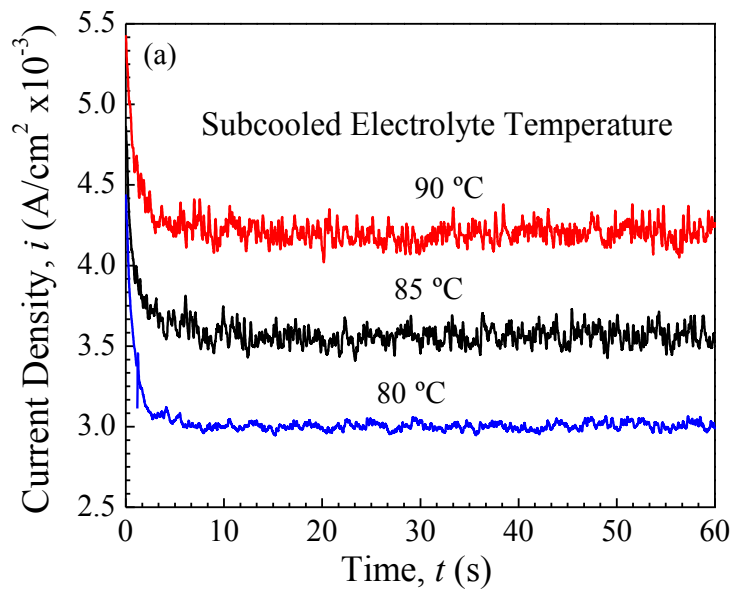
Figures 3-4. Cathodic polarization curves for ferri-/ferrocyanide (a) and hydrogen peroxide (b) reactions for different electrolyte temperatures under natural convection condition

3.4.3 Mass transfer rate under subcooled boiling condition (Onset of nucleate boiling)

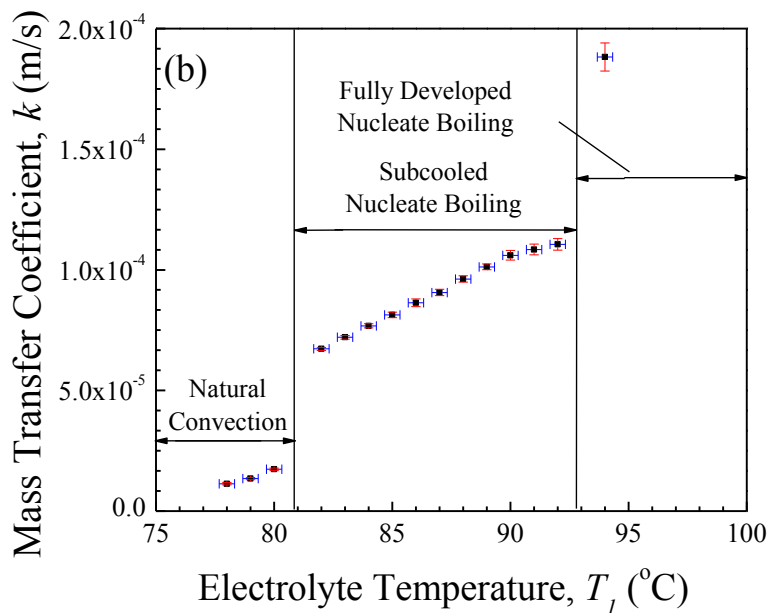
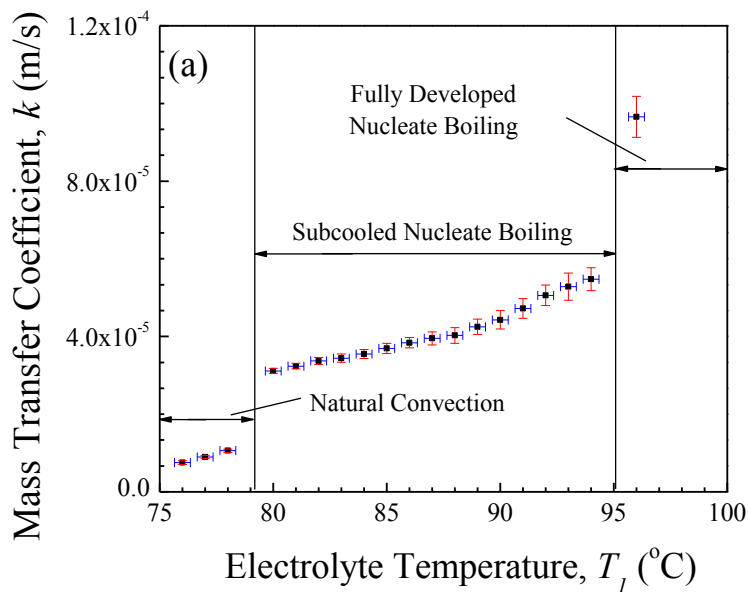
Figures 3-5 (a) and (b) show potentiostatic tests for the duration of 60 seconds for both potassium ferri-/ferrocyanide and hydrogen peroxide electrolytes under subcooled nucleate boiling condition. The potentiostatic test was used because it is a relatively quick test to overcome the developing subcooled boiling temperature. The potential of these tests was -1.0 V vs. SHE. All the subcooled boiling experiments were conducted at constant heat flux of 66 ± 2 kW/m² for the potassium ferri-/ferrocyanide electrolyte and 69 ± 2 kW/m² for the hydrogen peroxide electrolyte. It can be observed from Figures 3-5 (a) and (b) that the limiting current density increased with the increasing bulk boiling temperature under the subcooled boiling

condition, which indicated an increase in the mass transfer rates. Fluctuations in the current curves were also observed, with amplitudes increasing as the electrolyte temperature increased. The fluctuations of the current were caused by the bubble-induced forced convection. As the electrolyte temperature increased, the number of nucleate sites and/or the frequency of bubble generation increased in the subcooled boiling condition. Thus, the amplitudes of the fluctuation were enhanced at higher subcooled bulk temperatures [32].

Figures 3-6 (a) and (b) show the mass transfer coefficients obtained from natural convection, subcooled boiling and fully developed nucleate boiling conditions. The mass transfer coefficients were calculated using Eq. (1.6). The fully developed nucleate boiling data shown in Figures 3-6 (a) and (b) had nearly the same heat flux compared with that under subcooled nucleate boiling condition. The mass transfer coefficient showed a sudden increase at the onset of the subcooled nucleate boiling condition and at the start of the fully developed nucleate boiling condition. The sudden increase was caused by the increase in mass transfer enhancement factors. The mass transfer rate from the bulk solution to the boiling surface is influenced by three factors: the non-isothermal convection attributed to the temperature gradient [10], the convection caused by bubble generation, called micromixing [12] and the convection caused by detached bubble flow over the surface, known as macromixing [27, 28]. It can be summarized from Figures 3-6 (a) and (b) that under the subcooled boiling condition, the non-isothermal convection and micromixing influenced the mass transfer rate and caused the sudden increase in the mass transfer rate at the onset of subcooled boiling. Under the fully developed nucleate boiling condition, all three of the factors affected the mass transfer rate. It was the macromixing effect, which did not appear under subcooled boiling condition that led to a second sudden increase in the mass transfer coefficient.



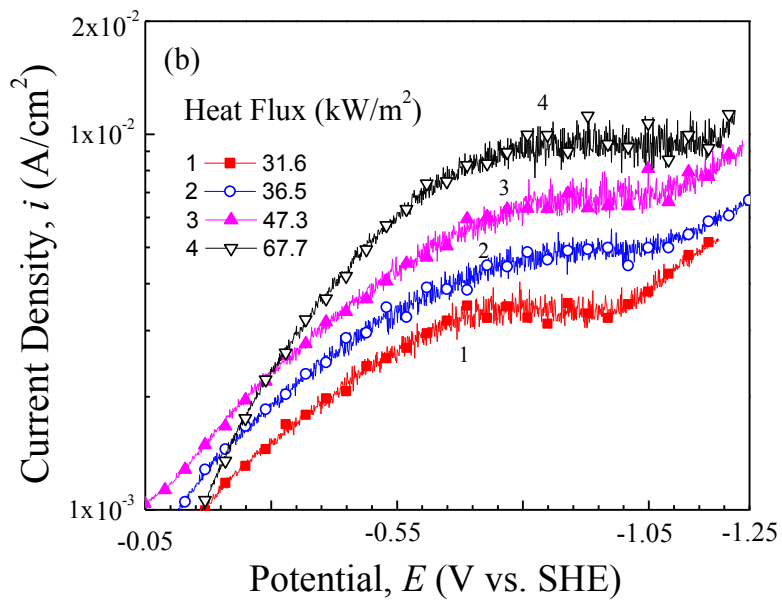
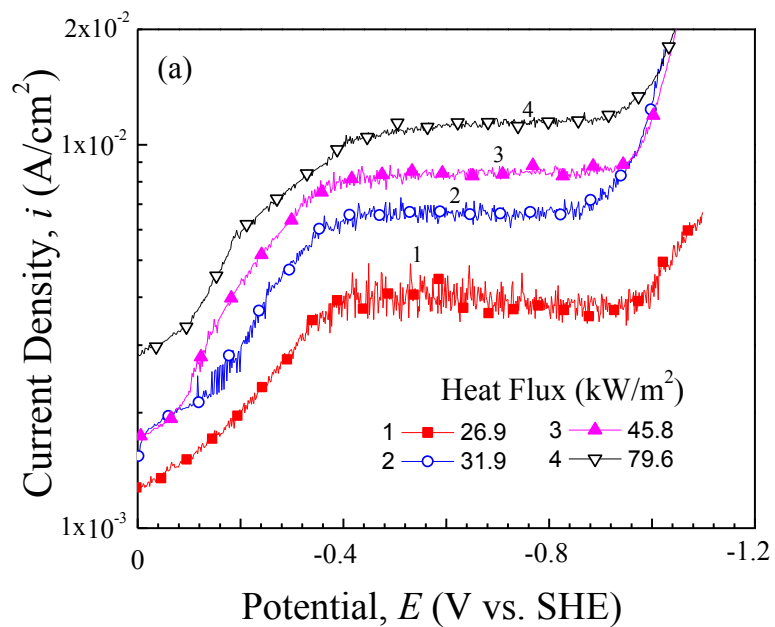
Figures 3-5. Potentiostatic test for (a) ferri-/ferrocyanide and (b) hydrogen peroxide reactions at subcooled nucleate boiling condition.



Figures 3-6. Mass transfer coefficients for (a) ferri-/ferrocyanide and (b) hydrogen peroxide reactions under natural convection, subcooled nucleate boiling and fully developed nucleate boiling conditions.

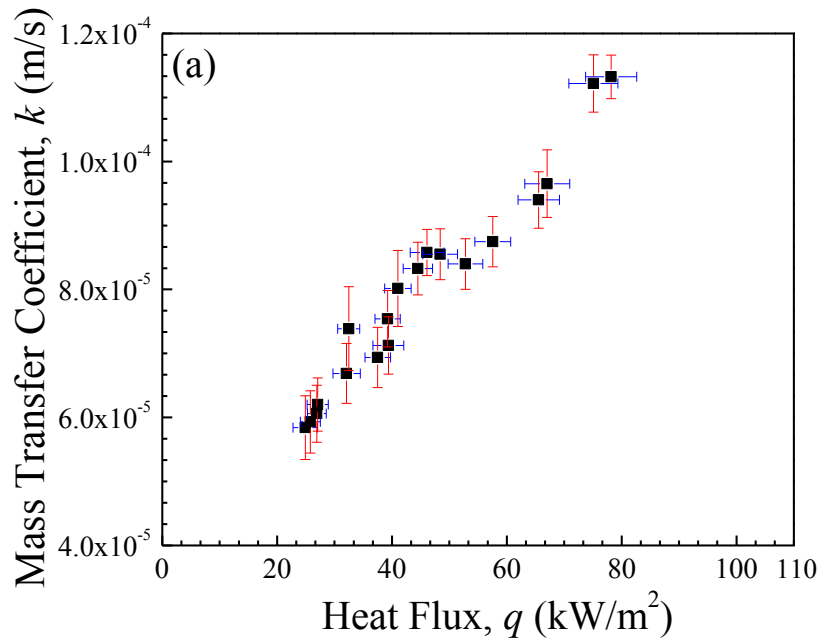
3.4.4 Mass transfer under fully developed boiling condition

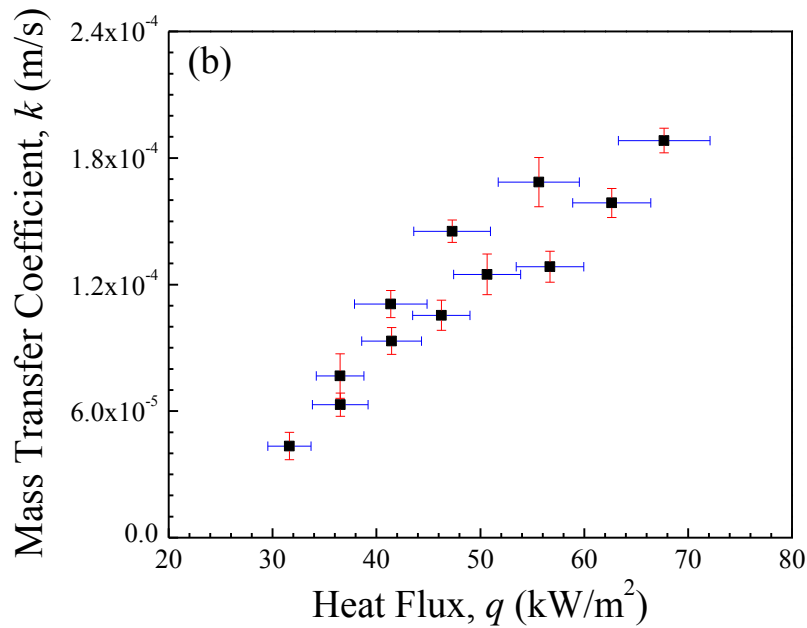
Figures 3-7 (a) and (b) show the polarization curves for the ferricyanide and hydrogen peroxide reactions obtained under fully developed boiling conditions for various heat fluxes, respectively. Figures 3-7 (a) clearly showed the current plateaus in the potential range between -0.55 and -0.95 V (SHE) for the ferricyanide reaction. This was strong evidence for the successful electrochemical measurement on the boiling surface. The current plateaus also indicated that this was the mass transfer controlled reaction region since the reaction rate (i.e. current) did not increase with the increasing driving force (i.e. potential). For the hydrogen peroxide tests shown in Figures 3-7 (b), the current plateaus were also observed between -0.90 and -1.05 V (SHE) but were shorter than those in the ferricyanide reaction, which indicated that it was more difficult to reach the mass transfer controlled region for this reaction. When the potential dropped below -1.05 V, water decomposed and hydrogen reaction began. This reaction was not mass transfer controlled. Figures 3-7 (a) and (b) also showed that the limiting current density increased with increasing heat flux under the fully developed boiling condition, indicating an increase in the mass transfer rate. The diffusion term did not significantly change since the solution temperature remained constant. Also, electromigration was eliminated due to the relatively high concentration of the supporting electrolyte. Therefore, the increase in limiting current density can only be attributed to the convection of electrolyte caused by the motions of the bubbles during the boiling condition. Thus, increasing the heat flux increased the bubble generation rate, leading to a higher mass transfer rate.



Figures 3-7. Cathodic polarization curves for (a) ferri-/ferrocyanide and (b) hydrogen peroxide reactions under fully developed nucleate boiling condition.

Figures 3-8 show the calculated the mass transfer coefficients as a function of heat flux for both ferricyanide and hydrogen peroxide reactions, respectively. The heat flux was calculated using Eq. (3.1). It can be seen that the mass transfer coefficient increased with increasing heat flux. Under the fully developed nucleate boiling region, the amount of vapor generation increased with increasing heat flux. With an increased number of bubble nucleation sites, and an increased vapor generation rate from each nucleation site, the departure and flow of bubbles enhanced the macromixing effect, which increased the mass transfer rate.





Figures 3-8. The mass transfer coefficients for ferri-/ferrocyanide (a) and hydrogen peroxide (b) reactions as a function of heat flux under fully developed nucleate boiling condition

3.4.5 Effect of surface roughness under fully developed nucleate boiling condition

Figure 3-9 shows the polarization curves for different average specimen surface roughnesses (Ras) varied between 0.95 and 0.10 μm obtained under fully developed nucleate pool boiling conditions. The surface different roughness was obtained by using different sand paper polishing, and measured by Pocket Surf tester. It is very clear that a rougher surface results in a higher limiting current value and consequently a higher mass transfer rate. Under nucleate boiling conditions, intense convection in the liquid adjacent to the heated tube wall is induced by the pumping motion of growing and departing bubbles which induced a remarkable localized forced convection process [26]. Rougher surfaces produced an increased number of active boiling

points on the specimen surface [33], which could cause more convection of the solution surrounding the specimen and thus a higher rate of mass transfer.

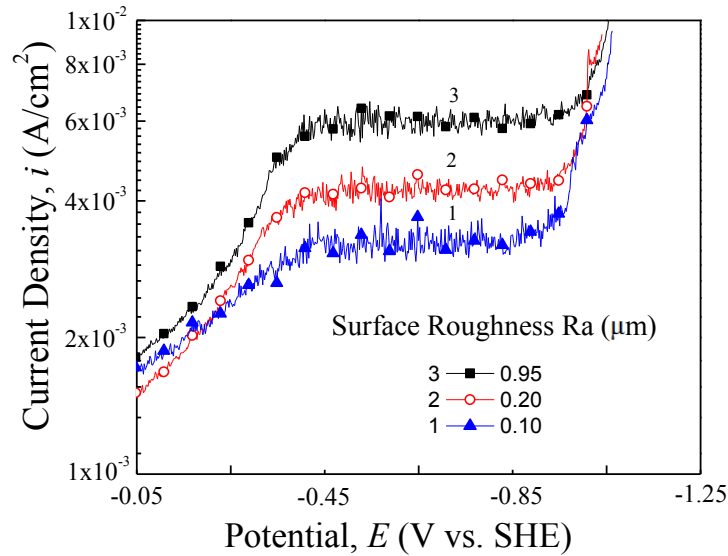
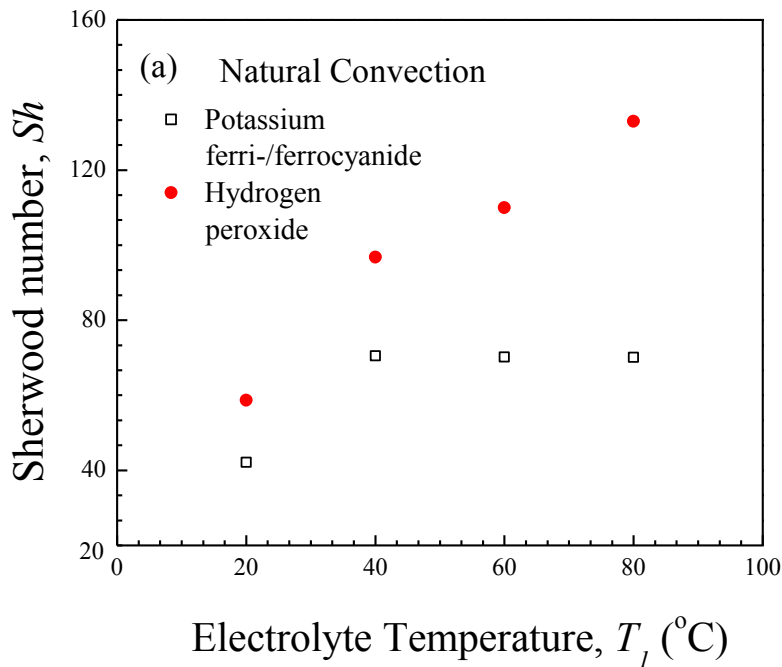


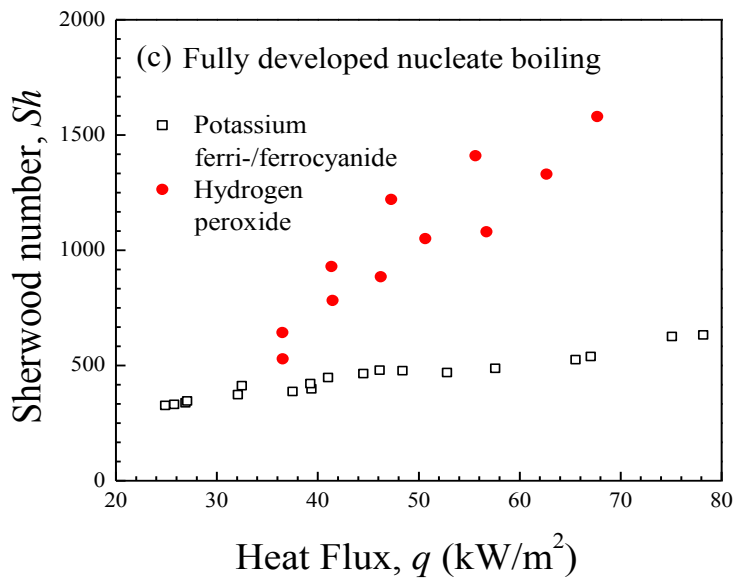
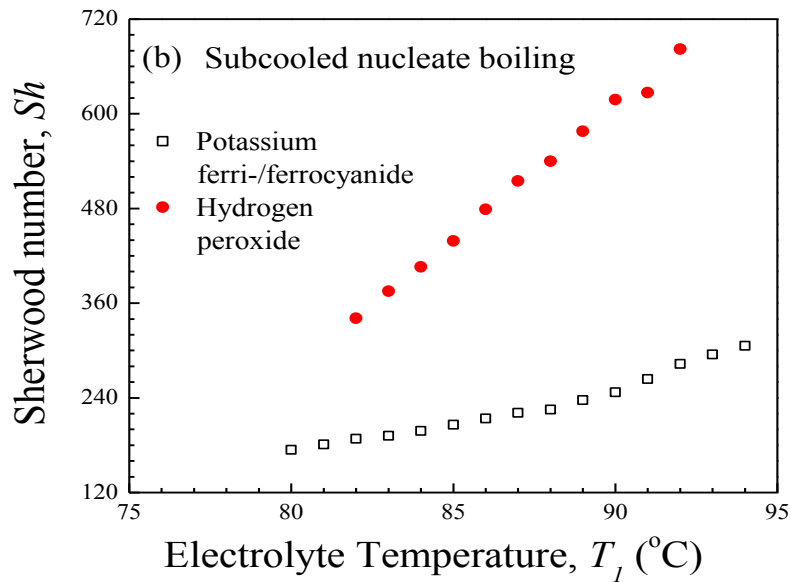
Figure 3-9. Polarization curves for various surface roughness under pool boiling condition.

3.4.6 Mechanism and difference between ferricyanide and hydrogen peroxide reactions

Figures 3-10 (a) and (b) show the Sherwood number as a function of electrolyte temperature in the natural convection and subcooled nucleate boiling conditions for the ferricyanide and hydrogen peroxide reactions. The electrolyte temperature was varied from 20 °C to 95 °C. Figure 3-10 (c) showed the Sherwood number as a function of heat flux under fully developed nucleate boiling conditions, where the electrolyte temperature remained relatively constant at 96 °C. The Sherwood number was calculated using Eq. (1.8). The Sherwood number is the ratio of convective mass transfer to the molecular diffusion. Therefore, it was expected that the

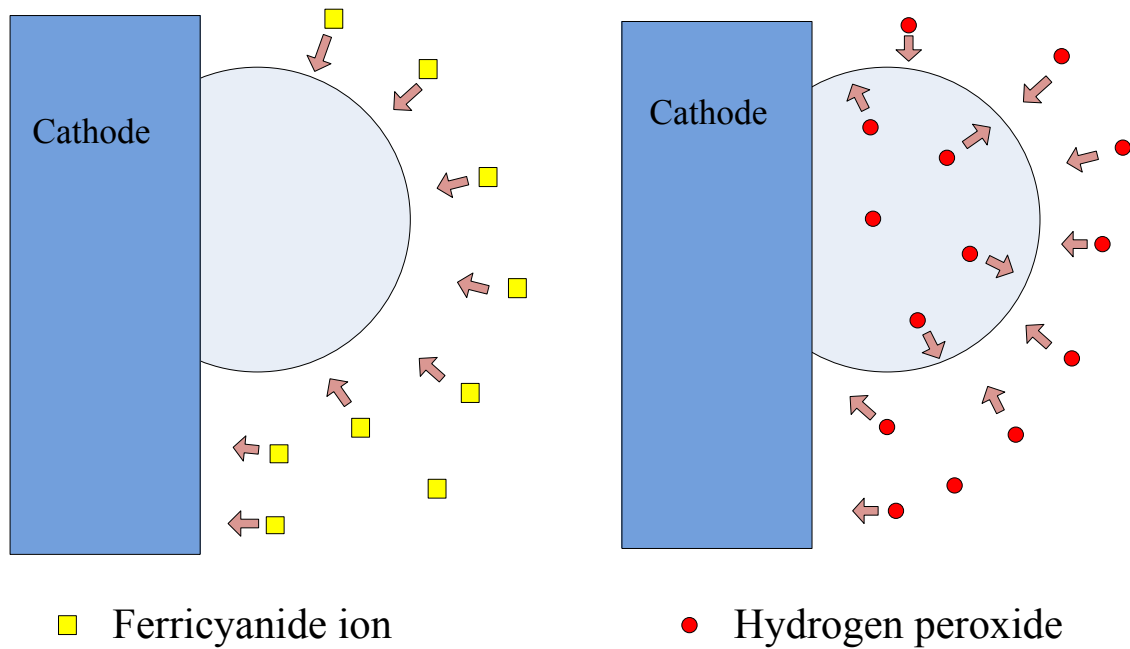
Sherwood numbers remained the same for both reactive species despite differences in their diffusivities [34]. However, it can be seen from Figure 3-10 (a) that, at any given temperature, the Sherwood numbers for ferricyanide and hydrogen peroxide were different. This indicated that the mass transfer correlation obtained from the ferricyanide reaction [15] cannot be directly applied to the hydrogen peroxide reaction. Figures 3-10 (b) and (c) also showed that the Sherwood numbers for hydrogen peroxide were higher than that of ferricyanide under the subcooled boiling and fully developed boiling conditions. The difference of Sherwood numbers for these two species could be attributed to the different natures of the non-volatile and volatile species. A detailed explanation is shown in Figure 3-11.





Figures 3-10. The Sherwood number of ferri-/ferrocyanide and hydrogen peroxide as a function of electrolyte temperature or heat flux for (a) natural convection, (b) subcooled nucleate boiling condition and (c) fully developed nucleate boiling conditions, respectively.

Figure 3-11 illustrates the proposed mechanism of the mass transport phenomenon for ferricyanide ions and hydrogen peroxide under boiling conditions. Under both the subcooled boiling and fully developed nucleate boiling conditions, part of the bubble surface could behave as the working electrode and enhance the electrochemical reaction [35]. The ferricyanide ions only exist in liquid phase, since it is a non-volatile species. The mass transfer of the ferricyanide ions from the bulk solution to the interface would only occur through the liquid phase as shown in Fig. 3-11. However, transfer of hydrogen peroxide could occur through both liquid and vapor phases since hydrogen peroxide would partition into the bubbles during reaction under the boiling condition. Also, the transport rate in vapor phase is much higher than in the liquid phase since the diffusivity of hydrogen peroxide in the vapor phase is several magnitudes higher than in the liquid phase [36]. Therefore, the Sherwood number of hydrogen peroxide increased at a higher rate than that of ferricyanide at both the subcooled nucleate boiling and fully developed nucleate boiling conditions as shown in Figures 3-10 (b) and (c).



Figures 3-11. The proposed mass transfer mechanisms of ferricyanide ion and hydrogen peroxide in the presence of bubbles under boiling condition.

3.4.7 Empirical correlation for mass transfer under pool boiling condition

Figure 3-12 (a) shows the mass and heat transfer coefficients as a function of heat flux. The mass transfer coefficient was calculated using Eq. (1.6) and the heat transfer coefficient was estimated by the Gorenflo correlation [37] with the consideration of the effect of both heat flux and surface roughness on heat transfer coefficient:

$$\frac{h}{h_0} = F(p_r) \left(\frac{q}{q_0} \right)^n \left(\frac{Ra}{Ra_0} \right)^{0.133} \quad (3.13)$$

where h is the heat transfer coefficient, p_r is the reduced pressure, q is the heat flux, $Ra_0 = 0.4 \mu\text{m}$, $h_0 = 5.6 \text{ kW/m}^2\text{K}$ and $q_0 = 20 \text{ kW/m}^2$ are reference values at standardized conditions, the function $F(p_r)$ is shown below:

$$F(p_r) = 1.73 \times p_r^{0.27} + \left(6.1 + \frac{0.68}{1 - p_r}\right)^e p_r^2 \quad (3.14)$$

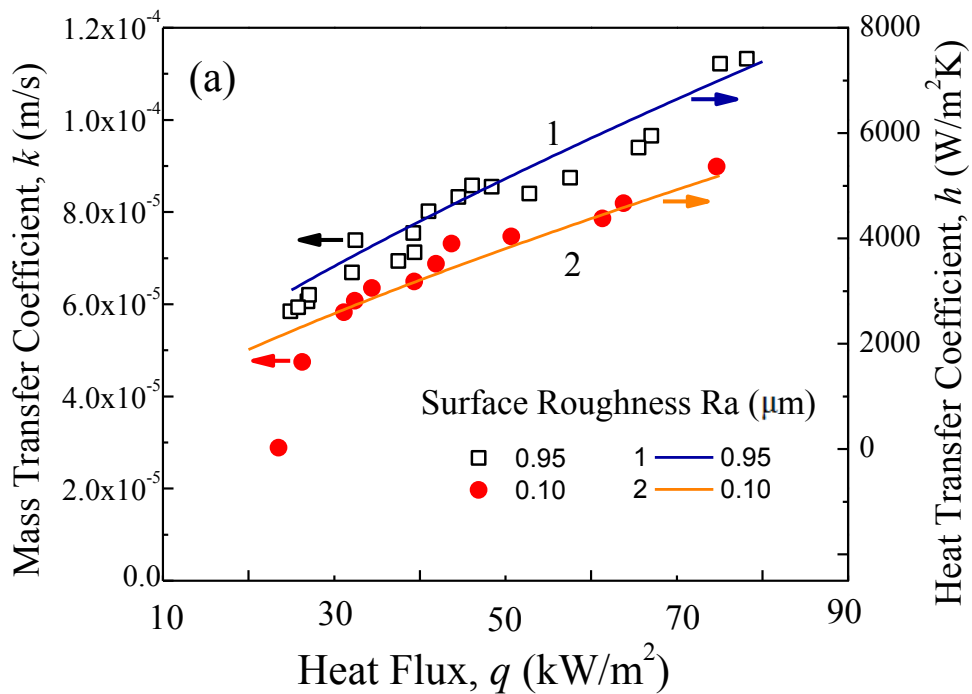
$$e = 0.9 - 0.3 \times p_r^{0.15} \quad (3.15)$$

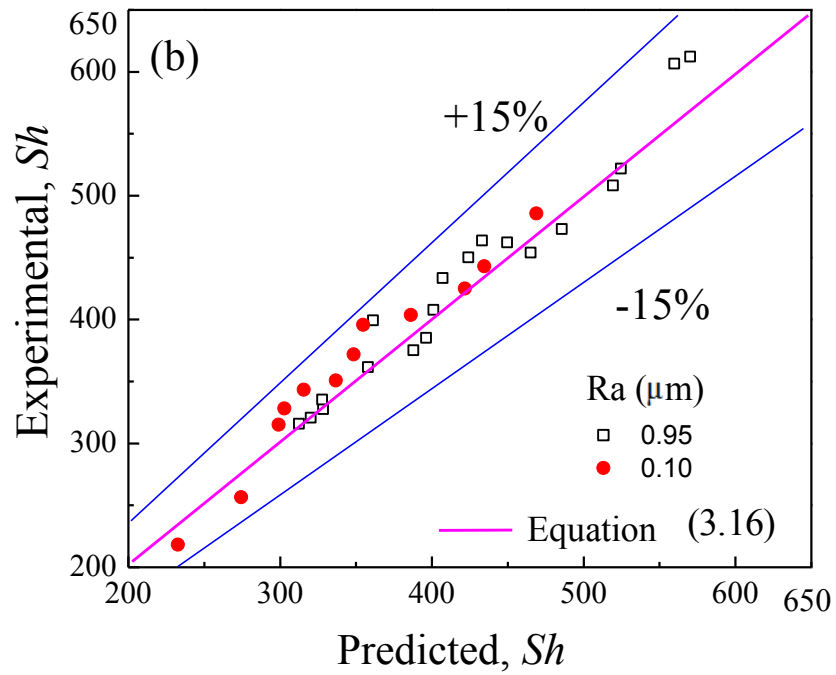
It is shown that the mass transfer coefficient increases with increasing heat flux. Since the increase in the heat flux increases the bubble generation rate which enhances forced convection and thus, increases the mass transfer. Figure 3-12 (a) also shows that the mass transfer coefficient of the rough surface is slightly higher than that of the smooth surface for the same heat flux. Since the rough surface provides more nucleate sites, the energy barrier for bubble generation decreases and increases the number of boiling active sites, resulting in an enhanced mass transfer rate. Moreover, it can be observed that the estimated heat transfer coefficient appears to parallel with the experimentally determined mass transfer coefficient.

As introduced in Section 3.3, all three influence factors: the convection caused by bubble generation, the convection caused by detached bubble flow over the surface, and the non-isothermal convection contribute to the total mass transport rate in the present study. The correlation constants a , b and c in Eq. (3.10) obtained using the experimental data and multiple linear-regression. Substituting the values of a , b and c in Eq. (3.10) gives the following equation:

$$Sh = 2.0898Re_G^{0.5}Sc^{0.487} + 0.0107 \times Ray^{0.5} + 0.0115 \times (Sc Gr)^{0.33} \quad (3.16)$$

Figure 3-12 (b) shows the comparison between the predicted and the experimentally determined *Sherwood* numbers under nucleate boiling conditions. The predicted values were calculated using Eq. (3.16) and the experimental values were obtained using Eq. (1.8). All of the data points are within $\pm 15\%$ error. Therefore, this equation is suitable for predicting the mass transfer behavior of dissolved non-volatile species at nucleate boiling surfaces in the heat flux range 23.4 to 82.7 kW/m² under atmospheric pressure.





Figures 3-12. Mass and heat transfer coefficient (a) and comparison of the experimentally determined and predicted *Sherwood* numbers (b) under pool boiling conditions.

3.5 Conclusions

A novel pool-boiling device was constructed and enabled us to conduct electrochemical measurement directly on boiling surface for the first time. The mass transfer coefficients of both ferricyanide and hydrogen peroxide were experimentally determined at different electrolyte temperatures, under subcooled boiling and fully developed boiling conditions using a novel pool-boiling device. The following conclusions were obtained:

- 1) It was found that the mass transfer rate increased with the increasing solution temperature for both species due to the increase in diffusivities under natural convection.
- 2) Under the subcooled nucleate boiling and fully developed nucleate boiling conditions, the mass transfer coefficient increased with increasing temperature and heat flux for both species, which was mainly ascribed to the forced convection.
- 3) The rate of increase of the Sherwood number of hydrogen peroxide was faster than that of ferricyanide ions with increasing heat flux. This result could be attributed to the fact that the mass transfer of ferricyanide ions only occurs through the liquid phase, while the mass transfer of hydrogen peroxide could occur through both the liquid and vapor phases during the reaction.
- 4) An empirical equation that considers the generation/expansion of the bubble (micromixing), the motion of the detached bubble (macromixing) and non-isothermal convection was proposed and proven to be valid in predicting mass transfer rate under nucleate boiling condition for potassium ferricyanide.

3.6 References

- [1] Lu, Y., "A Flow Impingement Facility for Corrosion and Electrochemical Studies in High Temperature Aqueous Solutions," *CORROSION* 2004, (2004).
- [2] Lu, Y., G. Goszczynski and S. Ramamurthy, "Degradation of alloy 800 under steam generator secondary side crevice conditions," 17th International Conference on Nuclear Engineering, (2009): pp. 1-9.
- [3] King, F., C.D. Litke, M.J. Quinn and D.M. LeNeveu, "The measurement and prediction of the corrosion potential of copper in chloride solutions as a function of oxygen concentration and mass-transfer coefficient," *Corrosion Science*, 37 (1995): pp. 833-851.
- [4] Turner, C.W. and S.J. Klimas, "Deposition of magnetite particles from flowing suspensions under flow-boiling and single-phase forced-convective heat transfer," *The Canadian Journal of Chemical Engineering*, 78 (2000): pp. 1065-1075.
- [5] Turner, C.W., S.J. Klimas and M.G. Brideau, "Thermal resistance of steam-generator tube deposits under single-phase forced convection and flow-boiling heat transfer," *The Canadian Journal of Chemical Engineering*, 78 (2000): pp. 53-60.
- [6] Sathiya Priya, A., V. Muralidharan and A. Subramania, "Development of novel acidizing inhibitors for carbon steel corrosion in 15% boiling hydrochloric acid," *Corrosion*, 64 (2008): pp. 541-552.
- [7] Qi, S.L., P. Zhang, R.Z. Wang and L.X. Xu, "Flow boiling of liquid nitrogen in micro-tubes: Part I – The onset of nucleate boiling, two-phase flow instability and two-phase flow pressure drop," *International Journal of Heat and Mass Transfer*, 50 (2007): pp. 4999-5016.
- [8] Wu, Y.W., G.H. Su, B.X. Hu and S.Z. Qiu, "Study on onset of nucleate boiling in bilaterally heated narrow annuli," *International Journal of Thermal Sciences*, 49 (2010): pp. 741-748.
- [9] Vogt, H., "Heat transfer in boiling and mass transfer in gas evolution at electrodes - The analogy and its limits," *International Journal of Heat and Mass Transfer*, 59 (2013): pp. 191-197.
- [10] Wragg, A.A. and A.K. Nasiruddin, "Ionic mass transfer by free convection with simultaneous heat transfer," *Electrochimica Acta*, 18 (1973): pp. 619-627.
- [11] Sarac, H., A. Wragg and M. Patrick, "An electrochemical mass transfer investigation in the presence of simultaneous subcooled pool boiling," *International Communications in Heat and Mass Transfer*, 30 (2003): pp. 909-920.

- [12] Stephan, K. and H. Vogt, "A model for correlating mass transfer data at gas evolving electrodes," *Electrochimica Acta*, 24 (1979): pp. 11-18.
- [13] Vogt, H., O. Aras and R.J. Balzer, "The limits of the analogy between boiling and gas evolution at electrodes," *International Journal of Heat and Mass Transfer*, 47 (2004): pp. 787-795.
- [14] Abdel-Aziz, M.H., I. Nirdosh and G.H. Sedahmed, "Liquid-solid mass and heat transfer behavior of a concentric tube airlift reactor," *International Journal of Heat and Mass Transfer*, 58 (2013): pp. 735-739.
- [15] Shen, C., A. Afacan, J.-L. Luo, A. Siddiqui and S.J. Klimas, "Mass transfer on nucleate boiling surfaces using the electrochemical method," *International Journal of Heat and Mass Transfer*, 78 (2014): pp. 289-293.
- [16] Shen, C., A. Afacan, J. Luo and S.J. Klimas, "Mass transfer of dissolved oxygen using rotating cylinder electrode under bulk boiling conditions," *International Journal of Heat and Mass Transfer*, 70 (2014): pp. 162-168.
- [17] Stewart, K.L. and A.A. Gewirth, "Mechanism of electrochemical reduction of hydrogen peroxide on copper in acidic sulfate solutions," *Langmuir*, 23 (2007): pp. 9911-9918.
- [18] Nickchi, T. and A. Alfantazi, "Kinetics of passive film growth on Alloy 800 in the presence of hydrogen peroxide," *Electrochimica Acta*, 58 (2011): pp. 743-749.
- [19] Nickchi, T. and A. Alfantazi, "Corrosion characteristics of alloy 800 in aqueous solutions up to 200 C," *Journal of The Electrochemical Society*, 160 (2013): pp. C64-C76.
- [20] Lin, C., Y. Kim, L. Niedrach and K. Ramp, "Electrochemical corrosion potential models for boiling-water reactor applications," *Corrosion*, 52 (1996): pp. 618-625.
- [21] Arvia, A.J., S.L. Marchiano and J.J. Podesta, "The diffusion of ferrocyanide and ferricyanide ions in aqueous solutions of potassium hydroxide," *Electrochimica Acta*, 12 (1967): pp. 259-266.
- [22] Hall, S.B., E.A. Khudaish and A.L. Hart, "Electrochemical oxidation of hydrogen peroxide at platinum electrodes. Part 1. An adsorption-controlled mechanism," *Electrochimica Acta*, 43 (1998): pp. 579-588.
- [23] Edward, J.T., "Molecular volumes and the Stokes-Einstein equation," *Journal of Chemical Education*, 47 (1970): pp. 261.
- [24] Coleman, H.W. and W.G. Steele, *Experimentation and uncertainty analysis for engineers* 1999: John Wiley & Sons Incorporated.
- [25] Holman, J.P., *Experimental methods for engineers* 2001: McGraw Hill.

- [26] Rohsenow, W.M., J.P. Hartnett and Y.I. Cho, *Handbook of heat transfer*. Vol. 3. 1998: McGraw-Hill New York.
- [27] Fukunaka, Y., K. Suzuki, A. Ueda and Y. Kondo, "Mass-Transfer Rate on a Plane Vertical Cathode with Hydrogen Gas Evolution," *Journal of The Electrochemical Society*, 136 (1989): pp. 1002-1009.
- [28] Alkire, R. and P.-Y. Lu, "Effect of Hydrogen Evolution on Current Distribution during Electrodeposition at Vertical Electrodes," *Journal of The Electrochemical Society*, 126 (1979): pp. 2118-2124.
- [29] Hall, P. and B. Selinger, "Better estimates of exponential decay parameters," *The Journal of Physical Chemistry*, 85 (1981): pp. 2941-2946.
- [30] Nickchi, T. and A. Alfantazi, "Electrochemical corrosion behaviour of Incoloy 800 in sulphate solutions containing hydrogen peroxide," *Corrosion Science*, 52 (2010): pp. 4035-4045.
- [31] Ferrell, R.T. and D.M. Himmelblau, "Diffusion coefficients of nitrogen and oxygen in water," *Journal of Chemical and Engineering Data*, 12 (1967): pp. 111-115.
- [32] Warriar, G.R. and V.K. Dhir, "Heat Transfer and Wall Heat Flux Partitioning During Subcooled Flow Nucleate Boiling---A Review," *Journal of Heat Transfer*, 128 (2006): pp. 1243-1256.
- [33] Kurihara, H. and J. Myers, "The effects of superheat and surface roughness on boiling coefficients," *AIChE Journal*, 6 (1960): pp. 83-91.
- [34] Pfeffer, R. and J. Happel, "An analytical study of heat and mass transfer in multiparticle systems at low Reynolds numbers," *AIChE Journal*, 10 (1964): pp. 605-611.
- [35] Tsai, W., P. Hsu, Y. Hwu, C. Chen, L. Chang, J. Je, H. Lin, A. Groso and G. Margaritondo, "Building on bubbles in metal electrodeposition," *Nature*, 417 (2002).
- [36] McMurtrie, R. and F. Keyes, "A measurement of the diffusion coefficient of hydrogen peroxide vapor into air," *Journal of the American Chemical Society*, 70 (1948): pp. 3755-3758.
- [37] Collier, J.G. and J.R. Thome, *Convective boiling and condensation* 1994: Oxford University Press.

Chapter 4 Phase III -- flow boiling conditions

In previous Phases I and II, the mass transfer coefficients were obtained under bulk boiling and pool boiling conditions. In both phases, the experiments were conducted under atmospheric pressure and for electrolyte temperatures were varied up to 125 °C. In this chapter (Phase III), a flow loop is designed and constructed to determine the mass transfer coefficient under the flow boiling condition. The electrolyte flow rate, temperatures and operating pressure will be varied.

4.1 Introduction

The mass transfer under the flow boiling condition is a fundamental issue that can cause many industrial problems, such as fouling in the boiler [1]; film cooling in the ducts [2]; and the material degradation of the wire plating cells [3] and the electrochemical reactors [4], as well the exchange tubing in the steam generator [5]. The flow boiling is a complex condition, which can include the elevated pressures and temperatures (above 100 °C), heat transfer, vapor generation (gas bubbling on the solid surface) and vapor-liquid two-phase flow [6-8].

The electrochemical approach to investigating mass transfer behavior in annular shape tubing under isothermal conditions has been reported previously [9]. Lin et al. [10] examined the mass transfer rate from a flowing electrolyte to the inside surface in a annular shape tubing. They measured the mass transfer rate for the cathodic reaction of ferricyanide ion and quinone. Their results showed good agreement with Leveque's (1928) equation in the laminar flow region and with Chilton-Colburn's equation (1934) in the turbulent flow region. Ross and Wragg [11, 12]

investigated free and forced convective mass transfer around the horizontal electrode and annuli. The mass transfer rates have been determined using the electrochemical method of depositing copper from acidified copper sulphate solutions on to copper cathodes. Ross and Wragg [11, 12] proposed a semi-empirical equation for predicting the mass transfer rate on the inner wall of an annular flow cell for both laminar and turbulent flow regions. They stated that their equation represent their data very well. They also stated that the mass transfer behavior under flow boiling condition studies are very limited in the open literature. The reason for the lack of investigation is the experimental difficulties of conduct measurement on the flow boiling surface. Although the flow boiling phenomenon has been extensively studied in the field of heat transfer [13-15]. However, the traditional analysis between heat and mass transfer cannot be applied to the flow boiling condition due to the boundary layer discontinuity [16]. Therefore, there is no available theory to explain solid-liquid mass transfer behavior under flow boiling condition [17].

It can be concluded from the above literature survey that there is a knowledge gap for the mass transfer behavior under flow boiling conditions both experimentally and theoretically. In this chapter, a novel flow boiling setup is designed and constructed. The mass transfer rates are first measured for elevated temperatures and pressures as well as various electrolyte flow rates under a single-phase condition to verify the experimental setup. Then, the mass transfer coefficient of hydrogen peroxide on a boiling surface electrode under a flow boiling condition will be obtained and a new empirical correlation will also be proposed to represent the mass transfer behavior under a flow boiling condition.

4.2 Experimental setup

To measure the mass transfer of dissolved species in flow boiling condition, a novel experimental setup is designed. The schematic diagram of the flow loop is shown in Figure 4-1. Two stainless steel storage tanks were used to store the chemistry-controlled working fluid and to collect the return working fluid. A positive displacement pump (Neptune 525-S-N3) with a maximum discharge pressure up to 6.2 MPa was used to circulate electrolyte solution and its flow rate was measured using a turbine meter (Omega FTB504-CK). The electrolyte solution temperature was controlled using an electrically heated preheater. Then, the electrolyte solution temperature was further heated to the boiling point in the flow cell using hot oil flowing between heating bath (Cole-Parmer SS 13L) and the inner tube. The mineral oil (SIL 180), which had a heat capacity of 1.51 kJ/kg K, was used as heating oil. The electrochemical measurements were conducted in the electrochemical flow cell under flow boiling condition. The electrolyte solution was cooled to near room temperature using a shell and tube heat exchanger (S.E.C. Heat exchangers Model C-8.2) before returned back to the Solution Tank 2. The pressure of the loop was controlled using a backpressure regulator (Equilibra GSD4-SS316) and a check valve. K-type thermocouples were used to measure the electrolyte temperatures after preheating and just entering to the electrochemical flow cell as well as the temperatures of the heating oil before entering and after leaving the specimen (T_2 and T_3).

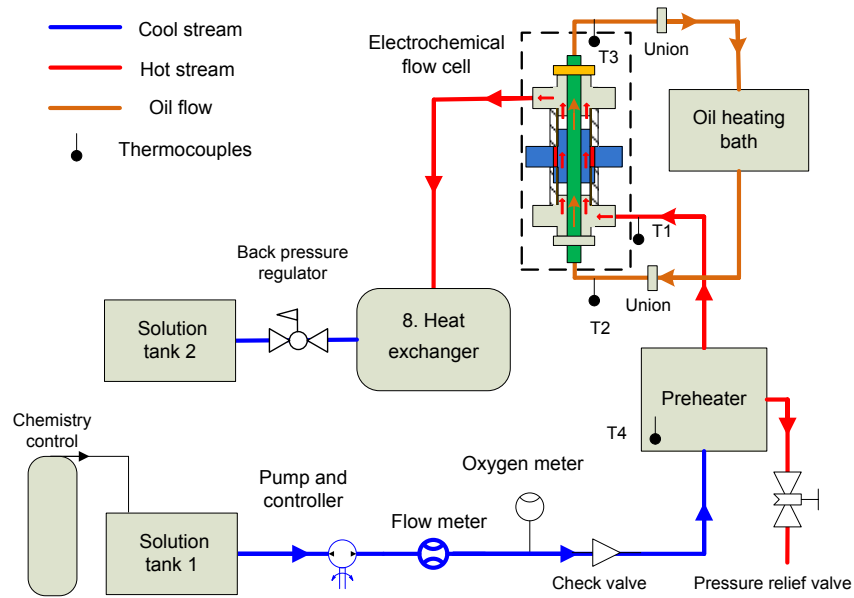


Figure 4-1. Schematic diagram of flow loop

Figures 4-2 and 4-3 show the detailed schematic of the electrochemical flow cell. The flow cell contained a double tube structure. The heated oil flows through the inner tube and the electrolyte solution flows through the annular space between the two tubes. The inner tube was made of Alloy 800, and was used as a working electrode. In the center of the tube, 30 mm of bare metal was exposed to the electrolyte solution. Other parts of the cell were insulated electrically using PTFE coating. A cross union was located in the middle of the electrochemical flow cell and was used to hold the counter and the reference electrodes as shown in Figure 4-3. A platinum tube ring with a diameter of 15.5 mm and length 30 mm was used as a counter electrode. A pressure balanced Ag/AgCl reference electrode (Corr Instruments, LLC), which can be operated up to 250 °C was used to provide constant potential during the measurement.

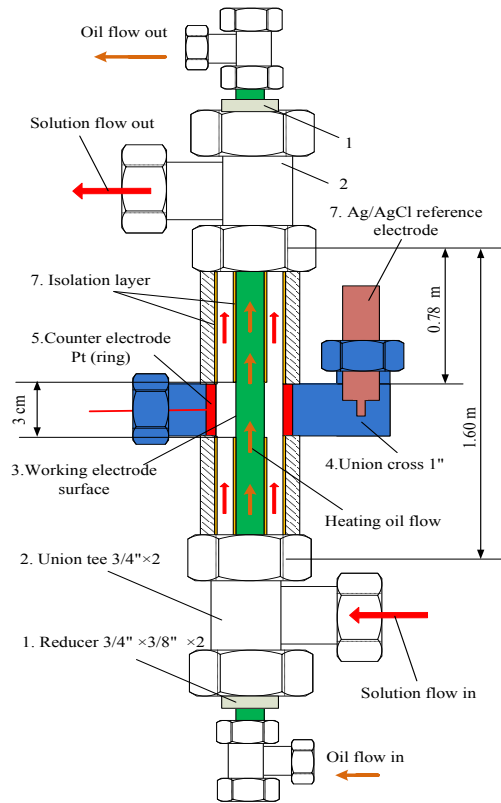


Figure 4-2. Schematic diagram of electrochemical flow cell

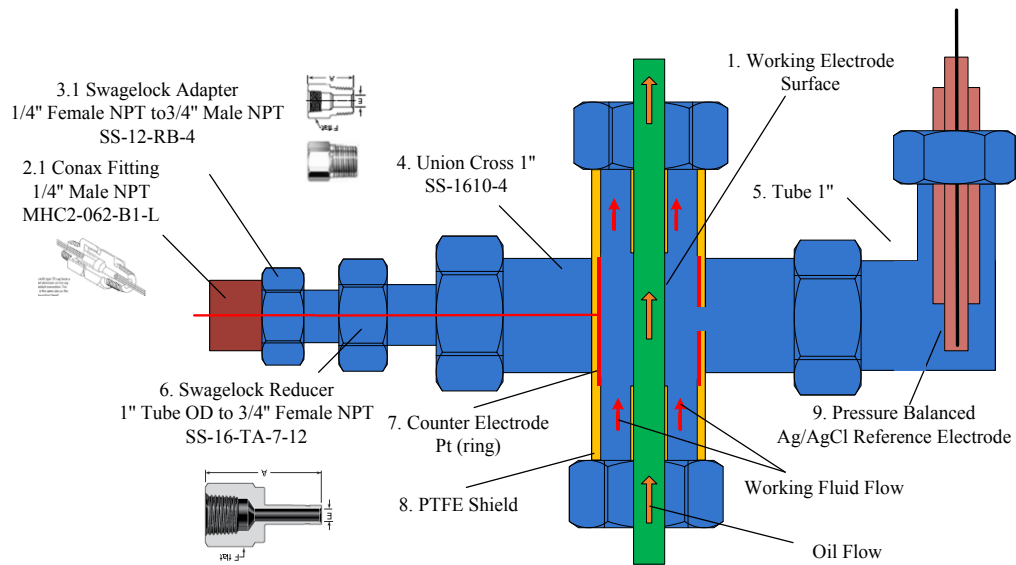


Figure 4-3. Schematic diagram of the experimental part

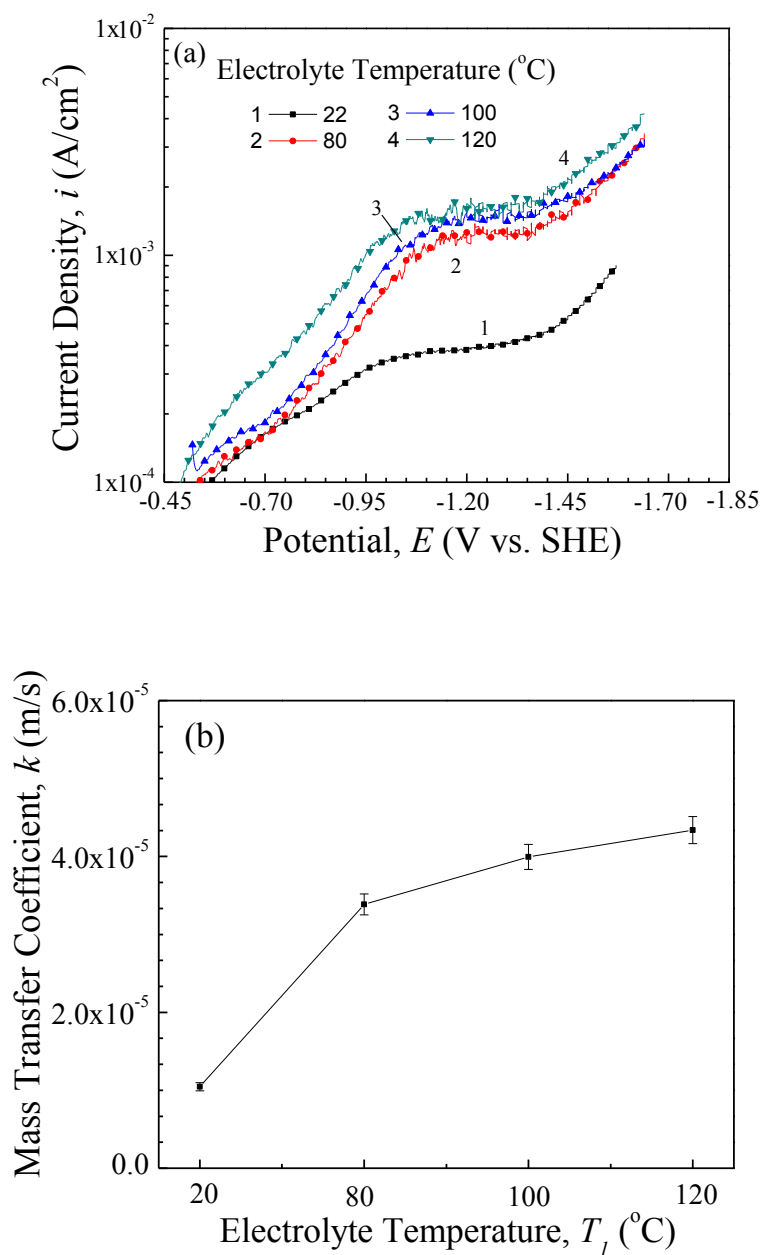
4.3 Experimental procedure

Before each test, the specimens were polished using #60 grit sand paper to obtain an average roughness of $0.95\ \mu\text{m}$ so that the roughness was close to the conventional operating condition of heat exchanger tubes in the steam generators. The surface roughness was tested by the Pocket Surf roughness tester. The electrolyte contained $0.025\ \text{M Na}_2\text{SO}_4$ as a supporting electrolyte, and a $0.002\ \text{M H}_2\text{O}_2$ solution was used as the reaction species. Before each measurement, the electrolyte solution was deoxygenated by purging the solution with pure nitrogen gas for 2 hours. The electrochemical measurements were conducted using a Gamry Reference 600 electrochemical station. Potentiodynamic polarization was applied by sweeping the potential in the negative direction at rate of $2\ \text{mV/s}$ until the current density reached $1\ \text{mA/cm}^2$. The mass transfer coefficient and heat flux were calculated using Eqs (1.6) and (3.1), respectively. The mass transfer rate of H_2O_2 was first investigated under single-phase flow and flow boiling conditions. Under the single-phase condition, the experiments were conducted under electrolyte temperature up to $120\ ^\circ\text{C}$, flow rate up to $44.6\ \text{kg/m}^2\text{s}$ and pressure up to $652\ \text{kPa}$. Under the flow boiling condition, the measurements were conducted under electrolyte entrance temperature up to $85\ ^\circ\text{C}$, flow rate up to $44.6\ \text{kg/m}^2\text{s}$, oil temperature up to $160\ ^\circ\text{C}$ and the operating pressure kept constant at $100\ \text{kPa}$. The diffusivity values of hydrogen peroxide are also included in Table 3-1 where the diffusivity at $20\ ^\circ\text{C}$ was obtained from literature [18] and the values for other temperatures were calculated using the Stokes-Einstein equation [19].

4.4 Results and discussion

4.4.1 Effect of temperature on mass transfer rate

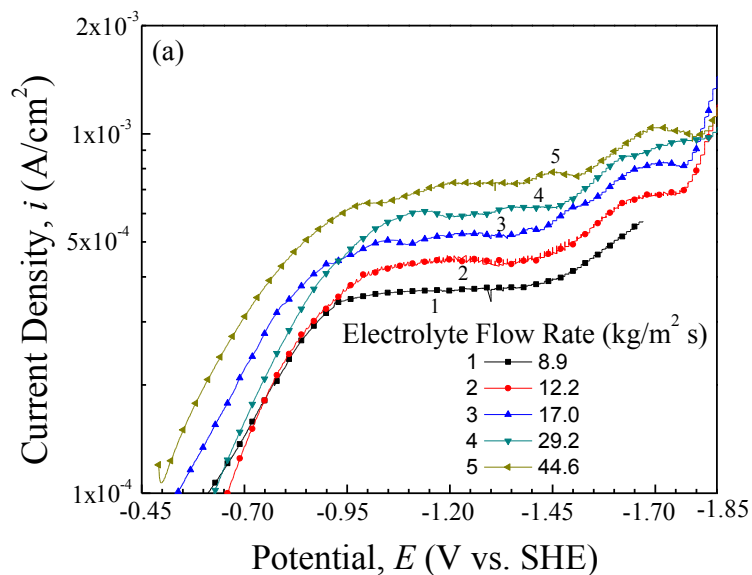
Figures 4-4 (a) and (b) show the polarization curves and mass transfer coefficient for the hydrogen peroxide reaction as a function of the solution temperature while keeping the operating pressure and electrolyte flow rate constant at 445 kPa and 17 kg/m² s, respectively. At this operating pressure, the saturation point of water is above 145 °C. Therefore, it is believed that the flow type for all temperatures is a single-phase flow (i.e. non-boiling). It can be observed from the Figure 4-4 (a) that for all electrolyte solution temperatures, the current plateaus in the potential range between -1.15 to -1.35 V vs. standard hydrogen electrode (SHE) for the hydrogen peroxide reaction. These plateaus indicate that the mass transfer controlled region can be reached for all these tests. It can also be seen that the current value of plateau region increases with the increasing the electrolyte solution temperature, which indicates that the mass transfer controlled reaction rate increases. Then, the mass transfer coefficients were calculated using Eq. (1.6) and the experimental determined limiting current density. The mass transfer coefficient increased 5.1 times with the increasing the electrolyte temperature from 22 °C to 120 °C as shown in Figure 4-4 (b). The increase in the electrolyte temperature increases the diffusivity of the dissolved species (i.e. hydrogen peroxide). Therefore, the enhancement in the mass transfer coefficient is only due increase in diffusivity of hydrogen peroxide.

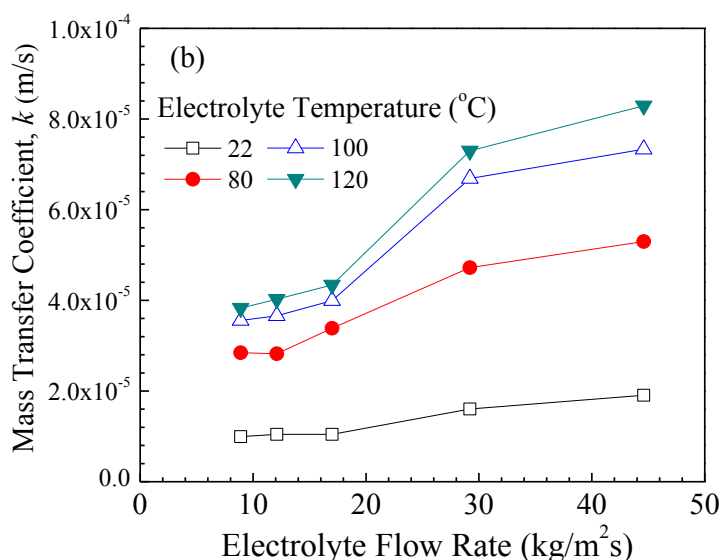


Figures 4-4. (a) Cathodic polarization curves and (b) the calculated mass transfer coefficient for the flow loop system at various electrolyte temperatures (Electrolyte flow rate 17.0 kg/m²s; Operating pressure 445 kPa).

4.4.2 Effect of the flow rate on the mass transfer rate

Figure 4-5 (a) shows the polarization curves for the hydrogen peroxide reaction as a function of electrolyte flow rates, while keeping the operating pressure and electrolyte temperature constant at 445 kPa and 22 °C, respectively. It can be observed from Figure 4-5 (a) that there are clear current plateaus in the potential range between -1.95 to -1.45 V vs SHE for the hydrogen peroxide reaction. These plateaus indicate that the mass transfer controlled region can be reached in these tests. It can be seen that the similar plateaus were also obtained for the electrolyte temperatures of 22, 80, 100 and 120 °C. Figure 4-5 (b) shows the calculated mass transfer coefficient as a function of the electrolyte flow rate for various electrolyte temperatures while keeping the operating pressure constant at 445 kPa. The mass transfer rate is increases with the increasing electrolyte flow rate for all electrolyte temperatures. The higher electrolyte flow rate will induce more forced convection. Thus, the mass transfer coefficient will increase when the electrolyte flow rates increase. These trends agree well with the classic Leveque equation [20].



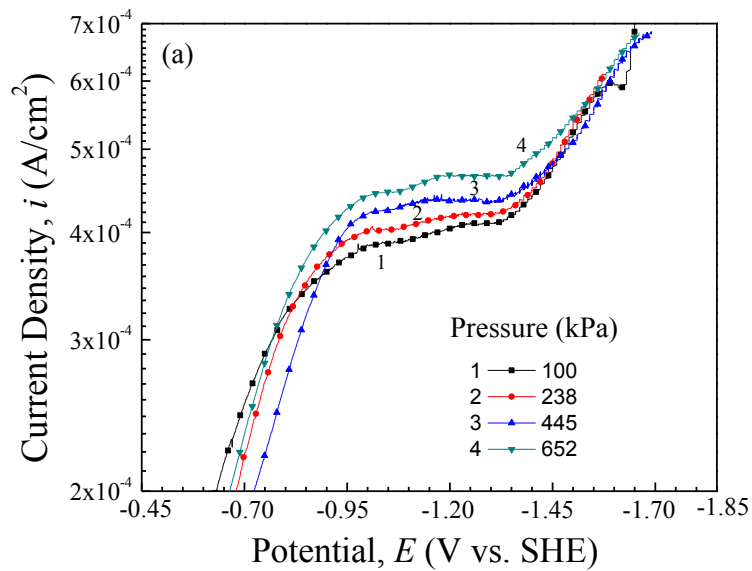


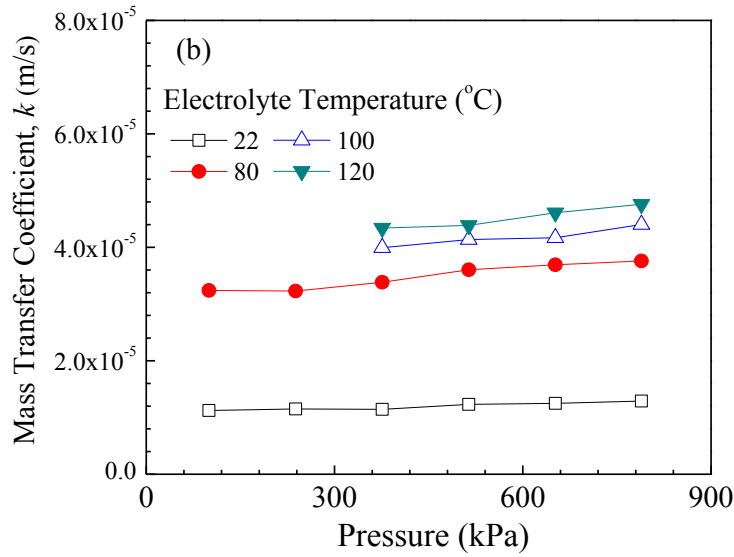
Figures 4-5. (a) Cathodic polarization curves (Electrolyte temperature 22 °C; Operating pressure 445 kPa) and (b) the calculated mass transfer coefficient as a function electrolyte flow rate for various electrolyte temperatures (Operating pressure 445 kPa).

4.4.3 Effect of the operating pressure on the mass transfer rate

Figure 4-6 (a) shows the polarization curves obtained for various operating pressures while keeping the electrolyte temperature and the flow constant at 22 °C and 17.0 kg/m² s, respectively. It can be observed from the Figure 4-6 (a) that there are clear current plateaus in the potential range between -0.95 to -1.35 V vs SHE for the hydrogen peroxide reaction. These plateaus indicate that the mass transfer controlled region can be reached in these tests. Figure 4-6 (b) shows the calculated mass transfer coefficients as a function of operating pressure for various electrolyte temperatures. In these tests, the operating pressure was varied from 100 to 652 kPa and for each operating pressure, the electrolyte temperature was varied from 22 to 120 °C. The electrolyte flow rate was kept constant at 17.0 kg/m² s. The data points for the operating

pressures of 100 and 238 kPa at 100 and 120 °C are not included because the electrolyte temperature was exceeded the saturation point. The mass transfer coefficient is increased when the operating pressure increased. It can be seen that the increase in the mass transfer rate is about 15% when the operating pressure is increased from 100 to 789 kPa. The increase of pressure enhanced the inner energy of the electrolyte solution, thus increasing the movement of dissolved hydrogen peroxide [21]. As a result, the mass transfer coefficient increases with the increase of the operating pressure as it was expected





Figures 4-6. (a) Cathodic polarization curves (Electrolyte temperature 22 °C; Electrolyte flow rate 17.0 kg/m² s) and (b) the calculated mass transfer coefficient as a function of operating pressure and for various electrolyte temperatures (Electrolyte flow rate 17.0 kg/m² s).

Carbin and Gabe [22] also studied the mass transfer behavior through the annular geometry but only considering the effect of the electrode length. They proposed the following correlation based on Ross and Wragg's work [11]:

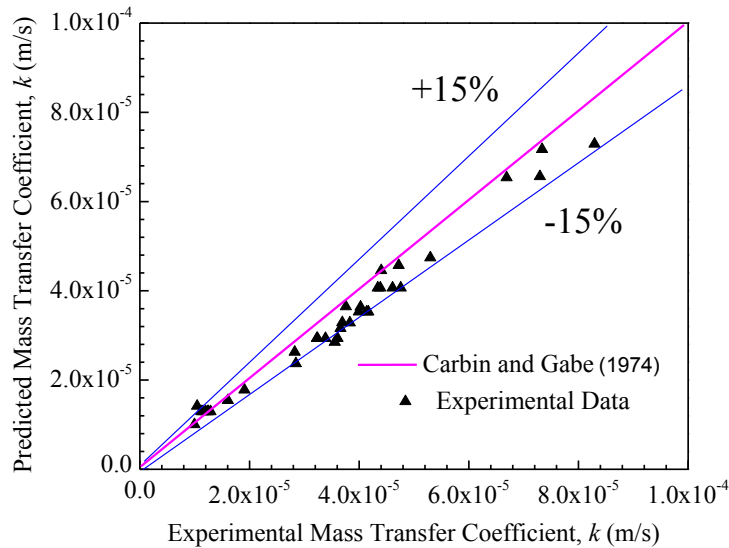
$$Sh = 3.93 Re^{0.32} Sc^{0.33} \left(\frac{d_c}{L_e} \right)^{0.35} \quad (4.1)$$

Therefore, the single phase mass transfer coefficient can be obtained based on Eq. (4.1), within the range of $100 < Re < 50000$ and $100 < Sc < 2000$:

$$k_{sp} = 3.93 \frac{D}{d_c} Re^{0.32} Sc^{0.33} \left(\frac{d_c}{L_e} \right)^{0.35} \quad (4.2)$$

where d_c is the hydraulic diameter and L_e is the length of the electrode. They stated that their correlation agreed well with other's work [9, 10].

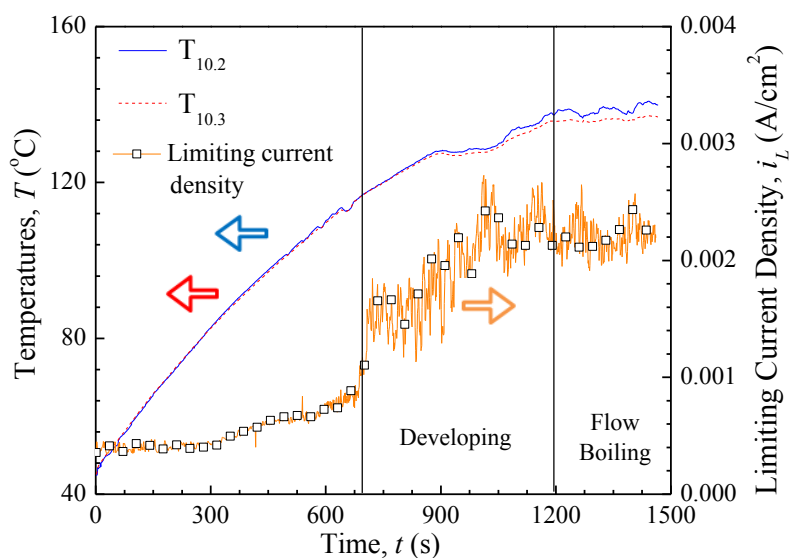
Figure 4-7 shows a comparison between the experimentally determined mass transfer coefficient and the predicted mass transfer coefficient obtained using the Eq. (4.2). It can be observed that 95% of the data under the single phase condition agree with the correlation within $\pm 15\%$ error. This indicates that the electrochemical method can be used to measure the mass transfer coefficient under single phase flow conditions.



Figures 4-7. Comparison between the experimentally determined present studies mass transfer coefficient and predicted value.

4.4.4 Mass transfer measurement under the flow boiling condition

Figure 4-8 shows the electrolyte solution temperature and limiting current density as a function of time. In these tests, the electrolyte solution temperature in the flow cell was varied using hot mineral oil flowing between heating bath and the inner tube. The mineral oil temperature was varied from room temperature to 150 °C while the applied potential was kept constant at -1.2 vs. SHE. For all above test, the mass transfer controlled reaction region was obtained. The flow rate of electrolyte solution was varied such that the flow regime varied from single phase to flow boiling condition (two-phase flow). The temperatures of the heating oil before entering, T_2 and after leaving the specimen, T_3 before and after the electrochemical measurement region are also shown in Figure 4-8. It can be seen that there is a sudden increase in the electrolyte temperature and in the limiting current density at 700 s. This sudden increase would attribute to the phase changing in the electrolyte solution. It is speculated that at 700 s, the flow boiling (two-phase flow) regime would occurs when the oil temperature reaches to 110 °C, which is higher than the saturation point of the electrolyte solution. The initiation and expand of the boiling bubbles induced a sudden enhancement of the forced convection on the specimen and bubble surfaces. Therefore, the measured current value shows a sudden increase. Between the time between 700 s and 1200 s, the limiting current density increases with the increasing temperatures, which indicates that the mass transfer rate was increased. The reason for this increase may due to the flow regime changed from the subcooled flow boiling to the fully developed flow boiling condition. After 1200 s, both the temperature and the current density remain constant. This indicates that the fully developed flow boiling regime is reached and the mass transfer controlled reaction has a stable reaction rate.



Figures 4-8. Potentiostatic tests for increasing oil temperatures (Operating pressure 100 kPa; Electrolyte flow rate $17.0 \text{ kg/m}^2 \text{ s}$).

Figure 4-9 shows the cathodic polarization curves for the single-phase and flow boiling conditions. Both measurements were conducted under the constant electrolyte solution flow rate of $17 \text{ kg/m}^2 \text{ s}$, entrance electrolyte solution temperature $85 \text{ }^\circ\text{C}$ and operating pressure at 100 kPa. For the single-phase flow condition, the oil temperature was kept at $85 \text{ }^\circ\text{C}$ and for the flow boiling condition; the oil temperature was increased to $150 \text{ }^\circ\text{C}$. Clear current plateaus can be observed for both single-phase and flow boiling conditions. According to the open literature, this is the first time the mass transfer rate is experimentally determined in-situ under flow boiling condition using the electrochemical method. Also, it can be calculated that the mass transfer coefficient for single phase and flow boiling conditions are 3.24×10^{-5} and $6.38 \times 10^{-5} \text{ m/s}$, respectively. The mass transfer controlled reaction rate under the flow boiling condition is 1.97 times higher than that under the single-phase flow condition. There are two main reasons causing

this enhancement. First, the surface electrolyte temperature under the flow boiling condition is higher than that under the single-phase flow condition. But the mass transfer enhancement caused by the temperature increase is limited. The experimental results show that for each 20 °C rise causes the mass transfer rate increase by only 10 %. The other reason for the mass transfer enhancement is the effect of boiling bubbles. The micro-mixing and macro-mixing effects caused by the generation and movement of boiling bubbles enhanced the forced convection, also the two-phase flow breaks the diffusion layer and reduced the concentration gradient. Thus the mass transfer rate increased vastly due to the effect of boiling bubbles.

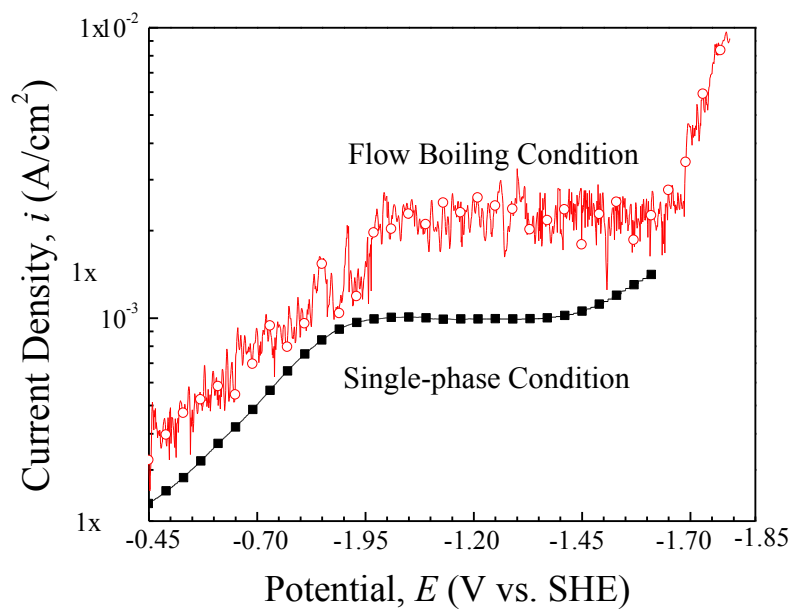
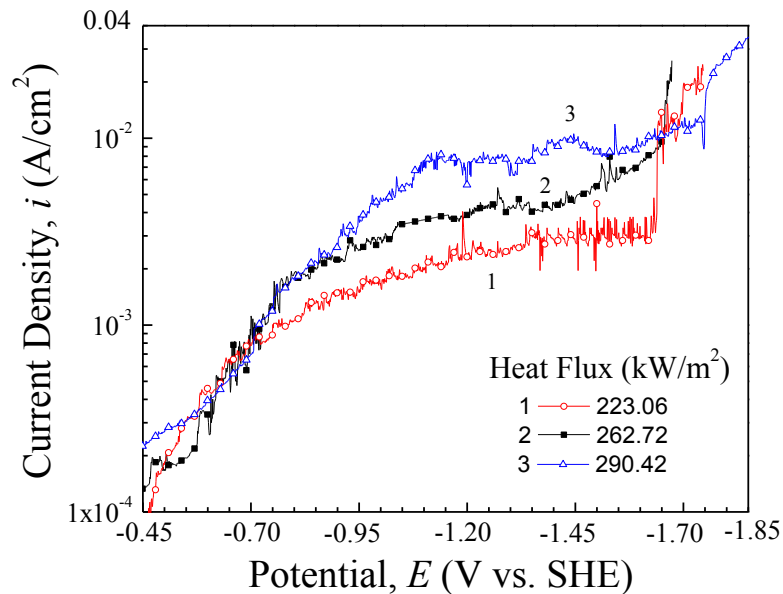


Figure 4-9. Cathodic polarization curves for single-phase and flow boiling conditions. (Operating pressure 100 kPa; Electrolyte flow rate 17.0 kg/m² s).

Figure 4-10 shows the cathodic polarization curves for the hydrogen peroxide reaction under flow boiling conditions for various heat fluxes. It can be seen that for all heat fluxes, the current plateaus in the potential range between -1.2 and -1.5 V (SHE). These curves prove that the mass

transfer rate can be measured successfully under the flow boiling condition using the electrochemical method. When the potential in the potentiostatic test drops below 1.60 V, water began to decompose and the hydrogen evolution reaction begins. This reaction is not mass transfer controlled. Figure 4-10 also shows that the values of the current plateau increase with the increasing of the heat flux. Because the increasing heat flux increases the vapor generation rate, which means more boiling and hence more bubbles are generated on the surface of the specimen. When the bubbles expand and detach, the diffusion layer was broke by the movement [23, 24], decrease the concentration gradient and increase the forced convection. All of these effects increase the mass transfer rate from the bulk solution to the specimen interface, thus leading to a higher mass transfer coefficient.



Figures 4-10. Cathodic polarization curves under the flow boiling condition (Operating pressure 100 kPa).

4.4.5 Empirical correlation for mass transfer behavior under the flow boiling condition

One of the classic correlation for the flow boiling heat transfer coefficient was developed by Chen (1966) [25]. The heat transfer coefficient is the summation of heat transfer coefficient contributed by both the pool boiling effect and the flow rate effect. This correlation has been further refined by Gungor and Winterton (1986) [26] for applications for both vertical and horizontal flows under saturated and subcooled boiling conditions shown as follows:

$$h_{fb} = E_1 h_{pool} + E_2 h_{sp} \quad (4.3)$$

where h is the heat transfer coefficient, the subscripts *pool* and *sp* refer to pool boiling and single-phase forced convection, respectively. The variable E_1 is the suppression factor and E_2 is the enhancement factor. The following the Dittus-Bolter (1930) [27] and Cooper (1984) [28] correlations can be used to determine the heat transfer coefficients contributed by the pool boiling and the single phase forced convective terms:

$$h_{pool} = 55Pr^{0.12}(\log_{10} Pr)^{-0.55}M^{-0.5}q^{0.67} \quad (4.4)$$

$$h_{sp} = 0.023\frac{\lambda}{d}Re^{0.8}Pr^{0.4} \quad (4.5)$$

where Pr is the Prandtl number, M is the molecular weight, q is the heat flux, λ is the thermal conductivity and d is the tubing diameter.

The suppression factor, E_1 and the enhancement factor, E_2 can be calculated using the following equations

$$E_1 = 1 + 24000 Bo^{1.16} + 1.37 (1/X_{tt})^{0.67} \quad (4.6)$$

$$E_2 = \frac{1}{1 + 1.15 \times 10^{-6} E_1^2 Re^{1.17}} \quad (4.7)$$

where Bo is the boiling number and X_{tt} is the Martinelli parameter [26]. Gungor and Winterton's study [26] stated that the mean deviation between the calculated and measured flow boiling heat transfer coefficient was within $\pm 21.4\%$ for the saturated boiling region.

Using the similar analogy, the flowing correlation is proposed to predict the mass transfer coefficient for the two-phase flow condition. The proposed correlation is the summation of the mass transfer coefficient from pool boiling effect and the flow effect. Thus:

$$k_{fb} = F_1 k_{pool} + F_2 k_{sp} \quad (4.8)$$

where k_{pool} is the mass transfer coefficient due to pool boiling and k_{sp} is the mass transfer coefficient due to the flow rate effect. According to Carbin and Gabe's [22] study, the mass transfer coefficient for the single phase annular flow condition, k_{sp} have been showed in Eq. (4.2). Also, from the analysis in the previous study [29], there are three factors contribute to the total mass transfer under pool boiling condition: micro-mixing, macro-mixing and non-isothermal convection. The mass transfer coefficient due to pool boiling, k_{pool} can be obtained based on Eq. (3.16) shown as follows:

$$k_{pool} = \frac{2.09}{d_c} \left(\frac{V_G d_b D}{A} \right)^{0.5} + \frac{0.01 D Ray^{0.5}}{d_c} + \frac{0.012 D (Sc Gr)^{0.33}}{d_c} \quad (4.9)$$

where V_G is the gas evolution rate, d_b is the break off diameter of the gas bubbles and can be estimated using the following Equations. [30, 31]:

$$V_G = \frac{J_L}{V_M M \lambda_L} \quad (4.10)$$

$$d_b = 0.851 \theta \left(\frac{2\sigma_s}{g(\rho_L - \rho_G)} \right)^{0.5} \quad (4.11)$$

where J_L is the power of latent heat, V_M is the molar volume, λ_L is the latent heat of evaporation, θ is the contact angle, σ_s is the surface tension, g is the gravity, ρ_L and ρ_G are the density of liquid and vapor phases, respectively.

Then, using a linear regression algorithm between Eq. (4.8) in conjunction with the flow boiling mass transfer experimental data the following the proposed mass transfer correlation was obtained:

$$k_{fb} = 0.69 k_{pool} + 1.12 k_{sp} \quad (4.12)$$

In equation (4.12) the constant F_1 is smaller than unity, which indicates that the boiling bubble enhancement in mass transfer in the flow boiling environment is not significant as opposed to the pool boiling condition. Also, the constant F_2 is larger than unity reflects that the single phase forced convection mass transfer under the flow boiling is higher compare to the single-phase condition.

Figure 4-11 shows the comparison between the experimental and predicted mass transfer coefficients calculated using Eq (4.12). It can be seen that all experimentally determined the mass transfer coefficients are within $\pm 10\%$ error of the predicted values. Therefore, this equation is valid to predict mass transfer behavior under flow boiling in annuli for the Reynolds number, Re range of 200 and 1000 and a heat flux up to 280 kW/m^2 .

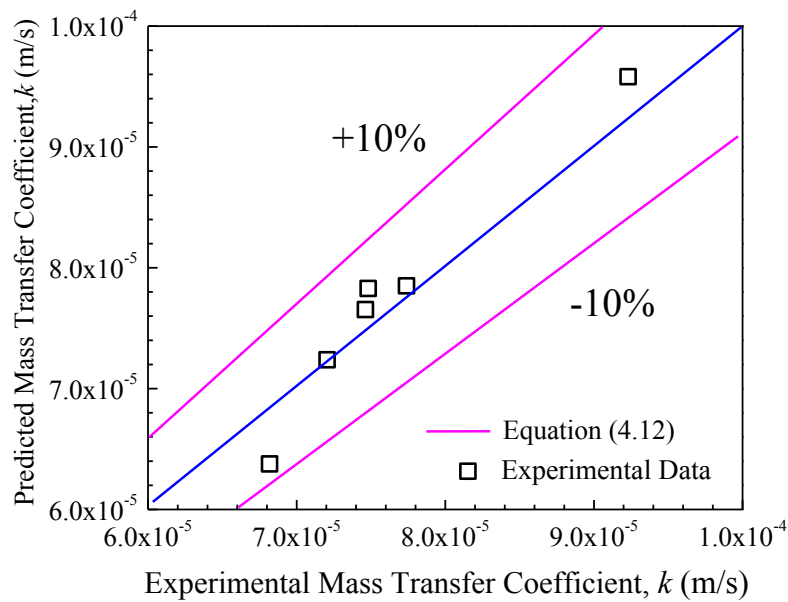


Figure 4-11. Comparison between the experimentally determined and predicted mass transfer coefficient under the flow boiling condition.

4.5 Conclusions

The mass transfer coefficients of hydrogen peroxide under both single-phase flow and two-phase flow boiling conditions were obtained using a novel flow loop setup and the electrochemical method for the first time. The following conclusions were obtained:

- 1) Under single-phase flow condition, the mass transfer rate was found to increase with the increasing electrolyte temperature, flow rate and operating pressure. The experimental data obtained under single-phase flow condition showed good agreement with the empirical equation given in the literature.

- 2) Under flow boiling condition, for the first time, the mass transfer coefficients of the hydrogen peroxide were successfully obtained experimentally using electrochemical method at elevated temperatures and pressures for both single-phase flow and flow boiling conditions. A new mass transfer correlation was proposed and found to be valid to represent the experimental data within $\pm 10\%$ of error for the flow boiling condition. We believed that this correlation filled the knowledge gap for the mass transfer under a flow boiling condition and provides a reference for the future studies.

4.6 References

- [1] Khumsa-Ang, K. and D. Lister, "Initial Oxide Particle Deposition Under Low-Temperature Cooling Water Conditions: Experiments Under Subcooled Boiling at High pH," *Heat Transfer Engineering*, 34 (2013): pp. 702-711.
- [2] Oduoza, C.F., "Electrochemical mass transfer at a heated electrode in a vertical annular flow cell," *Chemical Engineering and Processing: Process Intensification*, 43 (2004): pp. 921-928.
- [3] Tvarusko, A., "Dimensionless correlation of mass transfer in wire electroplating cells of various designs," *Journal of The Electrochemical Society*, 120 (1973): pp. 87-89.
- [4] Losey, M.W., M.A. Schmidt and K.F. Jensen, "Microfabricated multiphase packed-bed reactors: characterization of mass transfer and reactions," *Industrial & Engineering Chemistry Research*, 40 (2001): pp. 2555-2562.
- [5] Diercks, D.R., W.J. Shack and J. Muscara, "Overview of steam generator tube degradation and integrity issues," *Nuclear engineering and design*, 194 (1999): pp. 19-30.
- [6] Krishnamurthy, S. and Y. Peles, "Flow boiling of water in a circular staggered micro-pin fin heat sink," *International Journal of Heat and Mass Transfer*, 51 (2008): pp. 1349-1364.
- [7] Qi, S.L., P. Zhang, R.Z. Wang and L.X. Xu, "Flow boiling of liquid nitrogen in micro-tubes: Part I – The onset of nucleate boiling, two-phase flow instability and two-phase flow pressure drop," *International Journal of Heat and Mass Transfer*, 50 (2007): pp. 4999-5016.
- [8] Basu, N., G.R. Warrier and V.K. Dhir, "Wall Heat Flux Partitioning During Subcooled Flow Boiling: Part II---Model Validation," *Journal of Heat Transfer*, 127 (2005): pp. 141-148.
- [9] Friend, W.L. and A. Metzner, "Turbulent heat transfer inside tubes and the analogy among heat, mass, and momentum transfer," *AIChE Journal*, 4 (1958): pp. 393-402.
- [10] Lin, C.S., E.B. Denton, H.S. Gaskill and G.L. Putnam, "Diffusion-Controlled Electrode Reactions," *Industrial & Engineering Chemistry*, 43 (1951): pp. 2136-2143.
- [11] Ross, T.K. and A.A. Wragg, "Electrochemical mass transfer studies in annuli," *Electrochimica Acta*, 10 (1965): pp. 1093-1106.

- [12] Wragg, A.A., "Free convection mass transfer at horizontal electrodes," *Electrochimica Acta*, 13 (1968): pp. 2159-2165.
- [13] Gedupudi, S., Y.Q. Zu, T.G. Karayiannis, D.B.R. Kenning and Y.Y. Yan, "Confined bubble growth during flow boiling in a mini/micro-channel of rectangular cross-section Part I: Experiments and 1-D modelling," *International Journal of Thermal Sciences*, 50 (2011): pp. 250-266.
- [14] Hakeem, M.A. and M. Kamil, "Onset of nucleate boiling of binaries in a vertical thermosiphon reboiler," *Chemical Engineering Research and Design*, 85 (2007): pp. 1670-1677.
- [15] Zeitoun, O. and M. Shoukri, "Axial void fraction profile in low pressure subcooled flow boiling," *International Journal of Heat and Mass Transfer*, 40 (1997): pp. 869-879.
- [16] Vogt, H., O. Aras and R.J. Balzer, "The limits of the analogy between boiling and gas evolution at electrodes," *International Journal of Heat and Mass Transfer*, 47 (2004): pp. 787-795.
- [17] Vogt, H., "Heat transfer in boiling and mass transfer in gas evolution at electrodes - The analogy and its limits," *International Journal of Heat and Mass Transfer*, 59 (2013): pp. 191-197.
- [18] Hall, S.B., E.A. Khudaish and A.L. Hart, "Electrochemical oxidation of hydrogen peroxide at platinum electrodes. Part 1. An adsorption-controlled mechanism," *Electrochimica Acta*, 43 (1998): pp. 579-588.
- [19] Edward, J.T., "Molecular volumes and the Stokes-Einstein equation," *Journal of Chemical Education*, 47 (1970): pp. 261.
- [20] Berger, F.P. and K.F.F.L. Hau, "Mass transfer in turbulent pipe flow measured by the electrochemical method," *International Journal of Heat and Mass Transfer*, 20 (1977): pp. 1185-1194.
- [21] Schock, G. and A. Miquel, "Mass transfer and pressure loss in spiral wound modules," *Desalination*, 64 (1987): pp. 339-352.
- [22] Carbin, D.C. and D.R. Gabe, "Electrochemical mass transfer in an annulus," *Electrochimica Acta*, 19 (1974): pp. 653-654.
- [23] Engstrom, R.C., M. Weber, D.J. Wunder, R. Burgess and S. Winqvist, "Measurements within the diffusion layer using a microelectrode probe," *Analytical Chemistry*, 58 (1986): pp. 844-848.

- [24] Janssen, L.J.J. and J.G. Hoogland, "The effect of electrolytically evolved gas bubbles on the thickness of the diffusion layer," *Electrochimica Acta*, 15 (1970): pp. 1013-1023.
- [25] Chen, J.C., "Correlation for boiling heat transfer to saturated fluids in convective flow," *Industrial & Engineering Chemistry Process Design and Development*, 5 (1966): pp. 322-329.
- [26] Gungor, K.E. and R.H.S. Winterton, "A general correlation for flow boiling in tubes and annuli," *International Journal of Heat and Mass Transfer*, 29 (1986): pp. 351-358.
- [27] Dittus, F.W. and L.M.K. Boelter, "Heat transfer in automobile radiators of the tubular type," *International Communications in Heat and Mass Transfer*, 12 (1985): pp. 3-22.
- [28] Cooper, M. *Saturation nucleate pool boiling - a simple correlation*. in *Inst. Chem. Eng. Symp. Ser.* 1984.
- [29] Shen, C., A. Afacan, J.-L. Luo, A. Siddiqui and S.J. Klimas, "Mass transfer on nucleate boiling surfaces using the electrochemical method," *International Journal of Heat and Mass Transfer*, 78 (2014): pp. 289-293.
- [30] Stephan, K. and H. Vogt, "A model for correlating mass transfer data at gas evolving electrodes," *Electrochimica Acta*, 24 (1979): pp. 11-18.
- [31] Son, G. and V. Dhir, "Numerical simulation of film boiling near critical pressures with a level set method," *Journal of Heat Transfer*, 120 (1998): pp. 183-192.

Chapter 5 Conclusions

Mass transfer under flow boiling condition is an important phenomenon that encountered in the nuclear industry. The theoretical and experimental study of mass transfer on a boiling surface under a flow boiling condition has not been reported due to experimental difficulties and the lack of an appropriate experimental facility. To achieve creative understanding of this knowledge gap, the objectives of this thesis were to develop a novel technique to determine the mass transfer rate under flow boiling condition experimentally. This goal have been fulfilled step by step and the following conclusions were obtained:

- (1) Under the bulk boiling condition, the mass transfer coefficients of oxygen and ferricyanide were measured using a rotating cylinder electrode in under a simulated flow condition. An empirical correlation was proposed that works for both species under the non-boiling condition. It was found that due to the generation and rupture of the boiling bubbles, the mass transfer rates obtained under the bulk boiling condition were 38% higher than those obtained just below the boiling point.
- (2) Under pool boiling condition, a novel experimental setup was constructed to implement the direct electrochemical measurement on nucleate boiling surface thus investigate the mass transfer behavior under pool boiling condition. Successful measurements have been obtained using the new device, which is the first time according to the open literature. It was found that the increase of the mass transfer coefficient of hydrogen peroxide was faster than that of ferricyanide ions with increasing heat flux. This result could be

attributed to the fact that the mass transfer of ferricyanide ions only occurs through the liquid phase, while the mass transfer of hydrogen peroxide could occur through both the liquid and vapor phases of the reaction. Furthermore, an empirical equation was proposed and proven to work for predicting the mass transfer rate for potassium ferricyanide under nucleate boiling conditions.

- (3) Under flow boiling condition, a novel electrochemical flow loop system was designed and constructed to develop a technique of direct flow boiling mass transfer measurement. Aspiringly, this flow loop system successfully accomplished the first in-situ mass transfer measurement under the flow boiling condition. Furthermore, a new correlation represents the experimental data within 10 % of error for mass transfer under the flow boiling condition was proposed. The above work made valuable contribution on the mass transfer study under flow boiling condition. This correlation filled the knowledge gap for the mass transfer under flow boiling condition and provides reference for the future studies.

Chapter 6 Recommendations and future work

In the present study, two new experimental setups were constructed. These setups allowed us to measure the mass transfer behavior under pool boiling and flow boiling conditions. The mass transfer behavior of different species under bulk boiling, subcooled boiling and fully developed nucleate boiling conditions was studied. Furthermore, the mass transfer coefficient under the flow boiling condition was successfully detected for the first time. This was a very inspiring and the results can be applied to wide area.

In order to conduct more accurate measurement and expand the operating parameter range, the flow loop can be further revised based on the following aspects:

- (1) The current pump can be updated to a more accurate and high flow rate pump, for example Agilent SD-1 Solvent Delivery Module, to allow higher pressure and higher flow rate experiments.
- (2) The design of the preheating re-boiler could change to a tubing coil structure. It means insert a stainless steel tubing coil inside the original re-boiler vessel, and the working fluid will flow inside the tubing coil during the preheating process. While silicon oil can be used to fill the re-boiler vessel work as the heating media. This design could reduce the operating pressure inside the vessel, reduce the reaction time and increase the stability of the experiment.

- (3) The heating oil could change from SIL 180 to SIL 300 or other high temperature heating oil, to enable up to 300 °C oil temperature and expand the reachable boiling regime.

By updating the flow loop device, more experimental work could be done to allow further investigation of mass transfer in flow boiling regime:

- (1) Increasing operating parameters such as temperature, flow rate, different concentrations of electro-active species and different operating pressures. The onset of the nucleate boiling point and the mass transfer behavior in that region would be interesting to study.
- (2) More species, such as Cu, could be used as reaction agents to compare current results under different conditions.
- (3) A theoretical model of the mass transfer could be created from a single bubble under the boiling condition. The experimental results could be used to confirm and revise the modeling work.

Bibliography

Abdel-Aziz, M. H., I. Nirdosh and G. H. Sedahmed. "Liquid-solid mass and heat transfer behavior of a concentric tube airlift reactor." *International Journal of Heat and Mass Transfer* (2013) 58(1-2):PP. 735-739.

Abdel-Aziz, M. S. M., A. H. El-Shazly, H. A. Farag and G. H. Sedahmed. "Mass transfer behavior of rotating square cylinder electrochemical reactor in relation to wastewater treatment." *Energy Conversion and Management* (2011) 52(8-9):PP. 2870-2875.

Abraham, J. P., E. M. Sparrow and W. J. Minkowycz. "Internal-flow Nusselt numbers for the low-Reynolds-number end of the laminar-to-turbulent transition regime." *International Journal of Heat and Mass Transfer* (2011) 54(1-3):PP. 584-588.

Akerlof, G. and G. Kegeles. "The density of aqueous solutions of sodium hydroxide." *Journal of the American Chemical Society* (1939) 61(5):PP. 1027-1032.

Al-Dahhan, M., W. HighFill and B. T. Ong. "Drawbacks of the Dissolution Method for Measurement of the Liquid-Solid Mass-Transfer Coefficients in Two-Phase Flow Packed-Bed Reactors Operated at Low and High Pressures." *Industrial & Engineering Chemistry Research* (2000) 39(8):PP. 3102-3107.

Alkire, R. and P.-Y. Lu. "Effect of Hydrogen Evolution on Current Distribution during Electrodeposition at Vertical Electrodes." *Journal of The Electrochemical Society* (1979) 126(12):PP. 2118-2124.

Aoki, K., K. Honda, K. Tokuda and H. Matsuda. "Voltammetry at microcylinder electrodes: Part I. Linear sweep voltammetry." *Journal of Electroanalytical Chemistry and Interfacial Electrochemistry* (1985) 182(2):PP. 267-279.

Arvia, A. J., S. L. Marchiano and J. J. Podesta. "The diffusion of ferrocyanide and ferricyanide ions in aqueous solutions of potassium hydroxide." *Electrochimica Acta* (1967) 12(3):PP. 259-266.

Azumi, K., T. Ohtsuka and N. Sato. "Impedance of Iron Electrode Passivated in Borate and Phosphate Solutions." *J. Jpn. Inst. Met.* (1985) 49(9):PP. 729-736.

Baehr, H. and K. Stephan. "Heat and Mass Transfer, Springer, Berlin, 1998."PP.

Bartelmus, G. "Local solid-liquid mass transfer coefficients in a three-phase fixed bed reactor." *Chemical Engineering and Processing: Process Intensification* (1989) 26(2):PP. 111-120.

Bastidas, J. M., C. L. Torres, E. Cano and J. L. Polo. "Influence of molybdenum on passivation of polarised stainless steels in a chloride environment." *Corrosion Science* (2002) 44(3):PP. 625-633.

Basu, N., G. R. Warriar and V. K. Dhir. "Onset of nucleate boiling and active nucleation site density during subcooled flow boiling." *Journal of Heat Transfer* (2002) 124(4):PP. 717-728.

Basu, N., G. R. Warriar and V. K. Dhir. "Wall Heat Flux Partitioning During Subcooled Flow Boiling: Part II---Model Validation." *Journal of Heat Transfer* (2005) 127(2):PP. 141-148.

Beckmann, A., B. A. Coles, G. Richard, P. Grandler, F. Marken and A. Neudeck. "Modeling hot wire electrochemistry. Coupled heat and mass transport at a directly and continuously heated wire." *The Journal of Physical Chemistry B* (2000) 104(4):PP. 764-769.

Beckmann, A., A. Schneider and P. Grundler. "Electrically heated cylindrical microelectrodes. Electrochemical measurements in THF." *Electrochemistry Communications* (1999) 1(1):PP. 46-49.

Benzina, M., D. Mowla and G. Lacoste. "Mass transfer studies in porous electrodes: Application of the limiting current technique." *The Chemical Engineering Journal* (1983) 27(1):PP. 1-7.

Berger, F. P. and K. F. F. L. Hau. "Mass transfer in turbulent pipe flow measured by the electrochemical method." *International Journal of Heat and Mass Transfer* (1977) 20(11):PP. 1185-1194.

Boden, P. "Corrosion of Cu and Cu-base alloys under conditions of boiling heat transfer-I. Corrosion of Cu." *Corrosion Science* (1971) 11(6):PP. 353-362.

Brunner, E. *Z. physik. Chem.* (1904) 47(56):PP.

Burns, J. R. and R. J. J. Jachuck. "Determination of liquid-solid mass transfer coefficients for a spinning disc reactor using a limiting current technique." *International Journal of Heat and Mass Transfer* (2005) 48(12):PP. 2540-2547.

Carbin, D. C. and D. R. Gabe. "Electrochemical mass transfer in an annulus." *Electrochimica Acta* (1974) 19(10):PP. 653-654.

Cardoso, M. V., S. T. Amaral and E. M. A. Martini. "Temperature effect in the corrosion resistance of Ni-Fe-Cr alloy in chloride medium." *Corrosion Science* (2008) 50(9):PP. 2429-2436.

Carranza, R. M. and M. G. Alvarez. "The effect of temperature on the passive film properties and pitting behaviour of a Fe-Cr-Ni alloy." *Corrosion Science* (1996) 38(6):PP. 909-925.

Chang, L. S., T. E. Carleson and J. C. Berg. "Heat and mass transfer to a translating drop in an electric field." *International Journal of Heat and Mass Transfer* (1982) 25(7):PP. 1023-1030.

Chao, C., L. Lin and D. Macdonald. "A point defect model for anodic passive films I. Film growth kinetics." *Journal of The Electrochemical Society* (1981) 128(6):PP. 1187-1194.

Chen, J. C. "Correlation for boiling heat transfer to saturated fluids in convective flow." *Industrial & Engineering Chemistry Process Design and Development* (1966) 5(3):PP. 322-329.

Chiba, A., I. Muto, Y. Sugawara and N. Hara. "Pit Initiation Mechanism at MnS Inclusions in Stainless Steel: Synergistic Effect of Elemental Sulfur and Chloride Ions." *Journal of The Electrochemical Society* (2013) 160(10):PP. C511-C520.

Chin, D.-T. and K.-L. Hsueh. "An analysis using the Chilton-Colburn analogy for mass transfer to a flat surface from an unsubmerged impinging jet." *Electrochimica Acta* (1986) 31(5):PP. 561-564.

Cobo, O. A., S. L. Marchiano and A. J. Arvia. "Ionic mass transfer at rotating electrodes formed by solids of revolution. Rotating one-base spherical segment electrodes." *Electrochimica Acta* (1972) 17(3):PP. 503-509.

Coleman, H. W. and W. G. Steele (1999). *Experimentation and uncertainty analysis for engineers*, John Wiley & Sons Incorporated.

Collier, J. G. and J. R. Thome (1994). *Convective boiling and condensation*, Oxford University Press.

Coney, M. (1981). *Erosion-corrosion: the Calculation of Mass-transfer Coefficients*, CEGB.

Cooper, M. (1984). Saturation nucleate pool boiling - a simple correlation. *Inst. Chem. Eng. Symp. Ser.*

Cornet, I., R. Greif, J. T. Teng and F. Roehler. "Mass transfer to rotating rods and plates." *International Journal of Heat and Mass Transfer* (1980) 23(6):PP. 805-811.

Cowan, R. and A. Kaznoff. "Electrochemical measurements of corrosion processes in a boiling water nuclear reactor." *Corrosion* (1973) 29(4):PP. 123-132.

Daguenet, M. "Etude du transport de matiere en solution, a l'aide des electrodes a disque et a anneau tournants." *International Journal of Heat and Mass Transfer* (1968) 11(11):PP. 1581-1596.

Dang-Vu, T., H. D. Doan and A. Lohi. "Local Mass Transfer in a Packed Bed: Experiments and Model." *Industrial & Engineering Chemistry Research* (2005) 45(3):PP. 1097-1104.

Dawson, D. A. and O. Trass. "Mass transfer at rough surfaces." *International Journal of Heat and Mass Transfer* (1972) 15(7):PP. 1317-1336.

Dedov, A. V., A. T. Komov, A. N. Varava and V. V. Yagov. "Hydrodynamics and heat transfer in swirl flow under conditions of one-side heating. Part 2: Boiling heat transfer. Critical heat fluxes." *International Journal of Heat and Mass Transfer* (2010) 53(21-22):PP. 4966-4975.

Delaunay, G., A. Storck, A. Laurent and J.-C. Charpentier. "Electrochemical study of liquid-solid mass transfer in packed beds with upward cocurrent gas-liquid flow." *Industrial & Engineering Chemistry Process Design and Development* (1980) 19(4):PP. 514-521.

Despic, A. R., M. V. Mitrovic, B. Z. Nikolic and S. D. Cvijovic. "Mass transfer at a rotating disc with rectangular patch electrodes." *Journal of Electroanalytical Chemistry and Interfacial Electrochemistry* (1975) 60(2):PP. 141-149.

Diercks, D., W. Shack and J. Muscara. "Overview of steam generator tube degradation and integrity issues." *Nuclear engineering and design* (1999) 194(1):PP. 19-30.

Diercks, D. R., W. J. Shack and J. Muscara. "Overview of steam generator tube degradation and integrity issues." *Nuclear engineering and design* (1999) 194(1):PP. 19-30.

Dittus, F. W. and L. M. K. Boelter. "Heat transfer in automobile radiators of the tubular type." *International Communications in Heat and Mass Transfer* (1985) 12(1):PP. 3-22.

Dutta, R. S., R. Purandare, A. Lobo, S. K. Kulkarni and G. K. Dey. "Microstructural aspects of the corrosion of Alloy 800." *Corrosion Science* (2004) 46(12):PP. 2937-2953.

Edward, J. T. "Molecular volumes and the Stokes-Einstein equation." *Journal of Chemical Education* (1970) 47(4):PP. 261.

Eisenberg, M., C. W. Tobias and C. R. Wilke. "Ionic mass transfer and concentration polarization at rotating electrodes." *Journal of The Electrochemical Society* (1954) 101(6):PP. 306-320.

El-Shazly, Y. M., R. R. Zahran, H. A. Farag and G. H. Sedahmed. "Mass transfer in relation to flow induced corrosion of the bottom of cylindrical agitated vessels." *Chemical Engineering and Processing: Process Intensification* (2004) 43(6):PP. 745-751.

Engstrom, R. C., M. Weber, D. J. Wunder, R. Burgess and S. Winquist. "Measurements within the diffusion layer using a microelectrode probe." *Analytical Chemistry* (1986) 58(4):PP. 844-848.

Fenech, E. J. and C. W. Tobias. "Mass transfer by free convection at horizontal electrodes." *Electrochimica Acta* (1960) 2(4):PP. 311-325.

Ferrell, R. T. and D. M. Himmelblau. "Diffusion coefficients of nitrogen and oxygen in water." *Journal of Chemical and Engineering Data* (1967) 12(1):PP. 111-115.

Filinovsky, V. J., I. V. Kadija, B. Nolic and M. B. Nakic. "Mass transfer on the rotating double ring electrodes: Reactions without gas evolution." *Journal of Electroanalytical Chemistry and Interfacial Electrochemistry* (1974) 54(1):PP. 39-46.

Friend, W. L. and A. Metzner. "Turbulent heat transfer inside tubes and the analogy among heat, mass, and momentum transfer." *AIChE Journal* (1958) 4(4):PP. 393-402.

Fukunaka, Y., K. Suzuki, A. Ueda and Y. Kondo. "Mass-Transfer Rate on a Plane Vertical Cathode with Hydrogen Gas Evolution." *Journal of The Electrochemical Society* (1989) 136(4):PP. 1002-1009.

Ge, H.-H., G.-D. Zhou and W.-Q. Wu. "Passivation model of 316 stainless steel in simulated cooling water and the effect of sulfide on the passive film." *Applied Surface Science* (2003) 211(1–4):PP. 321-334.

Gedupudi, S., Y. Q. Zu, T. G. Karayiannis, D. B. R. Kenning and Y. Y. Yan. "Confined bubble growth during flow boiling in a mini/micro-channel of rectangular cross-section Part I: Experiments and 1-D modelling." *International Journal of Thermal Sciences* (2011) 50(3):PP. 250-266.

Geringer, J. and D. D. Macdonald. "Modeling fretting-corrosion wear of 316L SS against poly(methyl methacrylate) with the Point Defect Model: Fundamental theory, assessment, and outlook." *Electrochimica Acta* (2012) 79:PP. 17-30.

Greggory, D. P. and A. C. Riddiford. "Dissolution of copper in sulfuric acid solutions." *Journal of The Electrochemical Society* (1960) 107:PP. 950–956.

Grundler, P., T. Zerihun, A. Kirbs and H. Grabow. "Simultaneous joule heating and potential cycling of cylindrical microelectrodes." *Analytica Chimica Acta* (1995) 305(1,Äi3):PP. 232-240.

Gungor, K. E. and R. H. S. Winterton. "A general correlation for flow boiling in tubes and annuli." *International Journal of Heat and Mass Transfer* (1986) 29(3):PP. 351-358.

Hakeem, M. A. and M. Kamil. "Onset of nucleate boiling of binaries in a vertical thermosiphon reboiler." *Chemical Engineering Research and Design* (2007) 85(12 A):PP. 1670-1677.

Hall, P. and B. Selinger. "Better estimates of exponential decay parameters." *The Journal of Physical Chemistry* (1981) 85(20):PP. 2941-2946.

Hall, S. B., E. A. Khudaish and A. L. Hart. "Electrochemical oxidation of hydrogen peroxide at platinum electrodes. Part 1. An adsorption-controlled mechanism." *Electrochimica Acta* (1998) 43(5–6):PP. 579-588.

Hall, S. B., E. A. Khudaish and A. L. Hart. "Electrochemical oxidation of hydrogen peroxide at platinum electrodes. Part IV: phosphate buffer dependence." *Electrochimica Acta* (1999) 44(25):PP. 4573-4582.

Hall, S. B., E. A. Khudaish and A. L. Hart. "Electrochemical oxidation of hydrogen peroxide at platinum electrodes. Part V: inhibition by chloride." *Electrochimica Acta* (2000) 45(21):PP. 3573-3579.

Han, P. and D. M. Bartels. "Temperature dependence of oxygen diffusion in H₂O and D₂O." *The Journal of Physical Chemistry* (1996) 100(13):PP. 5597-5602.

Harvey, A. H. "Semiempirical correlation for Henry's constants over large temperature ranges." *AIChE Journal* (1996) 42(5):PP. 1491-1494.

Highfill, W. and M. Al-Dahhan. "Liquid-Solid Mass Transfer Coefficient in High Pressure Trickle Bed Reactors." *Chemical Engineering Research and Design* (2001) 79(6):PP. 631-640.

Ho, J. and G. Yu. "Pitting corrosion of Inconel 600 in chloride and thiosulfate anion solutions at low temperature." *Corrosion* (1992) 48(2):PP. 147-158.

Holman, J. P. (2001). *Experimental methods for engineers*, McGraw Hill.

Horvath, J. and H. Uhlig. "Critical Potentials for Pitting Corrosion of Ni, Cr, Ni-Cr, and Fe-Cr Related Stainless Steels." *Journal of The Electrochemical Society* (1968) 115(8):PP. 791-795.

Hsu, Y. Y. and R. W. Graham. "Transport processes in boiling and two-phase systems, including near-critical fluids." Washington, DC, Hemisphere Publishing Corp.; New York, McGraw-Hill Book Co., 1976. 559 p. (1976) 1:PP.

Huang, J., X. Wu and E.-H. Han. "Influence of pH on electrochemical properties of passive films formed on Alloy 690 in high temperature aqueous environments." *Corrosion Science* (2009) 51(12):PP. 2976-2982.

Huang, J., X. Wu and E.-H. Han. "Electrochemical properties and growth mechanism of passive films on Alloy 690 in high-temperature alkaline environments." *Corrosion Science* (2010) 52(10):PP. 3444-3452.

Ives, M. B., Y. C. Lu and J. L. Luo. "Cathodic reactions involved in metallic corrosion in chlorinated saline environments." *Corrosion Science* (1991) 32(1):PP. 91-102.

Janssen, L. J. J. and E. Barendrecht. "Mass transfer at a rotating ring-cone electrode and its use to determine supersaturation of gas evolved." *Electrochimica Acta* (1984) 29(9):PP. 1207-1212.

Janssen, L. J. J. and J. G. Hoogland. "The effect of electrolytically evolved gas bubbles on the thickness of the diffusion layer." *Electrochimica Acta* (1970) 15(6):PP. 1013-1023.

Jianping, W., H. Lin, Z. Yong, L. Chao and C. Yunlin. "Solid-liquid mass transfer in a gas-liquid-solid three-phase reversed flow jet loop reactor." *Chemical Engineering Journal* (2000) 78(2-3):PP. 231-235.

Jolls, K. R. and T. J. Hanratty. "Use of electrochemical techniques to study mass transfer rates and local skin friction to a sphere in a dumped bed." *AIChE Journal* (1969) 15(2):PP. 199-205.

Kear, G., K. Bremhorst, S. Coles and S.-H. Huang. "Rates of mass transfer to patch electrodes in disturbed flows using oxygen reduction under limiting current conditions." *Corrosion Science* (2008) 50(6):PP. 1789-1795.

Khumsa-Ang, K. and D. Lister. "Initial Oxide Particle Deposition Under Low-Temperature Cooling Water Conditions: Experiments Under Subcooled Boiling at High pH." *Heat Transfer Engineering* (2013) 34(8-9):PP. 702-711.

Kilian, R., N. Wieling and L. Stieding. "Corrosion resistance of SG tubing material Incoloy 800 mod. and Inconel 690 TT." *Materials and Corrosion* (1991) 42(9):PP. 490-496.

Kim, D. H., I. H. Kim and H. N. Chang. "Experimental study of mass transfer around a turbulence promoter by the limiting current method." *International Journal of Heat and Mass Transfer* (1983) 26(7):PP. 1007-1016.

Kim, J. "Review of nucleate pool boiling bubble heat transfer mechanisms." *International Journal of Multiphase Flow* (2009) 35(12):PP. 1067-1076.

King, F., C. D. Litke, M. J. Quinn and D. M. LeNeveu. "The measurement and prediction of the corrosion potential of copper in chloride solutions as a function of oxygen concentration and mass-transfer coefficient." *Corrosion Science* (1995) 37(5):PP. 833-851.

Kovatcheva, N., A. Polyanin and Z. Zapryanov. "The change of the diffusivity with the change of the concentration of the solvent in a solution." *Acta mechanica* (1989) 80(3):PP. 259-272.

Krishnamurthy, S. and Y. Peles. "Flow boiling of water in a circular staggered micro-pin fin heat sink." *International Journal of Heat and Mass Transfer* (2008) 51(5-6):PP. 1349-1364.

Kurihara, H. and J. Myers. "The effects of superheat and surface roughness on boiling coefficients." *AIChE Journal* (1960) 6(1):PP. 83-91.

Laitinen, T. "Localized corrosion of stainless steel in chloride, sulfate and thiosulfate containing environments." *Corrosion Science* (2000) 42(3):PP. 421-441.

Latifi, M. A., A. Laurent and A. Storck. "Liquid-solid mass transfer in a packed bed with downward cocurrent gas-liquid flow: An organic liquid phase with high Schmidt number." *The Chemical Engineering Journal* (1988) 38(1):PP. 47-56.

Lee, J. and J. B. Talbot. "A model of electrocodeposition on a rotating cylinder electrode." *Journal of The Electrochemical Society* (2007) 154(2):PP. D70-D77.

Leibovitz, J. "Theorems of electrochemical mass transport in dilute solutions of mixtures of electrolytes, including weak electrolytes and hydrolysis reactions." *Journal of The Electrochemical Society* (2005) 152(9):PP. E282-E297.

Li, X., J. Wang, E.-H. Han and W. Ke. "Corrosion behavior for Alloy 690 and Alloy 800 tubes in simulated primary water." *Corrosion Science* (2013) 67(0):PP. 169-178.

Lin, C., Y. Kim, L. Niedrach and K. Ramp. "Electrochemical corrosion potential models for boiling-water reactor applications." *Corrosion* (1996) 52(8):PP. 618-625.

Lin, C. S., E. B. Denton, H. S. Gaskill and G. L. Putnam. "Diffusion-Controlled Electrode Reactions." *Industrial & Engineering Chemistry* (1951) 43(9):PP. 2136-2143.

Lindberg, B., K. Hamrin, G. Johansson, U. Gelius, A. Fahlman, C. Nordling and K. Siegbahn. "Molecular spectroscopy by means of ESCA II. Sulfur compounds. Correlation of electron binding energy with structure." *Physica Scripta* (1970) 1(5-6):PP. 286.

Lolja, S. A. "Momentum and mass transfer on sandpaper-roughened surfaces in pipe flow." *International Journal of Heat and Mass Transfer* (2005) 48(11):PP. 2209-2218.

Losey, M. W., M. A. Schmidt and K. F. Jensen. "Microfabricated multiphase packed-bed reactors: characterization of mass transfer and reactions." *Industrial & Engineering Chemistry Research* (2001) 40(12):PP. 2555-2562.

Lu, B., J. Luo and Y. Lu. "Effects of pH on lead-induced passivity degradation of nuclear steam generator tubing alloy in high temperature crevice chemistries." *Electrochimica Acta* (2013) 87:PP. 824-838.

Lu, Y. "A Flow Impingement Facility for Corrosion and Electrochemical Studies in High Temperature Aqueous Solutions." *CORROSION 2004* (2004):PP.

Lu, Y., G. Goszczynski and S. Ramamurthy. "Degradation of alloy 800 under steam generator secondary side crevice conditions." 17th International Conference on Nuclear Engineering (2009):PP. 1-9.

Lu, Y., S. Ramamurthy and G. Goszczynski. "An aging assessment on ex-service Alloy 800 steam generator tubing." Nuclear engineering and design (2012) 242(0):PP. 91-99.

Luo, B. "Characterization of pH Effect on Corrosion Resistance of Nuclear Steam Generator Tubing Alloy by In-situ Scanning Electrochemical Microscopy." Acta Physico-Chimica Sinica (2014) 30(1):PP. 59-66.

Ma, H., D. Du, J. Sun, Y. Zhang and N. Deng. "Convective mass transfer from a horizontal rotating cylinder in a slot air jet flow." International Journal of Heat and Mass Transfer (2011) 54(1-3):PP. 186-193.

Ma, H., S. Hao, M. Wang, G. Yang and F. Wang. "Convective mass transfer from a horizontal rotating large-diameter cylinder." International Journal of Heat and Mass Transfer (2012) 55(4):PP. 1419-1422.

Macdonald, D. D., A. C. Scott and P. Wentreck. "External reference electrodes for use in high temperature aqueous systems." Journal of The Electrochemical Society (1979) 126(6):PP. 908-911.

Macdonald, D. D. and S. Sharifi-Asl. "Volt Equivalent diagrams as a means of displaying the electrochemical thermodynamics of the sulfur-water system." Corrosion Science (2014) 81(0):PP. 102-109.

Maceiras, R., X. R. Novoa, E. Alvarez and M. A. Cancela. "Local mass transfer measurements in a bubble column using an electrochemical technique." Chemical Engineering and Processing: Process Intensification (2007) 46(10):PP. 1006-1011.

Madden, A. J. and D. G. Nelson. "A novel technique for determining mass transfer coefficients in agitated solid-liquid systems." *AIChE Journal* (1964) 10(3):PP. 415-430.

Mahato, B. K., S. K. Voora and L. W. Shemilt. "Steel pipe corrosion under flow conditions-I. An isothermal correlation for a mass transfer model." *Corrosion Science* (1968) 8(3):PP. 173-193.

Mahinpey, N., M. Ojha and O. Trass. "Transient mass and heat transfer in a smooth pipe." *International Journal of Heat and Mass Transfer* (2001) 44(20):PP. 3919-3930.

McMurtrie, R. and F. Keyes. "A measurement of the diffusion coefficient of hydrogen peroxide vapor into air." *Journal of the American Chemical Society* (1948) 70(11):PP. 3755-3758.

Miller, C. T., M. M. Poirier, McNeil and A. S. Mayer. "Dissolution of trapped nonaqueous phase liquids: Mass transfer characteristics." *Water Resources Research* (1990) 26(11):PP. 2783-2796.

Mycroft, J. R., G. M. Bancroft, N. S. McIntyre, J. W. Lorimer and I. R. Hill. "Detection of sulphur and polysulphides on electrochemically oxidized pyrite surfaces by X-ray photoelectron spectroscopy and Raman spectroscopy." *Journal of Electroanalytical Chemistry and Interfacial Electrochemistry* (1990) 292(1-2):PP. 139-152.

Naumkin, A. V., A. Kraut-Vass, S. W. Gaarenstroom and C. J. Powell. "NIST X-ray Photoelectron Spectroscopy Database." *NIST Standard Reference Database 20, Version 4.1* (2000):PP.

Neal, A. L., S. Techkarnjanaruk, A. Dohnalkova, D. McCready, B. M. Peyton and G. G. Geesey. "Iron sulfides and sulfur species produced at hematite surfaces in the presence of sulfate-reducing bacteria." *Geochimica et Cosmochimica Acta* (2001) 65(2):PP. 223-235.

Newman, R., H. Isaacs and B. Alman. "Effects of sulfur compounds on the pitting behavior of type 304 stainless steel in near-neutral chloride solutions." *Corrosion* (1982) 38(5):PP. 261-265.

Nickchi, T. and A. Alfantazi. "Electrochemical corrosion behaviour of Incoloy 800 in sulphate solutions containing hydrogen peroxide." *Corrosion Science* (2010) 52(12):PP. 4035-4045.

Nickchi, T. and A. Alfantazi. "Kinetics of passive film growth on Alloy 800 in the presence of hydrogen peroxide." *Electrochimica Acta* (2011) 58:PP. 743-749.

Nickchi, T. and A. Alfantazi. "Corrosion characteristics of alloy 800 in aqueous solutions up to 200 C." *Journal of The Electrochemical Society* (2013) 160(2):PP. C64-C76.

Oduoza, C. F. "Electrochemical mass transfer at a heated electrode in a vertical annular flow cell." *Chemical Engineering and Processing: Process Intensification* (2004) 43(7):PP. 921-928.

Oh, K., S. Ahn, K. Eom, K. Jung and H. Kwon. "Observation of passive films on Fe–20Cr–xNi (x=0, 10, 20 wt.%) alloys using TEM and Cs-corrected STEM–EELS." *Corrosion Science* (2014) 79(0):PP. 34-40.

Olmedo, A., M. Villegas and M. Alvarez. "Corrosion behaviour of Alloy 800 in high temperature aqueous solutions: Electrochemical studies." *Journal of Nuclear Materials* (1996) 229:PP. 102-114.

Pao C, C. "Local liquid-solid mass transfer measurement in a trickle film flow model using an electrochemical technique." *International Journal of Heat and Mass Transfer* (1987) 30(11):PP. 2305-2317.

Park, Y., J. Galvele, A. Agrawal and R. Staehle. "Stress corrosion cracking and anodic behavior of AISI 304 stainless steel, Inconel 600, and Incoloy 800 straining in boiling NaOH solutions." *Corrosion* (1978) 34(12):PP. 413-418.

Parys, H. V., E. Tourwe, T. Breugelmans, M. Depauw, J. Deconinck and A. Hubin. "Modeling of mass and charge transfer in an inverted rotating disk electrode (IRDE) reactor." *Journal of Electroanalytical Chemistry* (2008) 622(1):PP. 44-50.

Patrick, M. A. and A. A. Wragg. "Optical and electrochemical studies of transient free convection mass transfer at horizontal surfaces." *International Journal of Heat and Mass Transfer* (1975) 18(12):PP. 1397-1407.

Persaud, S. Y., A. G. Carcea and R. C. Newman. "Electrochemical aspects of stress corrosion cracking of Ni-Cr-Fe alloys in acid sulfate solutions relevant to nuclear steam generators." *ECS Transactions* (2013) 53(21):PP. 3-14.

Pfeffer, R. and J. Happel. "An analytical study of heat and mass transfer in multiparticle systems at low Reynolds numbers." *AIChE Journal* (1964) 10(5):PP. 605-611.

Postelnicu, A. "Influence of a magnetic field on heat and mass transfer by natural convection from vertical surfaces in porous media considering Soret and Dufour effects." *International Journal of Heat and Mass Transfer* (2004) 47(6):PP. 1467-1472.

Pratt, A. R., I. J. Muir and H. W. Nesbitt. "X-ray photoelectron and Auger electron spectroscopic studies of pyrrhotite and mechanism of air oxidation." *Geochimica et Cosmochimica Acta* (1994) 58(2):PP. 827-841.

Qi, S. L., P. Zhang, R. Z. Wang and L. X. Xu. "Flow boiling of liquid nitrogen in micro-tubes: Part I – The onset of nucleate boiling, two-phase flow instability and two-phase flow pressure drop." *International Journal of Heat and Mass Transfer* (2007) 50(25-26):PP. 4999-5016.

Ratkovich, N., P. R. Berube and I. Nopens. "Assessment of mass transfer coefficients in coalescing slug flow in vertical pipes and applications to tubular airlift membrane bioreactors." *Chemical Engineering Science* (2011) 66(6):PP. 1254-1268.

Reiss, L. P. and T. J. Hanratty. "Measurement of instantaneous rates of mass transfer to a small sink on a wall." *AIChE Journal* (1962) 8(2):PP. 245-247.

Rivero, E. P., P. Granados, F. F. Rivera, M. Cruz and I. Gonzalez. "Mass transfer modeling and simulation at a rotating cylinder electrode (RCE) reactor under turbulent flow for copper recovery." *Chemical Engineering Science* (2010) 65(10):PP. 3042-3049.

Roberge, R. "Effect of the nickel content in the pitting of stainless steels in low chloride and thiosulfate solutions." *Corrosion* (1988) 44(5):PP. 274-280.

Rohsenow, W. M. and H. Y. Choi (1961). *Heat, mass, and momentum transfer*, Prentice-Hall New Jersey.

Rohsenow, W. M., J. P. Hartnett and Y. I. Cho (1998). *Handbook of heat transfer*, McGraw-Hill New York.

Rondelli, G., P. Torricelli, M. Fini and R. Giardino. "In vitro corrosion study by EIS of a nickel-free stainless steel for orthopaedic applications." *Biomaterials* (2005) 26(7):PP. 739-744.

Ross, T. K. and A. A. Wragg. "Electrochemical mass transfer studies in annuli." *Electrochimica Acta* (1965) 10(11):PP. 1093-1106.

Rousar, I., J. Hostomsky, V. Cezner and B. Stverak. "Limiting Local Current Densities for Electrodes Located on the Walls of a Rectangular Channel with Laminar Flow; Asymptotic Solution and Experimental Verification." *Journal of The Electrochemical Society* (1971) 118(6):PP. 881-884.

Sara, H., A. A. Wragg and M. A. Patrick. "Combined heat and mass transfer by natural convection at horizontal cylinder electrodes." *International Communications in Heat and Mass Transfer* (1991) 18(6):PP. 853-863.

Sarac, H., A. Wragg and M. Patrick. "An electrochemical mass transfer investigation in the presence of simultaneous subcooled pool boiling." *International Communications in Heat and Mass Transfer* (2003) 30(7):PP. 909-920.

Sathiya Priya, A., V. Muralidharan and A. Subramania. "Development of novel acidizing inhibitors for carbon steel corrosion in 15% boiling hydrochloric acid." *Corrosion* (2008) 64(6):PP. 541-552.

Sato, N. "Anodic Breakdown of Passive Films on Metals." *Journal of The Electrochemical Society* (1982) 129(2):PP. 255-260.

Saul, A. and W. Wagner. "International equations for the saturation properties of ordinary water substance." *Journal of Physical and Chemical Reference Data* (1987) 16(4):PP. 893-901.

Schock, G. and A. Miquel. "Mass transfer and pressure loss in spiral wound modules." *Desalination* (1987) 64(0):PP. 339-352.

Schutz, G. "Natural convection mass-transfer measurements on spheres and horizontal cylinders by an electrochemical method." *International Journal of Heat and Mass Transfer* (1963) 6(10):PP. 873-879.

Selman, J. R. and C. W. Tobias. "Mass transfer measurements by the limiting current technique." *Advances in Chemical Engineering* (1978) 10:PP. 211-318.

Shen, C., A. Afacan, J.-L. Luo, A. Siddiqui and S. J. Klimas. "Mass transfer on nucleate boiling surfaces using the electrochemical method." *International Journal of Heat and Mass Transfer* (2014) 78(0):PP. 289-293.

Shen, C., A. Afacan, J. Luo and S. J. Klimas. "Mass transfer of dissolved oxygen using rotating cylinder electrode under bulk boiling conditions." *International Journal of Heat and Mass Transfer* (2014) 70(0):PP. 162-168.

Siriwardane, R. V. and J. M. Cook. "Interactions of SO₂ with sodium deposited on CaO." *Journal of colloid and interface science* (1986) 114(2):PP. 525-535.

Sloppy, J. D., Z. Lu, E. C. Dickey and D. D. Macdonald. "Growth mechanism of anodic tantalum pentoxide formed in phosphoric acid." *Electrochimica Acta* (2013) 87:PP. 82-91.

Smestad, G., A. Ennaoui, S. Fiechter, H. Tributsch, W. Hofmann, M. Birkholz and W. Kautek. "Photoactive thin film semiconducting iron pyrite prepared by sulfurization of iron oxides." *Solar Energy Materials* (1990) 20(3):PP. 149-165.

Smith, A. F. J. and A. A. Wragg. "An electrochemical study of mass transfer in free convection at vertical arrays of horizontal cylinders." *Journal of Applied Electrochemistry* (1974) 4(3):PP. 219-228.

Son, G. and V. Dhir. "Numerical simulation of film boiling near critical pressures with a level set method." *Journal of Heat Transfer* (1998) 120(1):PP. 183-192.

Speccia, V., G. Baldi and A. Gianetto. "Solid-liquid mass transfer in concurrent two-phase flow through packed beds." *Industrial & Engineering Chemistry Process Design and Development* (1978) 17(3):PP. 362-367.

Staehele, R. and J. Gorman. "Quantitative assessment of submodes of stress corrosion cracking on the secondary side of steam generator tubing in pressurized water reactors: Part 1." *Corrosion* (2003) 59(11):PP. 931-994.

Staehele, R. and J. Gorman. "Quantitative assessment of submodes of stress corrosion cracking on the secondary side of steam generator tubing in pressurized water reactors: Part 2." *Corrosion* (2004) 60(1):PP. 5-63.

Staehele, R. and J. Gorman. "Quantitative assessment of submodes of stress corrosion cracking on the secondary side of steam generator tubing in pressurized water reactors: Part 3." *Corrosion* (2004) 60(2):PP. 115-180.

Stellwag, B. "Pitting Resistance of Alloy 800 as a Function of Temperature and Prefilming in High-Temperature Water." *Corrosion* (1997) 53(2):PP. 120-128.

Stephan, K. and H. Vogt. "A model for correlating mass transfer data at gas evolving electrodes." *Electrochimica Acta* (1979) 24(1):PP. 11-18.

Stewart, K. L. and A. A. Gewirth. "Mechanism of electrochemical reduction of hydrogen peroxide on copper in acidic sulfate solutions." *Langmuir* (2007) 23(19):PP. 9911-9918.

Sun, H., X. Wu and E.-H. Han. "Effects of temperature on the protective property, structure and composition of the oxide film on Alloy 625." *Corrosion Science* (2009) 51(11):PP. 2565-2572.

Tabet, N., I. Allam and R. C. Yin. "X-ray photoelectron spectroscopy study of the carburization of the nickel-based alloy Haynes 214." *Applied Surface Science* (2002) 195(1-4):PP. 166-174.

Takhar, H. S., A. J. Chamkha and G. Nath. "Flow and mass transfer on a stretching sheet with a magnetic field and chemically reactive species." *International Journal of Engineering Science* (2000) 38(12):PP. 1303-1314.

Tan, C.-S., S.-K. Liang and D.-C. Liou. "Fluid-solid mass transfer in a supercritical fluid extractor." *The Chemical Engineering Journal* (1988) 38(1):PP. 17-22.

Tapping, R., Y. Lu and M. Pandey (2007). Alloy 800 SG tubing: current status and future challenges. *Proceedings of the 13th International Conference on Environmental Degradation of Materials in Nuclear Power Systems-Water Reactors*.

Teng, J. T., R. Greif, I. Cornet and R. N. Smith. "Study of heat and mass transfer in pipe flows with non-newtonian fluids." *International Journal of Heat and Mass Transfer* (1979) 22(4):PP. 493-498.

Thomas, F. I. M. and M. J. Atkinson. "Ammonium uptake by coral reefs: Effects of water velocity and surface roughness on mass transfer." *Limnology and Oceanography* (1997) 42(1):PP. 81-88.

Tobias, C. W., M. Eisenberg and C. R. Wilke. "Fiftieth Anniversary: Diffusion and Convection in Electrolysis---A Theoretical Review." *Journal of The Electrochemical Society* (1952) 99(12):PP. 359C-365C.

Tsai, W.-T. and T.-F. Wu. "Pitting corrosion of alloy 690 in thiosulfate-containing chloride solutions." *Journal of Nuclear Materials* (2000) 277(2):PP. 169-174.

Tsai, W., P. Hsu, Y. Hwu, C. Chen, L. Chang, J. Je, H. Lin, A. Groso and G. Margaritondo. "Building on bubbles in metal electrodeposition." *Nature* (2002) 417(6885):PP.

Turner, C. W. and S. J. Klimas. "Deposition of magnetite particles from flowing suspensions under flow-boiling and single-phase forced-convective heat transfer." *The Canadian Journal of Chemical Engineering* (2000) 78(6):PP. 1065-1075.

Turner, C. W., S. J. Klimas and M. G. Brideau. "Thermal resistance of steam-generator tube deposits under single-phase forced convection and flow-boiling heat transfer." *The Canadian Journal of Chemical Engineering* (2000) 78(1):PP. 53-60.

Tvarusko, A. "Dimensionless correlation of mass transfer in wire electroplating cells of various designs." *Journal of The Electrochemical Society* (1973) 120(1):PP. 87-89.

Vogt, H. "Mechanisms of mass transfer of dissolved gas from a gas-evolving electrode and their effect on mass transfer coefficient and concentration overpotential." *Journal of Applied Electrochemistry* (1989) 19(5):PP. 713-719.

Vogt, H. "On the gas-evolution efficiency of electrodes I-Theoretical." *Electrochimica Acta* (2011) 56(3):PP. 1409-1416.

Vogt, H. "On the gas-evolution efficiency of electrodes. II-Numerical analysis." *Electrochimica Acta* (2011) 56(5):PP. 2404-2410.

Vogt, H. "Heat transfer in boiling and mass transfer in gas evolution at electrodes - The analogy and its limits." *International Journal of Heat and Mass Transfer* (2013) 59(0):PP. 191-197.

Vogt, H., O. Aras and R. J. Balzer. "The limits of the analogy between boiling and gas evolution at electrodes." *International Journal of Heat and Mass Transfer* (2004) 47(4):PP. 787-795.

Wang, Y. and K. Sefiane. "Effects of heat flux, vapour quality, channel hydraulic diameter on flow boiling heat transfer in variable aspect ratio micro-channels using transparent heating." *International Journal of Heat and Mass Transfer* (2012) 55(9-10):PP. 2235-2243.

Warrier, G. R. and V. K. Dhir. "Heat Transfer and Wall Heat Flux Partitioning During Subcooled Flow Nucleate Boiling---A Review." *Journal of Heat Transfer* (2006) 128(12):PP. 1243-1256.

Williams, D., R. Möller and H. Grabke. "The high-temperature corrosion of alloy 800 in carburizing, oxidizing, and sulfidizing environments." *Oxidation of Metals* (1981) 16(3):PP. 253-266.

Wragg, A. A. "Free convection mass transfer at horizontal electrodes." *Electrochimica Acta* (1968) 13(12):PP. 2159-2165.

Wragg, A. A. and A. K. Nasiruddin. "Ionic mass transfer by free convection with simultaneous heat transfer." *Electrochimica Acta* (1973) 18(9):PP. 619-627.

Wu, Y. W., G. H. Su, B. X. Hu and S. Z. Qiu. "Study on onset of nucleate boiling in bilaterally heated narrow annuli." *International Journal of Thermal Sciences* (2010) 49(5):PP. 741-748.

Xia, D.-H., R.-K. Zhu, Y. Behnamian, C. Shen, J.-L. Luo, Y.-C. Lu and S. Klimas. "pH Effect on Sulfur-Induced Passivity Degradation of Alloy 800 in Simulated Crevice Chemistries." *Journal of The Electrochemical Society* (2014) 161(4):PP. C201-C214.

Xia, D., S. Song, R. Zhu, Y. Behnamian, C. Shen, J. Wang, J. Luo, Y. Lu and S. Klimas. "A Mechanistic Study on Thiosulfate-enhanced Passivity Degradation of Alloy 800 in Chloride Solutions." *Electrochimica Acta* (2013):PP.

Xia, D. H., S. Z. Song, J. H. Wang and H. C. Bi. "Corrosion detection of metal cans for beverage packaging." *CIESC Journal* (2012) 63(6):PP. 1797-1802.

Xia, D. H., S. Z. Song, J. H. Wang, H. C. Bi and Z. W. Han. "Corrosion behavior of tinplate in NaCl solution." *Transactions of Nonferrous Metals Society of China* (2012) 22(3):PP. 717-724.

Yin, Q., G. Kelsall, D. Vaughan and N. Brandon. "Mathematical models for time-dependent impedance of passive electrodes." *Journal of The Electrochemical Society* (2001) 148(3):PP. A200-A208.

Young, D. F., B. R. Munson, T. H. Okiishi and W. W. Huebsch (2010). *A brief introduction to fluid mechanics*, Wiley. com.

Yuan, S., B. Liang, Y. Zhao and S. O. Pehkonen. "Surface chemistry and corrosion behaviour of 304 stainless steel in simulated seawater containing inorganic sulphide and sulphate-reducing bacteria." *Corrosion Science* (2013) 74(0):PP. 353-366.

Zanotto, F., V. Grassi, A. Balbo, C. Monticelli and F. Zucchi. "Stress corrosion cracking of LDX 2101® duplex stainless steel in chloride solutions in the presence of thiosulphate." *Corrosion Science* (2014) 80(0):PP. 205-212.

Zeitoun, O. and M. Shoukri. "Axial void fraction profile in low pressure subcooled flow boiling." *International Journal of Heat and Mass Transfer* (1997) 40(4):PP. 869-879.

Zhang, X. and D. W. Shoesmith. "Influence of temperature on passive film properties on Ni–Cr–Mo Alloy C-2000." *Corrosion Science* (2013) 76(0):PP. 424-431.

Appendix A Experimental data

A.1.1 Data for Phase I

Table A-1. Experimental data for oxygen reaction conducted under temperature of 20 °C

Speed (RPM)	Velocity (v, m/s)	k (m/s)	Sh	Re
Dissolved oxygen concentration 8.83 ppm				
100	0.06	6.27E-05	421.22	733.27
500	0.31	1.32E-04	885.50	3666.35
900	0.56	1.87E-04	1256.67	6599.44
1700	1.05	2.96E-04	1991.02	12465.60
2500	1.55	3.55E-04	2386.48	18331.77
3300	2.04	4.30E-04	2889.63	24197.93
Dissolved oxygen concentration 4.41 ppm				
100	0.06	6.85E-05	460.21	733.27
500	0.31	1.54E-04	1036.30	3666.35
900	0.56	2.10E-04	1411.38	6599.44
1700	1.05	3.20E-04	2151.77	12465.60
2500	1.55	3.72E-04	2496.97	18331.77
3300	2.04	4.21E-04	2829.73	24197.93
Dissolved oxygen concentration 2.21 ppm				
100	0.06	8.09E-05	543.27	733.27
500	0.31	1.50E-04	1005.10	3666.35
900	0.56	2.27E-04	1521.84	6599.44
1700	1.05	3.28E-04	2204.49	12465.60
2500	1.55	4.12E-04	2768.85	18331.77
3300	2.04	4.84E-04	3250.82	24197.93
Dissolved oxygen concentration 0.44 ppm				
100	0.06	2.27E-04	1523.66	733.27
500	0.31	3.36E-04	2255.21	3666.35
900	0.56	4.57E-04	3069.58	6599.44
1700	1.05	5.27E-04	3540.72	12465.60
2500	1.55	5.97E-04	4007.99	18331.77
3300	2.04	6.80E-04	4568.20	24197.93

Table A-2. Experimental data for oxygen reaction conducted under temperature of 40 °C

Speed (RPM)	Velocity (v, m/s)	k (m/s)	Sh	Re
Dissolved oxygen concentration 6.39 ppm				
100	0.06	9.20E-05	389.39	1088.08
500	0.31	2.15E-04	908.53	5440.38
900	0.56	3.07E-04	1300.21	9792.68
1700	1.05	5.07E-04	2145.69	18497.28
2500	1.55	6.44E-04	2727.80	27201.88
3300	2.04	8.06E-04	3410.40	35906.48
Dissolved oxygen concentration 3.20 ppm				
100	0.06	1.13E-04	478.25	1088.08
500	0.31	2.32E-04	983.13	5440.38
900	0.56	3.34E-04	1412.31	9792.68
1700	1.05	5.00E-04	2115.05	18497.28
2500	1.55	6.21E-04	2630.46	27201.88
3300	2.04	7.25E-04	3070.00	35906.48
Dissolved oxygen concentration 1.60 ppm				
100	0.06	1.42E-04	602.81	1088.08
500	0.31	2.73E-04	1153.82	5440.38
900	0.56	3.46E-04	1466.13	9792.68
1700	1.05	5.41E-04	2290.76	18497.28
2500	1.55	7.09E-04	2999.83	27201.88
3300	2.04	8.18E-04	3462.73	35906.48
Dissolved oxygen concentration 0.32 ppm				
100	0.06	3.12E-04	1319.48	1088.08
500	0.31	4.85E-04	2054.54	5440.38
900	0.56	5.91E-04	2501.33	9792.68
1700	1.05	7.92E-04	3351.18	18497.28
2500	1.55	9.70E-04	4107.52	27201.88
3300	2.04	1.18E-03	5009.24	35906.48

Table A-3. Experimental data for oxygen reaction conducted under temperature of 60 °C

Speed (RPM)	Velocity (v, m/s)	k (m/s)	Sh	Re
Dissolved oxygen concentration 4.79 ppm				
100	0.06	1.24E-04	367.17	367.17
500	0.31	3.06E-04	903.69	903.69
900	0.56	4.16E-04	1229.72	1229.72
1700	1.05	6.87E-04	2030.53	2030.53
2500	1.55	8.79E-04	2596.82	2596.82
3300	2.04	1.10E-03	3246.19	3246.19
Dissolved oxygen concentration 2.40 ppm				
100	0.06	1.71E-04	505.34	1537.01
500	0.31	3.19E-04	942.94	7685.07
900	0.56	4.71E-04	1391.47	13833.12
1700	1.05	7.34E-04	2169.21	26129.23
2500	1.55	9.57E-04	2827.80	38425.34
3300	2.04	1.12E-03	3307.14	50721.45
Dissolved oxygen concentration 1.20 ppm				
100	0.06	1.64E-04	484.21	1537.01
500	0.31	3.46E-04	1023.05	7685.07
900	0.56	4.83E-04	1427.61	13833.12
1700	1.05	7.83E-04	2312.24	26129.23
2500	1.55	9.49E-04	2803.68	38425.34
3300	2.04	1.20E-03	3540.87	50721.45
Dissolved oxygen concentration 0.24 ppm				
100	0.06	4.56E-04	1347.21	1537.01
500	0.31	8.58E-04	2536.01	7685.07
900	0.56	1.07E-03	3157.65	13833.12
1700	1.05	1.25E-03	3705.96	26129.23
2500	1.55	1.31E-03	3865.32	38425.34
3300	2.04	1.80E-03	5312.32	50721.45

Table A-4. Experimental data for oxygen reaction conducted under temperature of 80 °C

Speed (RPM)	Velocity (v, m/s)	k (m/s)	Sh	Re
Dissolved oxygen concentration 3.04 ppm				
100	0.06	1.81E-04	403.20	1982.88
500	0.31	3.89E-04	865.69	9914.40
900	0.56	4.97E-04	1106.26	17845.93
1700	1.05	7.82E-04	1741.58	33708.97
2500	1.55	9.76E-04	2174.37	49572.02
3300	2.04	1.22E-03	2708.48	65435.06
Dissolved oxygen concentration 1.52 ppm				
100	0.06	2.15E-04	479.08	1982.88
500	0.31	4.08E-04	908.99	9914.40
900	0.56	5.52E-04	1229.90	17845.93
1700	1.05	9.36E-04	2085.32	33708.97
2500	1.55	1.10E-03	2439.06	49572.02
3300	2.04	1.20E-03	2670.59	65435.06
Dissolved oxygen concentration 0.76 ppm				
100	0.06	2.55E-04	567.88	1982.88
500	0.31	5.00E-04	1113.35	9914.40
900	0.56	7.54E-04	1678.05	17845.93
1700	1.05	1.21E-03	2705.64	33708.97
2500	1.55	1.46E-03	3242.99	49572.02
3300	2.04	1.55E-03	3449.38	65435.06
Dissolved oxygen concentration 0.15 ppm				
100	0.06	1.16E-03	2572.11	1982.88
500	0.31	1.52E-03	3383.71	9914.40
900	0.56	1.78E-03	3957.21	17845.93
1700	1.05	1.96E-03	4363.33	33708.97
2500	1.55	2.09E-03	4653.68	49572.02
3300	2.04	2.22E-03	4933.26	65435.06

Table A-5. Experimental data for ferricyanide reaction under the concentration of 0.01 mol/L

Speed (RPM)	Velocity (v, m/s)	k (m/s)	Sh	Re
Reaction temperature 20 °C				
100	0.06	2.69E-05	492.35	733.27
500	0.31	7.40E-05	1356.22	3666.35
900	0.56	1.08E-04	1982.58	6599.44
1700	1.05	1.66E-04	3044.78	12465.60
2500	1.55	2.24E-04	4109.54	18331.77
3300	2.04	2.81E-04	5154.43	24197.93
Reaction temperature 40 °C				
100	0.06	3.72E-05	427.94	1088.08
500	0.31	1.11E-04	1282.04	5440.38
900	0.56	1.69E-04	1949.30	9792.68
1700	1.05	2.53E-04	2914.80	18497.28
2500	1.55	3.65E-04	4200.81	27201.88
3300	2.04	4.17E-04	4795.63	35906.48
Reaction temperature 60 °C				
100	0.06	5.42E-05	411.22	1537.01
500	0.31	1.58E-04	1197.39	7685.07
900	0.56	2.33E-04	1766.99	13833.12
1700	1.05	3.74E-04	2833.07	26129.23
2500	1.55	4.83E-04	3663.25	38425.34
3300	2.04	5.93E-04	4493.07	50721.45
Reaction temperature 100 °C (bulk boiling condition)				
100	0.06	2.00E-04	835.21	1982.88
500	0.31	3.35E-04	1399.76	9914.40
900	0.56	4.96E-04	2070.73	17845.93
1700	1.05	8.38E-04	3502.31	33708.97
2500	1.55	1.15E-03	4821.96	49572.02
3300	2.04	1.39E-03	5807.96	65435.06

A.1.2 Data for Phase II

Table A-6. Experimental data for ferricyanide reaction under pool boiling condition with the concentration of 0.01 mol/L

Inlet T_2 (°C)	Outlet T_3 (°C)	q (kW/m ²)	i_L (A/cm ²)	k (m/s)
Surface roughness 0.1 μm				
132.8	131.4	23.53	2.78E-03	2.89E-05
162	159.5	43.71	7.06E-03	7.32E-05
141.3	139.45	26.28	4.58E-03	4.75E-05
149.92	147.75	31.14	5.62E-03	5.83E-05
161.03	158.49	34.42	6.13E-03	6.35E-05
170.15	167.08	41.90	6.63E-03	6.88E-05
163.76	162.36	50.69	7.21E-03	7.47E-05
143.55	142.53	32.42	5.86E-03	6.07E-05
153.53	152.31	39.35	6.26E-03	6.49E-05
143.75	142.69	35.05	3.89E-03	4.03E-05
173	171.13	63.82	7.90E-03	8.19E-05
Surface roughness 0.2 μm				
163.32	161.6	71.29	9.00E-03	9.33E-05
143.44	142.19	46.17	7.22E-03	7.49E-05
172.96	170.98	73.85	9.83E-03	1.02E-04
143.73	142.51	45.36	7.52E-03	7.80E-05
153.52	152.2	48.82	7.97E-03	8.26E-05
132.53	131.24	32.09	6.20E-03	6.43E-05
163.67	161.45	57.13	8.31E-03	8.62E-05
132.33	131.14	25.50	5.03E-03	5.21E-05
153.47	151.63	41.07	7.05E-03	7.31E-05
143.23	141.69	38.74	6.90E-03	7.15E-05
173.17	170.55	67.29	8.94E-03	9.26E-05
140.75	139.39	19.82	3.00E-03	3.11E-05
157.34	155.03	35.33	6.73E-03	6.98E-05
152.1	150.27	30.27	6.24E-03	6.47E-05
171.03	168.41	43.89	7.00E-03	7.25E-05

Inlet T_2 (°C)	Outlet T_3 (°C)	q (kW/m ²)	i_L (A/cm ²)	k (m/s)
Surface roughness	0.95 μ m			
133.83	133.05	24.89	5.64E-03	5.84E-05
163.54	162.12	48.40	8.25E-03	8.55E-05
143.84	142.9	32.10	6.45E-03	6.69E-05
153.69	152.4	46.12	8.28E-03	8.58E-05
173.34	171.28	75.09	1.08E-02	1.12E-04
143.54	142.43	39.38	6.87E-03	7.13E-05
173.14	171.03	78.19	1.09E-02	1.13E-04
132.17	130.68	26.91	5.85E-03	6.06E-05
172.35	169.28	57.57	8.44E-03	8.75E-05
161.62	159.35	39.26	7.28E-03	7.54E-05
141.86	140.18	32.47	7.13E-03	7.39E-05
151.76	149.67	41.04	7.74E-03	8.02E-05
132.73	131.62	27.07	5.98E-03	6.20E-05
163.45	161.39	52.80	8.10E-03	8.40E-05
143.01	141.36	37.51	6.69E-03	6.94E-05
152.71	150.77	44.51	8.03E-03	8.33E-05
132.55	131.43	25.79	5.72E-03	5.93E-05
173.25	170.58	65.54	9.07E-03	9.40E-05

Table A-7. Experimental data for ferricyanide reaction under subcooled boiling condition with the concentration of 0.01 mol/L

Inlet T_2 (°C)	Outlet T_3 (°C)	q (kW/m ²)	i_L (A/cm ²)	k (m/s)
Set 1				
161.98	160.2	66.38	1.02E-03	1.06E-05
162.48	160.7	66.29	3.00E-03	3.11E-05
162.49	160.71	66.29	3.12E-03	3.24E-05
162.55	160.72	68.45	3.25E-03	3.37E-05
162.44	160.66	66.30	3.32E-03	3.44E-05
162.41	160.62	66.74	3.42E-03	3.55E-05
162.46	160.66	67.16	3.57E-03	3.70E-05
162.43	160.65	66.30	3.71E-03	3.84E-05
162.41	160.68	64.13	3.81E-03	3.95E-05
162.46	160.69	65.86	3.89E-03	4.03E-05
162.26	160.51	65.03	4.10E-03	4.25E-05
162.29	160.43	69.80	4.27E-03	4.43E-05
162.23	160.53	62.86	4.55E-03	4.72E-05
162.24	160.44	67.20	4.88E-03	5.06E-05
162.2	160.37	68.51	5.10E-03	5.28E-05
162.11	160.3	67.66	5.28E-03	5.48E-05
161.78	159.94	69.01	6.67E-03	6.91E-05
Set 2				
163.34	162.16	52.17	4.65E-03	4.82E-05
163.32	162.14	52.17	4.84E-03	5.02E-05
163.27	162.09	52.19	5.05E-03	5.23E-05
163.29	162.1	52.75	5.30E-03	5.49E-05
163.27	162.09	52.19	5.79E-03	6.00E-05
163.33	162.14	52.74	6.06E-03	6.28E-05
163.3	162.17	49.35	6.45E-03	6.68E-05
163.46	162.35	48.17	6.47E-03	6.71E-05
163.49	162.37	48.73	5.95E-03	6.17E-05
163.46	162.35	48.17	5.71E-03	5.92E-05
163.37	162.29	46.50	5.27E-03	5.46E-05
163.27	162.16	48.22	5.07E-03	5.25E-05

Table A-8. Experimental data for hydrogen peroxide reaction under pool boiling condition with the concentration of 0.00195 mol/L

Inlet T_2 (°C)	Outlet T_3 (°C)	q (kW/m ²)	i_L (A/cm ²)	k (m/s)
Surface roughness 0.1 μm				
132.01	130.16	31.76	1.36E-03	3.61E-05
142.32	140.21	36.51	2.69E-03	7.14E-05
153.48	150.99	46.83	3.53E-03	9.39E-05
163.73	160.83	54.70	4.50E-03	1.19E-04
132.57	131.21	32.70	1.96E-03	5.21E-05
142.89	141.15	42.90	3.11E-03	8.25E-05
152.58	150.37	56.85	4.39E-03	1.17E-04
163.51	160.98	65.07	5.54E-03	1.47E-04
132.31	131.18	39.57	3.86E-03	1.02E-04
142.35	141.05	46.18	5.11E-03	1.36E-04
152.28	150.6	59.71	6.03E-03	1.60E-04
162.34	160.46	66.55	6.46E-03	1.72E-04
Surface roughness 0.95 μm				
131.97	130.17	31.62	1.64E-03	4.35E-05
142.74	140.68	36.49	2.88E-03	7.66E-05
153.78	151.29	46.24	3.97E-03	1.05E-04
163.61	160.58	56.70	4.83E-03	1.28E-04
132.38	131.23	41.37	4.17E-03	1.11E-04
142.47	141.17	47.29	5.47E-03	1.45E-04
152.43	150.85	55.63	6.34E-03	1.69E-04
162.87	160.96	67.69	7.08E-03	1.88E-04
152.81	150.83	50.65	4.70E-03	1.25E-04
163.49	161.06	62.65	5.97E-03	1.59E-04
132.01	130.58	36.52	2.37E-03	6.30E-05
142.5	140.89	41.46	3.51E-03	9.33E-05

A.1.3 Data for Phase III

Table A-9. Experimental data for hydrogen peroxide reaction under single-phase condition with the concentration of 0.002 mol/L.

Temperature (°C)	Pressure (kPa)	Flow rate (kW/m ²)	i_L (A/cm ²)	k (m/s)
22	445	8.9	3.84E-04	9.96E-06
22	445	12.2	4.03E-04	1.04E-05
22	445	17.0	4.62E-04	1.20E-05
22	445	29.2	6.20E-04	1.61E-05
22	445	44.6	7.36E-04	1.91E-05
80	445	8.9	1.10E-03	2.85E-05
80	445	12.2	1.09E-03	2.82E-05
80	445	17.0	1.31E-03	3.38E-05
80	445	29.2	1.82E-03	4.72E-05
80	445	44.6	2.04E-03	5.30E-05
100	445	8.9	1.37E-03	3.56E-05
100	445	12.2	1.41E-03	3.66E-05
100	445	17.0	1.54E-03	3.99E-05
100	445	29.2	2.58E-03	6.69E-05
100	445	44.6	2.83E-03	7.34E-05
120	445	8.9	1.48E-03	3.83E-05
120	445	12.2	1.55E-03	4.02E-05
120	445	17.0	1.68E-03	4.34E-05
120	445	29.2	2.82E-03	7.30E-05
120	445	44.6	3.20E-03	8.29E-05
22	100	17.0	4.33E-04	1.12E-05
22	238	17.0	4.44E-04	1.15E-05
22	514	17.0	4.75E-04	1.23E-05
22	583	17.0	4.82E-04	1.25E-05
22	652	17.0	4.98E-04	1.29E-05

Temperature (°C)	Pressure (kPa)	Flow rate (kW/m ²)	i_L (A/cm ²)	k (m/s)
80	100	17.0	1.25E-03	3.24E-05
80	238	17.0	1.25E-03	3.23E-05
80	514	17.0	1.39E-03	3.61E-05
80	583	17.0	1.43E-03	3.69E-05
80	652	17.0	1.45E-03	3.76E-05
100	514	17.0	1.60E-03	4.14E-05
100	583	17.0	1.61E-03	4.17E-05
100	652	17.0	1.70E-03	4.40E-05
120	514	17.0	1.69E-03	4.39E-05
120	583	17.0	1.78E-03	4.61E-05
120	652	17.0	1.84E-03	4.76E-05

Table 6-1. Experimental data for hydrogen peroxide reaction under flow boiling condition with the concentration of 0.002 mol/L.

Inlet T_2 (°C)	Outlet T_3 (°C)	Flow rate (kW/m ²)	Pressure (kPa)	q (kW/m ²)	i_L (A/cm ²)	k (m/s)
144.21	141.23	8.9	100	223.057644	1.84E-03	4.77E-05
139.41	136.07	12.2	100	250.004205	2.95E-03	7.65E-05
136.25	133.25	12.2	100	224.554675	2.79E-03	7.24E-05
136.42	132.91	17.0	100	262.72897	3.02E-03	7.83E-05
132.13	129.06	29.2	100	229.794284	3.03E-03	7.85E-05
137.81	133.93	44.6	100	290.424046	3.70E-03	9.58E-05

Appendix B Calculations

B.1 Sample calculation

B.1.1 Calculation of dissolved oxygen concentration.

In order to calculate the mass transfer coefficient the oxygen concentration has to be calculated first. The concentration of dissolved oxygen under different temperatures will be calculated by Henry's law which indicated that the amount of a given gas that dissolves in a given type and volume of liquid is directly proportional to the partial pressure of that gas in equilibrium with that liquid.

$$p = K_H C \quad (\text{B.1})$$

where p is the partial pressure of the solute in the gas phase above the solution, C is the concentration of the solute and K_H is a Henry's law constant with the dimensions of pressure divided by concentration. Therefore, we can control the concentration of dissolved oxygen by control the partial pressure of oxygen in the experimental atmosphere.

The partial pressure of a certain gas is proportional to the mole ratio of that gas in the environment, therefore the oxygen partial pressure is controlled by the mole ratio of the oxygen in the inlet gas flow and the gas is bubbled continually in to the reactor during the reaction in order to keep that ratio constant. The value of oxygen mole ratio was controlled at 1%, 5%, 10% and 20% at the inlet.

For the calculation of K_H , a semiempirical correlation have been given by Harvey[1] over large temperature range:

$$\ln K_H = \ln P_l + \frac{A_1}{T^*} + \frac{A_2(1 - T^*)^{0.355}}{T^*} + A_3 e^{(1-T^*)(T^*)^{-0.41}} \quad (\text{B.2})$$

Where A_1 , A_2 and A_3 are the parameters and the values are -9.4025, 4.4923 and 11.3387 for O_2 in water, T^* is the reduced temperature which equal to T/T_c ; and T_c is the solvent's critical temperature, for water it is 647.096 K.

P_l is the solvent vapor pressure and can be calculated using the equation given by Saul and Wagner[2]:

$$\ln(P_l/P_c) = T_c/T(a_1\tau + a_2\tau^{1.5} + a_3\tau^3 + a_4\tau^{3.5} + a_5\tau^4 + a_6\tau^{7.5}) \quad (\text{B.3})$$

Where $a_1 \sim a_6$ are constant, the values are: $a_1 = -7.85823$, $a_2 = 1.89391$, $a_3 = -11.7811$, $a_4 = 22.6705$, $a_5 = -15.9393$, $a_6 = 1.77516$, P_c is the critical pressure for water which is 22064 kPa and $\tau = 1 - T^*$.

The dissolved oxygen concentration then can be calculated based on the Eq. (A-1), the results is shown in the Figure A-1. As it can be observed, the concentration of dissolved oxygen decreased with the increase of temperature when the temperature is below 100 °C and will increase after that. The dissolved concentration of O_2 of 20% O_2 at temperature of 20 °C and 40 °C are 8.95

and 6.73 ppm, respectively. These data have been used in the Phase I study to calculate the mass transfer coefficient.

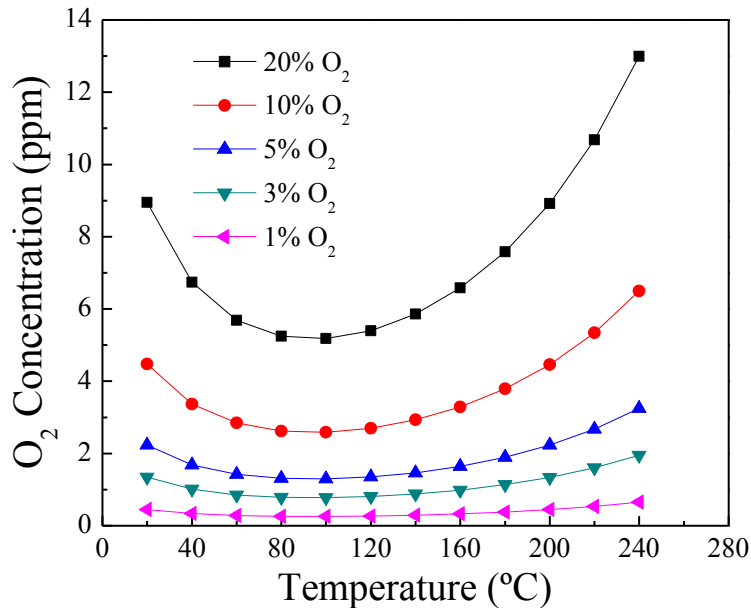


Figure B-1. Calculation results of dissolved O₂ concentration

B.1.2 Sample mass transfer coefficient calculation

There are a large number of parameters that need to be calculated in this thesis. The calculation has not been given by very detail due to the length control. In this section, a sample calculation of important such as mass transfer coefficient, Sherwood number, heat flux and the error bars is given. The data and constant used here is from Phase II experiment.

The experiment was mass transfer measurement of ferricyanide on fully developed nucleated boiling surface, conducted on the date Sep. 4th 2013. The concentration of ferricyanide C is 0.01 mol/L, the measured limiting current density is 0.00803 A/cm², the diffusivity of ferricyanide at saturation electrolyte temperature (100 °C) is 2.83×10^{-9} m²/s, surface area of the specimen A is

0.00149 m², the inlet oil temperature T_2 is 152.71 °C, out let oil temperature T_3 is 150.77 °C, the flow rate of the m oil is 0.025 kg/s and the heat capacity of oil is 1.51 kJ/kg K.

The mass transfer coefficient can be calculated as:

$$k = \frac{i_L}{nFC_b} = \frac{0.00803 \frac{\text{A}}{\text{cm}^2}}{1 \times 96485 \frac{\text{A s}}{\text{mol}} \times 0.01 \frac{\text{mol}}{\text{L}}} = 8.33 \times 10^{-5} \text{ m/s} \quad (\text{B.4})$$

The error of mass transfer coefficient can be estimated as:

$$\omega_{i_L} = \pm(0.003i_L + 2\sigma_{i_L}) \quad (\text{B.5})$$

$$\begin{aligned} \omega_{i_L} &= \pm(0.003i_L + 2\sigma_{i_L}) = \pm\left(0.003 \times 0.008 \frac{\text{A}}{\text{cm}^2} + 2 \times 0.00018 \frac{\text{A}}{\text{cm}^2}\right) \\ &= 0.00204 \frac{\text{A}}{\text{cm}^2} \end{aligned} \quad (\text{B.6})$$

$$\omega_{C_b} = \pm(0.04C_b) = 0.0004 \frac{\text{mol}}{\text{L}} \quad (\text{B.7})$$

$$\begin{aligned} \omega_k &= \pm \left[\left(\frac{\partial k}{\partial i_L} \omega_{i_L} \right)^2 + \left(\frac{\partial k}{\partial C_b} \omega_{C_b} \right)^2 \right]^{0.5} \\ &= 4.11 \times 10^{-6} \text{ m/s} \end{aligned} \quad (\text{B.8})$$

The Sherwood number can be calculated as:

$$Sh = \frac{kL}{D} = \frac{9.26 \times 10^{-5} \frac{\text{m}}{\text{s}} \times 0.00158 \text{ m}}{2.83 \times 10^{-9} \frac{\text{m}^2}{\text{s}}} = 450.28 \quad (\text{B.9})$$

The heat flux can be calculated as:

$$q = \frac{m(T_2 - T_3)C_p}{A} = \frac{0.0025 \frac{kg}{s} (152.71 - 150.77)K \times 1.51 \frac{kJ}{kg K}}{0.00149m^2} = 44.5 \frac{kW}{m^2} \quad (B.10)$$

$$\omega_q = \pm q \times \left\{ \left(\frac{\omega_{\dot{m}}}{\dot{m}} \right)^2 + \left(\frac{\omega_{c_p}}{c_p} \right)^2 + \left[\frac{\omega_{T_{in}}}{(T_{in} - T_{out})} \right]^2 + \left[\frac{\omega_{T_{out}}}{(T_{in} - T_{out})} \right]^2 + \left(\frac{\omega_A}{A} \right)^2 \right\}^{0.5} = 2.55 \frac{kW}{m^2} \quad (B.11)$$

This data was showed in Figure 3-8 (a), at Chapter 3 Phase II.

B.2 Calculation for design of phase III

B.2.1 Solution tank

The volume of the tank is estimated base on the experiment lasting 3 hours for the maximum flow rate.

$$\text{Vol} = \frac{m * A * 5h}{\rho @ 20^\circ C} = \frac{150 \text{ kg/m}^2\text{s} \times 0.0001235\text{m}^2 \times 3 \times 3600\text{s}}{998.2 \text{ kg/m}^3} = 212.02 \text{ L} \quad (B.12)$$

Therefore, the total volume for each solution tank would be around 200 L, the 55 gallon stainless steel drum (McMaster-Carr) was selected as the solution tank.

B.2.2 Pre heater

The power of preheater was calculated using the following equations. In our loop, the heating power is selected to be less than 20 kW due to the limitation of the power availability.

$$m = 50 \text{ kg/m}^2\text{s} \quad (\text{B.13})$$

$$V = \frac{m}{\rho@20^\circ\text{C}} = \frac{100 \text{ kg/m}^2\text{s}}{998.2 \text{ kg/m}^3} = 0.05 \text{ m/s} \quad (\text{B.14})$$

$$\begin{aligned} E_{pre} &= m * A * (H_{200^\circ\text{C}} - H_{20^\circ\text{C}}) \quad (\text{B.15}) \\ &= 50 \text{ kg/m}^2\text{s} \times 0.0001235\text{m}^2 \times (851.9 - 83.8) \text{ kJ/kg} = 4.7 \text{ kW} \end{aligned}$$

$$\begin{aligned} E_{vap} &= m * A * 10\% * H_{vap} \quad (\text{B.16}) \\ &= 50 \text{ kg/m}^2\text{s} \times 0.0001235\text{m}^2 \times 10\% \times 1937.3 \text{ kJ/kg} = 1.195 \text{ kW} \end{aligned}$$

$$E_{tot} = E_{pre} + E_{vap} = 5.89 \text{ kW} < 10\text{kW} \quad (\text{B.17})$$

Therefore the selected flow rate is under the limitation of the preheater.

B.2.3 Entrance length

The entrance length L_e for the electrochemical flow cell was calculated using the following equations [3]:

Hydraulic diameter, D

$$D = \frac{4 \times \text{flow area}}{\text{frictional wetted perimeters}} \quad (\text{B.18})$$

$$= \frac{4\pi(D_1^2 - D_2^2)}{4\pi(D_1 + D_2)} = D_1 - D_2 = 6.2 \text{ mm}$$

$$Re = \frac{\rho \cdot D \cdot V}{\mu} = 2664 \quad (\text{B.19})$$

For laminar flow for maximum $Re=2100$

$$L_e = 0.06 \cdot D \cdot Re = 0.06 \cdot 6.2 \text{ mm} \cdot 2100 = 0.78 \text{ m} \quad (\text{B.20})$$

For turbulent flow, even for Re as high as 80000:

$$L_e = 4.4 \cdot D \cdot Re^{\frac{1}{6}} = 4.4 \cdot 6.2 \text{ mm} \cdot 80000^{\frac{1}{6}} = 0.18 \text{ m} \quad (\text{B.21})$$

Therefore the 0.78 m was selected as the design entrance length.

Table B-1. Dimensions of the flow loop and electrochemical flow cell as well as the operating range.

Descriptions	Dimensions
Outer tube (Stainless Steel)	19.05mm OD; 15.75 mm, ID
Inner tube (Alloy 800)	9.53mm OD; ID=7.80 mm ID
Entrance length	0.78 m
Total length of the cell	1.6 m
Surface roughness	$Ra = \sim 1 \mu\text{m}$
Operating Conditions	
Temperature	200 °C
Pressures	6.2 Mpa
Heat flux at the working electrode surface	Up to 300 kW/m ²
Working Fluid mass flow rate	Up to 50 kg/m ² s

B.3 References

- [1] Harvey, A.H., "Semiempirical correlation for Henry's constants over large temperature ranges," *AIChE Journal*, 42 (1996): pp. 1491-1494.
- [2] Saul, A. and W. Wagner, "International equations for the saturation properties of ordinary water substance," *Journal of Physical and Chemical Reference Data*, 16 (1987): pp. 893-901.
- [3] Young, D.F., B.R. Munson, T.H. Okiishi and W.W. Huebsch, *A brief introduction to fluid mechanics* 2010: Wiley. com.

Appendix C Effect of Boiling Bubbles on Passivation

Degradation of Alloy 800 in Thiosulphate-containing Aqueous

Solution

C.1 Introduction

Alloy 800 has been widely used in steam generators (SGs) tubing materials in CANada Deuterium Uranium (CANDU^{®TM}) reactors and German designed Pressurized Water Reactor (PWR) systems due to its excellent strength and corrosion resistance [1, 2]. Although SG tubes eventually approach their design lifetime, Alloy 800 SG tubing degradation has been found in a very small number of cases [3]. Concentrated impurities in local aggressive environments [4, 5] are key factors in material degradation such as pitting and stress cracking corrosion (SCC). Sulphate is a major impurity in SG feed water; it can be reduced to sulphide and deposited within tube sheet crevices, assisted by hydrazine (N₂H₄) during full power operating conditions. Sulphide can also be oxidised to thiosulphate/polythionate under oxidizing conditions that occur during shutdown stage [6, 7]. Thiosulphate (S₂O₃²⁻) is one of the most aggressive intermediate oxidation state of sulphur and the effect is more severe in the presence of the common impurity chloride, Cl⁻ [7, 8]. The combined effect of thiosulphate and chloride ions has been reported to lower the pitting potentials for 304 stainless steel, Alloy 600 and Alloy 690 in neutral chloride solutions [8-11]. Corrosion degradation of Alloy 800 have been experimentally investigated from room temperature up to 300 °C using various electrochemical methods such as electrochemical impedance spectroscopy (EIS), electrochemical noise (EN), polarization curve, and scanning electrochemical microscope (SECM), etc. [12-16]. Several semi-empirical models such as electrochemical equivalent circuit, point defect, energy-band [17-20] have been developed for

corrosion degradation of the passive films at different temperatures. However, there are limited investigations conducted under flow boiling conditions which are the common working condition in SG, involving elevated temperature, vapour generation and gas-liquid two-phase flow [21, 22]. Most of the previous high temperature studies took place in autoclaves where continuous boiling was not likely to occur [15, 23]. Thus the effect of boiling bubbles on the corrosion behavior of Alloy 800 is still unknown. In the open literature, the experimental studies on material degradation under two-phase boiling conditions are scarce.

In this study, the effects of boiling bubbles on sulphur-induced passivity degradation of Alloy 800 in simulated crevice chemistry have been investigated using electrochemical and surface-analysis techniques. The effects and possible mechanisms of boiling bubbles on sulphur-induced passivity degradation are discussed.

C.2 Experimental

C.2.1 Experimental set up

A schematic diagram of the experimental set-up is shown in Fig. 1. A modulated speed rotator (Pine Instrument Co.) was used to provide variable rotating speed and conductivity from a rotating shaft to the specimen. A section in 10 mm length of an Alloy 800 (Sandvik, heat number 516809) heat exchange tube with inner and outer diameters of 15.8 mm, 13.4 mm, respectively, was used as the specimen. The composition of this alloy is: Fe 43.20, Ni 32.78, Cr 21.78, Mn 0.50, Ti 0.48, Si 0.46, Al 0.29, Cu 0.02, C 0.017, N 0.016, P 0.012, Co 0.01, and S 0.001 wt.%. A platinum coil circle around the specimen with a circle diameter of 60 mm was used as the counter electrode. An Ag/AgCl reference electrode (Fisher Scientific) with an operating

temperature range of -5 °C to +110 °C was utilized to provide the reference potential during the experiment. All potentials reported have been converted to standard hydrogen potentials (SHE) at the corresponding temperature using the following correlation[24]:

$$E_{SHE} = E_{Ag/AgCl} + 0.2866 - 0.001\Delta T + 1.745 \times 10^{-7}\Delta T^2 - 3.0310^{-9}\Delta T^3 \quad (C.1)$$

Where

$$\Delta T = T_{Experiment} - T_{room} \quad (C.2)$$

The temperature of the electrolyte was controlled using an external oil-circulating bath (Cole-Parmer PolyStat Co.) in a temperature range from room temperature (20 °C) to boiling. A condenser was used to maintain the constant electrolyte concentration. This set-up allows us to simulate the flow boiling conditions needed to study flow enhanced material degradation. An SI 1287 Electrochemical Interface (Solartron Analytical Co.) was used as the electrochemical station to conduct all the electrochemical measurements. Composition of the testing electrolyte is listed in Table C-1.

Table C-1. Composition of testing electrolyte

Composition	NaCl	KCl	CaCl ₂	Na ₂ S ₂ O ₃	pH _{20°C}
Concentration (mol/L at 20 °C)	0.30	0.05	0.15	0.075	7.01

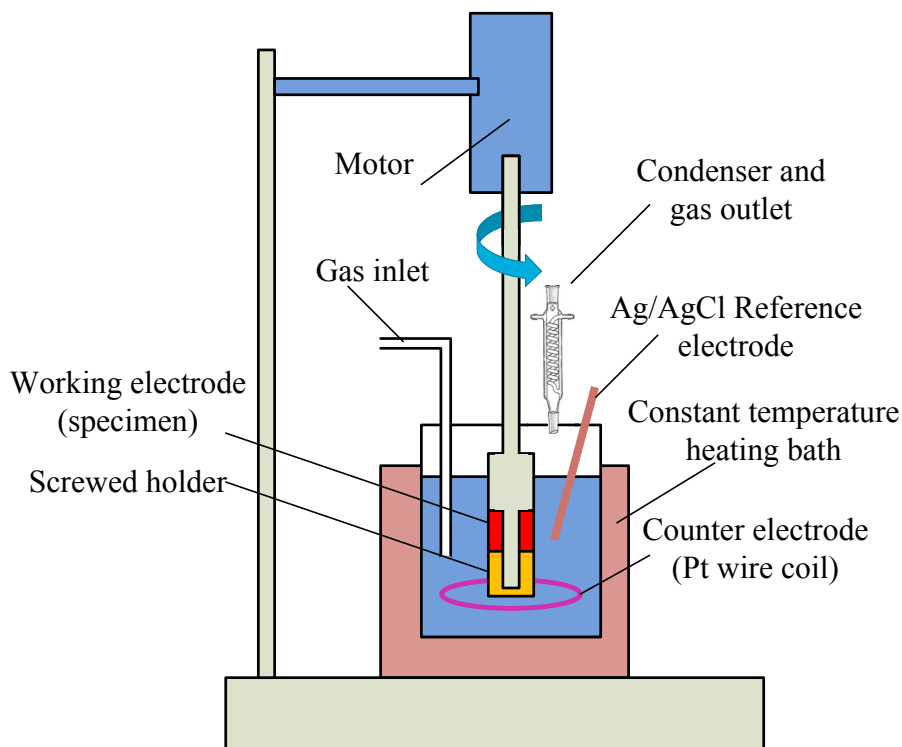


Figure C-1. Rotating electrode electrochemical experimental set-up.

C.2.2 Experimental procedure

Before each test, the specimens were grounded using 600#, 800# and 1200# grit sand papers and rinsed with distilled water followed by ethanol. Then, the specimens were air dried in a desiccator for 12 hours. All the test solutions were de-aerated with high purity Argon (99.99%) for 2 hours before each test. Argon flow was maintained throughout the electrochemical measurements to eliminate the presence of oxygen in the experiments.

To investigate the surface electrode reaction, cyclic voltammetry (CV) was performed by sweeping the potential in the passivity region according to polarization curves and then in the reverse direction back to the initial value at the potential scan rate of 50 mV s^{-1} . Before each CV test, the specimen was cathodic polarized ($-1.2 \text{ V}_{\text{SHE}}$) for 15 minutes trying to get a fresh metal surface.

The same cathodic polarization ($-1.2 V_{\text{SHE}}$) was applied for the specimen for 15 minutes as the initial conditioning step to reduce the air-formed oxide film on the specimen surface. Then, the specimen was immersed in the de-aerated test solutions at open-circuit overnight before the potentiodynamic and EIS measurements.

Potentiodynamic polarization curves were measured by sweeping the potential in the positive direction at 0.1667 mV/s until the current density reached 1 mA/cm^2 . EIS measurements were performed at the free corrosion potential with an AC potential signal of 10 mV amplitude and the frequencies from 100 kHz to 0.01 Hz . The results were analyzed using an equivalent circuit to evaluate the resistance of the anodic film at different solution temperatures. For the reproducibility, at least 3 measurements were performed for each specimen.

Scanning electron microscopy (SEM) analyses were carried out to test the surface morphology of corrosion pits on the specimens after electrochemical measurements using a field-emission scanning electron microscope (FE-SEM, Hitachi, Japan) equipped with Genesis XM2 energy dispersive spectroscopy (EDS).

Time-of-flight secondary ion mass spectrometry (ToF SIMS) analysis was carried out using a ToF SIMS IV instrument (ION-ToFGmbH) to test the depth profiles of the main elements in the anodic films formed at the different solution temperatures. The information depth of ToF SIMS analysis is limited to the top 1-20 monolayers. Ions from mass 1 (hydrogen) to $\sim 9000 \text{ amu}$ (cluster ions) were detected with resolutions in the range of 1 ppb to ppm concentrations (by

weight), depending on the element. In the current work, the analysis source used was Ga⁺, operating at 15 kV; the sputtering source was Cs⁺, operating at 1 kV. The samples were immersed in the solution for 7 days at different temperatures and then cleaned with distilled water before the SIMS test.

X-ray photoelectron spectroscopy (XPS) measurements were performed using an Axis-ULTRA spectrometer (Kratos Analytical) controlled by a SUN workstation to test the valence of main elements in the anodic films. Photoelectron emission was excited by an aluminum (monochromatised) source operated at 210 W with initial photon energy of 1486.71 eV. The survey spectra were recorded in steps of 0.33 eV using 160 eV pass energy, and high-resolution spectra were taken in steps of 0.1 eV using 20 eV pass energy. The base pressure was approximately 5×10^{-10} Torr. The photoelectrons were collected at a take-off angle of 90° with respect to the sample surface. The C1 peak at 284.6 eV from adventitious carbon was used as a reference to correct for charging shifts. The samples were immersed in the solution for 7 days at different temperatures before the SIMS test. Specimens were cleaned using distilled water, before each test. The binding energies for the targeted components are listed in Table C-2.

Table C-2. Binding energies of XPS peaks

Element	Species	Binding Energy (eV)	References
S	SO ₄ ²⁻ (2p)	168.1-169.4	Neal et al. (2001) [25]
			Lindberg et al. (1970) [26]
	SO ₃ ²⁻ (2p)	166.0-167.0	Yuan et al. (2013) [27]
			Siriwardane et al. (1986) [28]
	S ⁰ (2p)	164.4	Pratt et al. (1994) [29]
	S ²⁻ (2p)	162.5	Mycroft et al. (1990) [30]
Fe	Fe ⁰ (2p 3/2)	707.2	Lu et al. (2013) [31]
	Fe ⁰ (2p 1/2)	720.2	NIST (2000) [32]
	FeS (2p 3/2)	710.1	Smestad et al. (1990) [33]
	Fe ²⁺ _{ox} (2p 3/2)	710.5	NIST (2000) [32]
Ni	Ni ⁰ (2p 3/2)	852.8	Tabet et al. (2002) [34]
	Ni ⁰ (2p 1/2)	870.1	Tabet et al. (2002) [34]
	NiS (2p 3/2)	855.6	NIST (2000) [32]
	Ni ²⁺ _{OH} (2p 3/2)	856.0	Lu et al. (2013) [31]
Cr	Cr ⁰ (2p 3/2)	573.9	Hamm et al. (2002) [35]
	Cr ⁰ (2p 1/2)	583.0	Hamm et al. (2002) [35]
	Cr ³⁺ _{ox} (2p 3/2)	576.1	Lu et al. (2013) [31]
	Cr ³⁺ _{ox} (2p 1/2)	585.5	Lu et al. (2013) [31]
	Cr ³⁺ _{OH} (2p 3/2)	577.6	NIST (2000) [32]
	Cr ³⁺ _{OH} (2p 1/2)	587.7	NIST (2000) [32]

C.3 Results and discussion

C.3.1 Corrosion potential

Figure C-2 shows the corrosion potential of Alloy 800 in de-aerated solution as a function of temperatures. Below the boiling point, the corrosion potential decreases with increasing the solution temperature ($E_{\text{corr}1} > E_{\text{corr}2} > E_{\text{corr}3}$). Increasing the solution temperature accelerates both anodic and cathodic reactions. However, the acceleration rate of anodic reactions is higher than that of cathodic reaction [36], thus the corrosion potential presents a negative shift in the Evans diagram. This result is consistent with the result reported in the literature [37] for Alloy 625. The corrosion potential shifts positively under the boiling condition ($E_{\text{corr}3} < E_{\text{corr}4}$) compared to the condition just below boiling point (99 °C). The effect of temperature could be excluded since the change in temperature is small. The boiling bubble enhanced the forced convection and decreased the thickness of diffusive layer. The mass transfer of reactive species from bulk solution to the electrode increase significantly by the boiling bubbles [38]. The cathodic reaction rate increased with the increase of mass transport in the solution. This increase in the cathodic reaction leads to a positive shift in the corrosion potential in the Evans diagram.

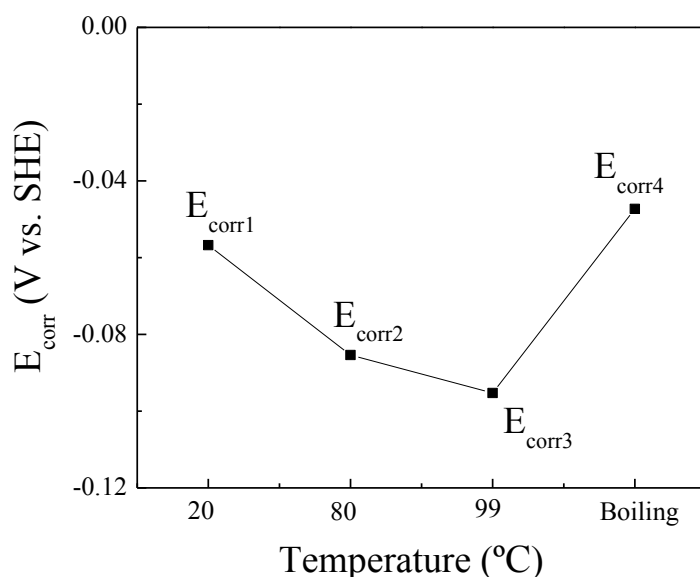


Figure C-2. Corrosion potentials for Alloy 800 in deaerated testing electrolyte at various temperatures.

C.3.2 Anodic polarization

Figure C-3 shows anodic polarization curves of Alloy 800 at various electrolyte temperatures including the bulk boiling condition. As expected, Alloy 800 showed self-passivation characteristics in a wide passive potential range (0–620 mV_{SHE}) with a passivation current density round 1 $\mu\text{A}/\text{cm}^2$ at room temperature. Such a small current density indicates that the passive layer of Alloy 800 has a low dissolution rate. The passive film appears to breakdown when the anodic polarization reaches the critical pitting potential. The current density increases dramatically at the pitting potential indicating that pitting corrosion is taking place. Figure C-3 also shows that the pitting potential decreases as the temperature increases and the passive current density increases with increasing temperature from room temperature to 99 °C. Shrinkage of the passive potential range and an increase in current density indicate the degradation of the stability and corrosion resistance of the passive film. The effects of

temperature on the degradation of the passive layers observed are consistent with other's work [37]. Under bulk boiling condition, the critical pitting potential further decreased to approximately 280 mV_{SHE} and the passive current density increased to 8 μA/cm². The increase in boiling bubbles in the bulk boiling condition might cause an increase in convection of the electrolyte, that is, the reactant and corrosion product would be transported faster under boiling condition than under below boiling condition. This higher transport rate could lead to an increasing corrosion reaction rate indicting an enhancement of passive layer degradation. Xia et al. [39] pointed out that the breakdown of passive film is related to its semi-conductivity, and the passive film in the testing electrolyte is considered as n-type semiconductor. N-type semiconductors are easy to breakdown but are more resistant than p-type semiconductors to anodic dissolution [40].

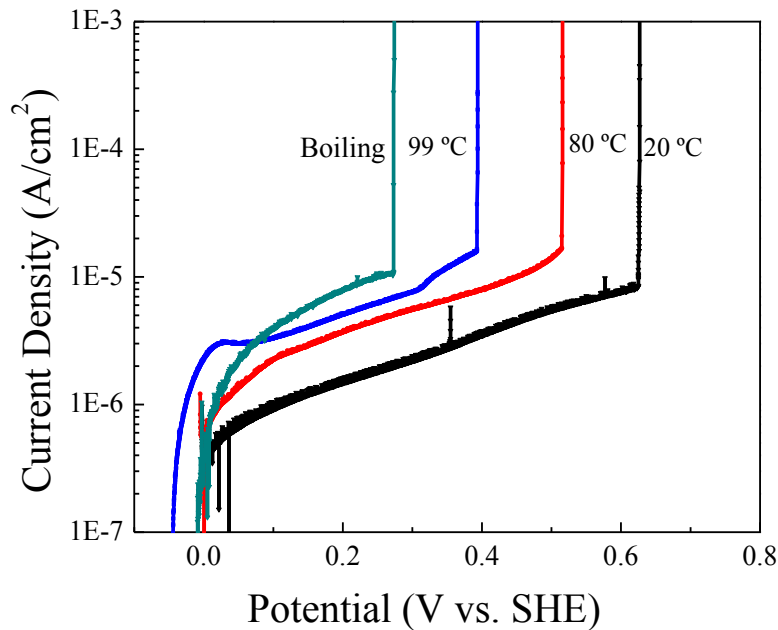


Figure C-3. Anodic potentiodynamic polarization curves for Alloy 800 in deaerated testing electrolyte at various temperatures.

C.3.3 Electrochemical impedance spectroscopy (EIS)

The Nyquist plot in the testing electrolyte at different temperatures and the equivalent circuit are shown in Figure C-4. The symbols represent experimental measured data and the solid lines represent the fit line obtained using the electrochemical equivalent circuit (EEC) which is well accepted model for a passive system. Where the solution resistance is represented by R_s . The R_s (Q_1R_1)(Q_2R_2) model [41, 42] uses Q_1 and R_1 to present the double layer capacitance and the charge transfer resistance, respectively, and Q_2 and R_2 to present the film capacitance and film resistance, respectively. This two layer model is well accepted and presented the real structure of the passive film [43, 44], therefore, is employed in this work. The mathematical expression of the impedance of this electrode system is given as:

$$Z = R_s + \frac{1}{\frac{1}{R_1} + Y_1(j\omega)^{n_1}} + \frac{1}{\frac{1}{R_2} + Y_2(j\omega)^{n_2}} \quad (\text{C. 3})$$

This model fits our experimental data well and the fitting parameters are shown in Table C-3.

Table C-3. Constants of the EEC model.

Temp. (°C)	R_s ($\Omega \cdot \text{cm}^2$)	R_l ($\Omega \cdot \text{cm}^2$)	Q_1 ($\mu\text{F cm}^{-2}$)	n_1	R_2 ($\Omega \cdot \text{cm}^2$)	Q_2 ($\mu\text{F cm}^{-2}$)	n_2	χ^2 (%)
20	47.18	3.25×10^4	3.41	0.61	4.08×10^5	38.6	0.89	0.018
80	24.30	1.82×10^4	5.74	0.65	1.12×10^5	85.1	0.91	0.023
99	23.52	1.17×10^4	5.79	0.65	0.74×10^5	97.6	0.92	0.413
Boiling	54.35	2.55×10^4	6.83	0.71	0.58×10^5	84.3	0.79	2.843

It can be seen from Table C-3, that R_s decreases with the increase of temperature before boiling due to an increase in the diffusivity of ions. Also, the film resistance, R_2 decreases with the increase of the temperature since the dissolution rate of passive film is higher at elevated temperatures. Table 3 also shows that the solution temperatures of 99 °C and at the boiling condition, the film resistance, R_2 further decreases. Since the temperature difference is very small in these two cases, the main reason could be that the boiling bubbles enhance the forced convection of the electrolyte and leads to flow accelerate corrosion. The corrosion resistance of Alloy 800 is dependent on the composition, nature and thickness of the passive film. It's well known that the temperature has significant influence on composition, structure and thickness of passive film or corrosion product film formed on the Ni-base alloys. Huang et al. [45] investigated the electrochemical properties and growth mechanism of passive films on Alloy 690 in solutions in the temperature ranged from 20 °C to 300 °C. They found that the thickness of the passive films increases with increasing solution temperature, and the donor density in the passive films increases and in turn results in an increase of the passive current density. This was believed to be due to increased diffusion rates of metallic ions with increasing temperature. In summary, an increased in solution temperature, increased the diffusivity of charged ions, increased diffusion rates of metallic ions, eventually decrease the film resistance and corrosion resistance.

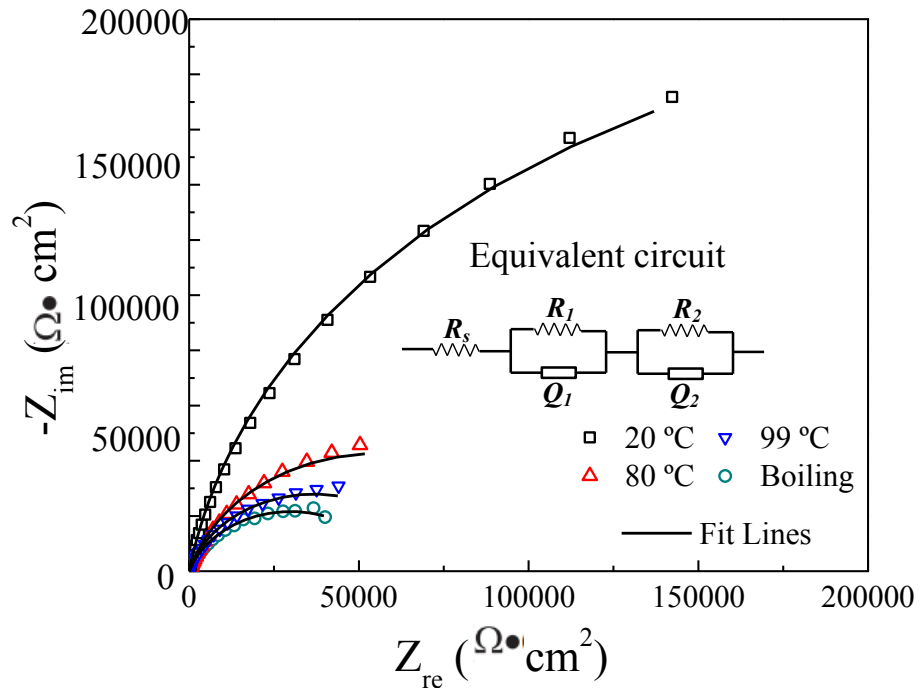


Figure C-4. EIS for Alloy 800 in deaerated testing electrolyte at various temperatures.

C.3.5 Secondary ion mass spectrometry (SIMS)

The SMIS results of elements O and S of the specimen after immersion in test solution at various temperatures for 7 days are shown in Figures C-5 (a) and (b), respectively. It can be seen that the change of temperature and the existence of boiling bubbles have a significant effect on O and S intensity versus depth profiles. At the room temperature and 80 °C, the thicknesses of oxide and sulphide are under 30 nm. When the temperature is increased to 99 °C and the solution boils, the thickness of the anodic film increases to above 100 nm. The change in film thickness is attributed to an increase in the activation energy of the outer layer on the specimen surface at high temperature [46]. Thus the diffusion rate of vacancies and atoms in the film increases. Boiling bubble movement could dislodge the corrosion product in the anodic film and possibly

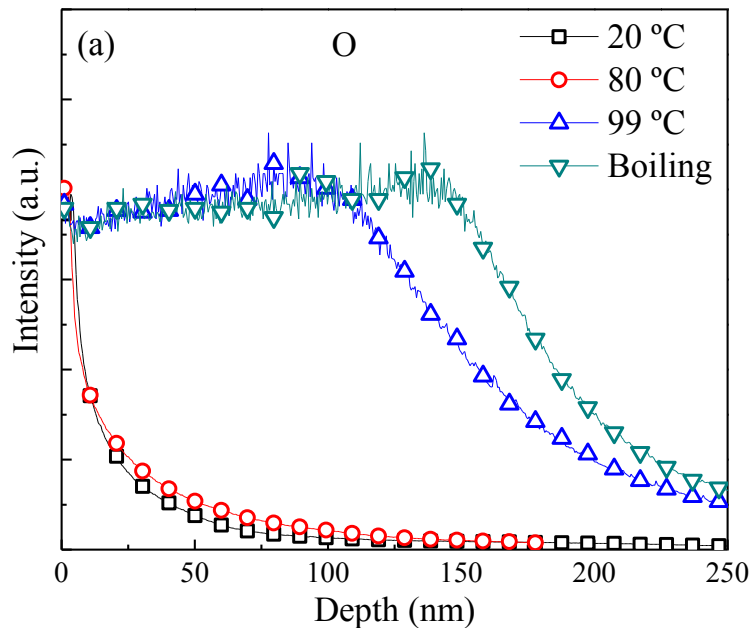
leading to two results: The first one is the porous structure of the film increasing and allowing the oxidation reaction to take place deeper in the matrix. The other one is S permeates deeper in the boiling condition, which indicates that the permeation of S into the passive layer is significant and hence the corrosion resistance of the anodic film has decreased in the boiling condition.

Since secondary ion yields depend on the chemical environment of the target, it is difficult to relate the strength of the SIMS signals to the concentration difference between different elements [31]. A comparison of the ratios of the intensities of $\text{Fe}/(\text{Fe}+\text{Ni}+\text{Cr})$, $\text{Ni}/(\text{Fe}+\text{Ni}+\text{Cr})$ and $\text{Cr}/(\text{Fe}+\text{Ni}+\text{Cr})$ are shown in Figures C-6 (a) to (c). It is important to determine whether certain elements are preferentially dissolved from the anodic film due to a change in temperature and an influence of boiling bubbles. The following phenomena can be observed from Figures C-6 (a) to (c).

- (1) The anodic films formed at room temperature and at 80 °C have a similar structure; both films are Ni-enriched as shown in Figure C-6 (b) and Cr-depleted in Figure C-6 (c). The $\text{Fe}/(\text{Fe}+\text{Ni}+\text{Cr})$ ratios in the anodic films are close to the ratio inside the matrix as shown in Figure C-6 (a). The results are consistent with the data reported in the literature [50].
- (2) At 99 °C, the anodic film start to behavior different than that below 80 °C. The change of intensity ratio of the metal elements happened at around 100 nm which indicate the anodic film is thicker than that at lower temperatures where the changes happened around 30 nm. This results is consistent with that of SMIS analyses of S and O as shown in

Figures C-5 (a) and (b). In this thicker anodic film, it can be observed that the relative content of Cr is less than that of Ni and Fe, indicating Cr depleted relatively faster than Ni and Fe at higher temperature.

(3) Under the boiling condition, the Ni/(Fe+Ni+Cr) intensity ratio is lower than the film formed at 99 °C, as shown in Figure C-6 (b), revealing that Ni is preferentially dissolved from the matrix in the boiling condition. When Ni is removed from the matrix metal, the pitting resistance of the specimen decrease [47]. It leads to a decrease of critical pitting potential at boiling condition, which is consistent with the anodic polarization measurements. Different from Ni, the intensity ratio of Cr under boiling condition is higher than that at 99 °C, as shown in Figure C-6 (c). The higher intensity ratio indicated that the Cr is less depleted under boiling condition.



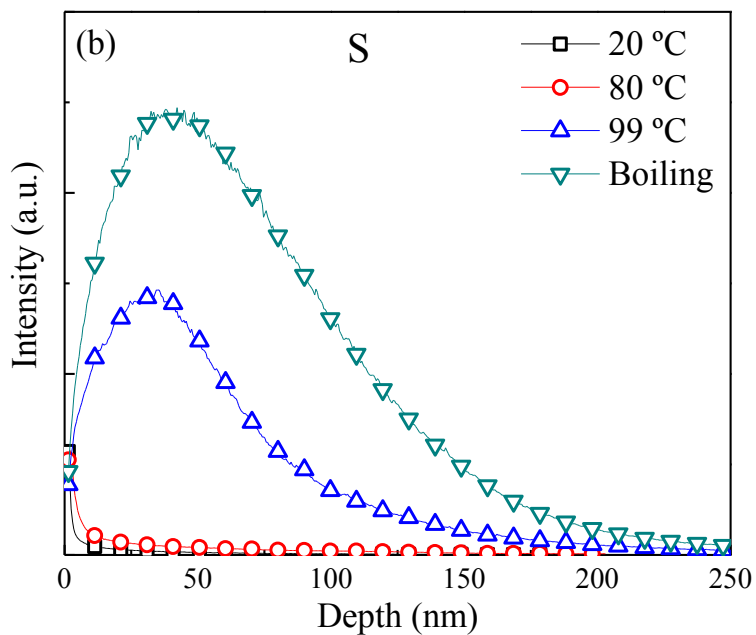
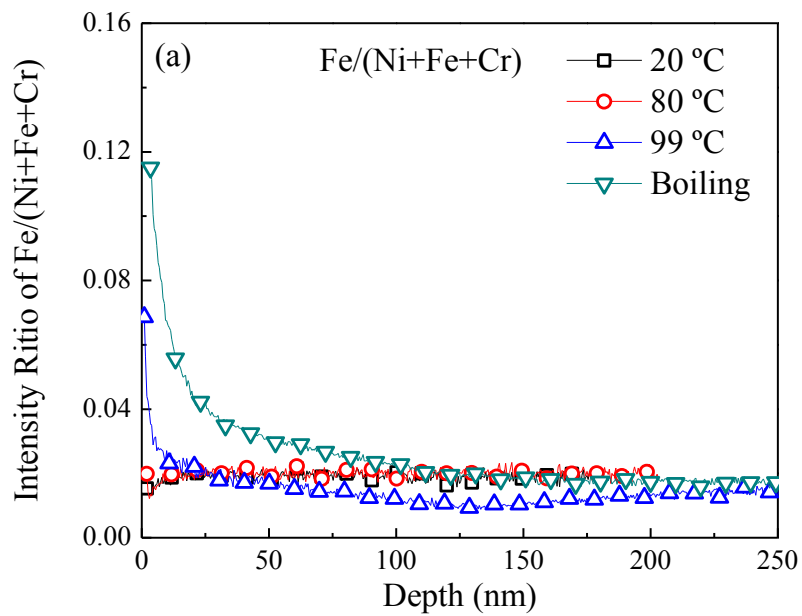


Figure C-5. SIMS analyses of O and S after immersion of the specimen in the test solution at various temperatures.



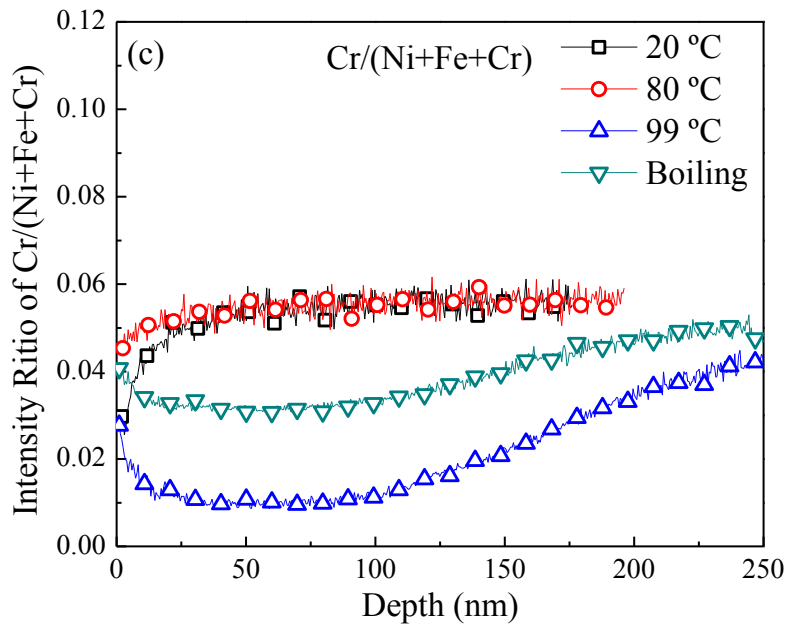
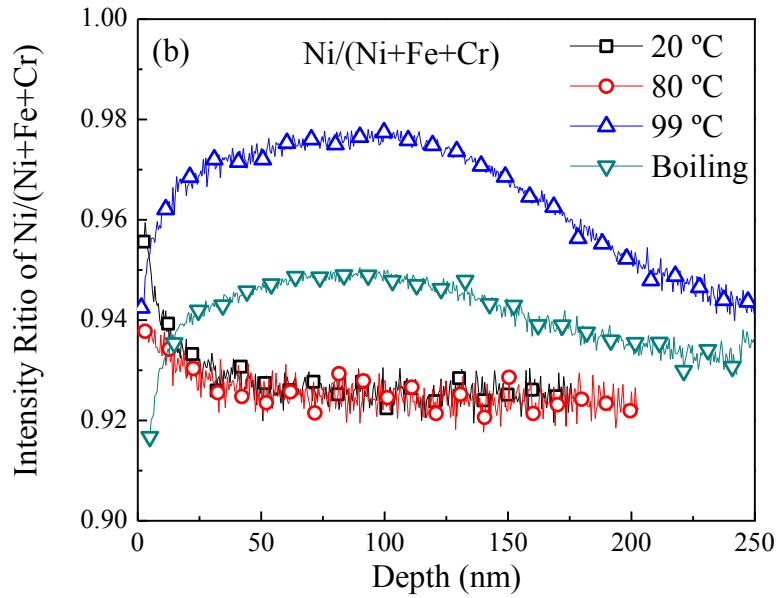


Figure C-6. SIMS analyses of Fe, Ni and Cr after immersion of the specimen in the test solution at various temperatures.

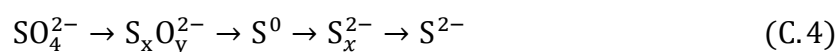
C.3.4 X-ray photoelectron spectroscopy (XPS)

Figures C-7 (a) to (d) and Figures C-8 (a) to (c) show the XPS spectra of Alloy 800 after the immersion tests. Table C-4 shows the atomic ratio of each S component over all S components under different conditions calculated from the results in Figures C-7 (a) to (d).

Table C-4. Atomic ratio of different S components over all S components at different temperatures

Conditions	SO ₄ ²⁻	SO ₃ ²⁻	S ⁰	S ²⁻	Total
20 °C	89.3 %	Little	little	10.7 %	100 %
80 °C	79.7 %	Little	little	20.3 %	100 %
99 °C	25.3 %	8.5 %	8.3 %	58.0 %	100 %
Boiling	14.7 %	9.0 %	11.6 %	64.6 %	100 %

According to sulphur redox chemistry, the transition from sulphate to sulphide can be viewed as occurring through the following intermediates [35]:



Thiosulphate (S₂O₃²⁻) is a polythiosulphate (S_xO₃²⁻) intermediate; it can decompose into sulphate and elemental sulphur when exposed in air:

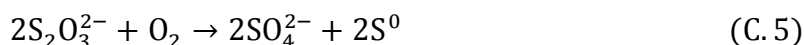


Table C-5. Possible reaction for thiosulphate

Reactions	ΔG^0 298K (kJ/mol ⁻¹)	Reference	Eq. No.
$S_2O_3^{2-} + 2O_2 + 2OH^- \rightleftharpoons 2SO_4^{2-} + H_2O$	-887	[48]	(6)
$S_2O_3^{2-} + 2OH^- \rightleftharpoons SO_4^{2-} + S^{2-} + H_2O$	-54	[49]	(7)
$2S_2O_3^{2-} + O_2 + 2H_2O \rightleftharpoons S_4O_6^{2-} + 4OH^-$	-62	[48]	(8)
$S_2O_3^{2-} + 6H^+ + 4e^- \rightleftharpoons 2S^0 + 3H_2O$	-193	[50]	(9)
$S_2O_3^{2-} + H^+ \rightleftharpoons S^0 + HSO_3^-$	-3.1	[51]	(10)

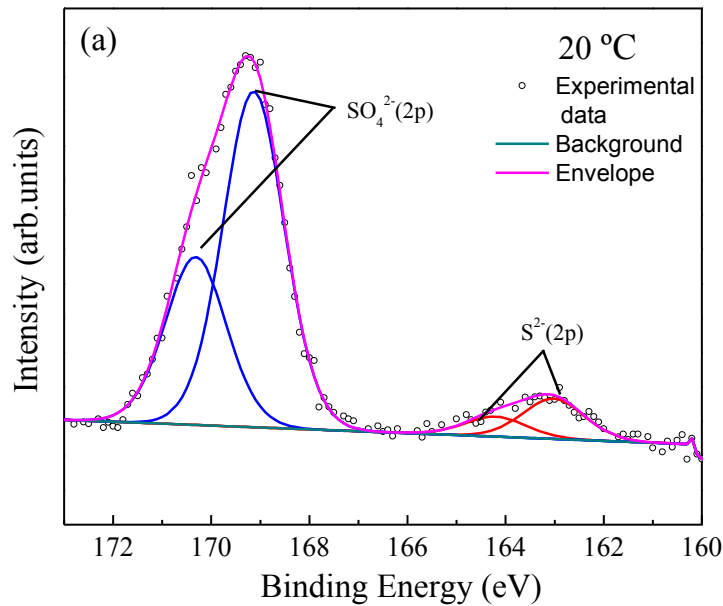
From Figures C-7 (a) to (d), it can be observed that $S_2O_3^{2-}$ unlikely exists in the passive film after the immersion test because all of the reactions shown in Table C-5 tend to proceed spontaneously in the forward direction. According to Table 4, SO_4^{2-} and S^{2-} exist in the Alloy 800 specimen after the immersion test at 20 °C, with the SO_4^{2-} being the dominant species. Under reducing conditions in the presence of metals, $S_2O_3^{2-}$ and/or elemental sulphur could react with the metal and produce metal sulphide. When the immersion temperature rises to 80 °C as shown in Fig. C-7 (b), the relative amount of S^{2-} increases, which indicate more SO_4^{2-} , $S_2O_3^{2-}$ and S^0 have been reduced to S^{2-} ; therefore, more metal has been oxidized to a sulfide species. After the solution temperature rises to 99 °C as shown in Figure C-7 (c), the intermediate sulphur species (SO_3^{2-} and S^0) appears in a passive film. Also, the relative ratio of SO_4^{2-} continues to decrease and S^{2-} becomes the dominant sulphur species. Figure C-7 (d) shows that when the specimen is immersed in a boiling test solution, the S^{2-} species is clearly dominant. This indicates that more corrosion products have formed in this condition due to bubble-enhanced convection and mass transfer of corrosion product. According to the potential vs. pH diagram for stability of a Ni-S-H₂O species in an aqueous environment, the NiS is stable under the condition investigated in this work. Therefore, with the accelerate effects from the boiling bubbles, the

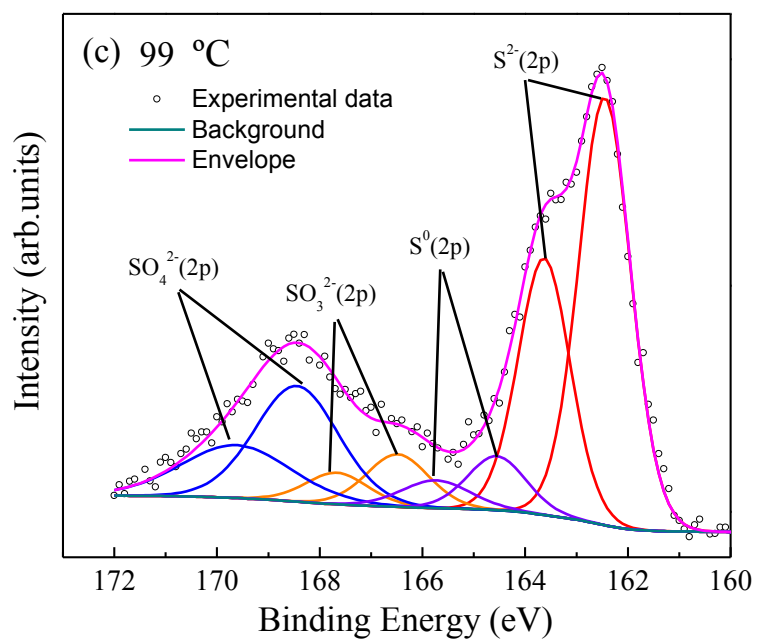
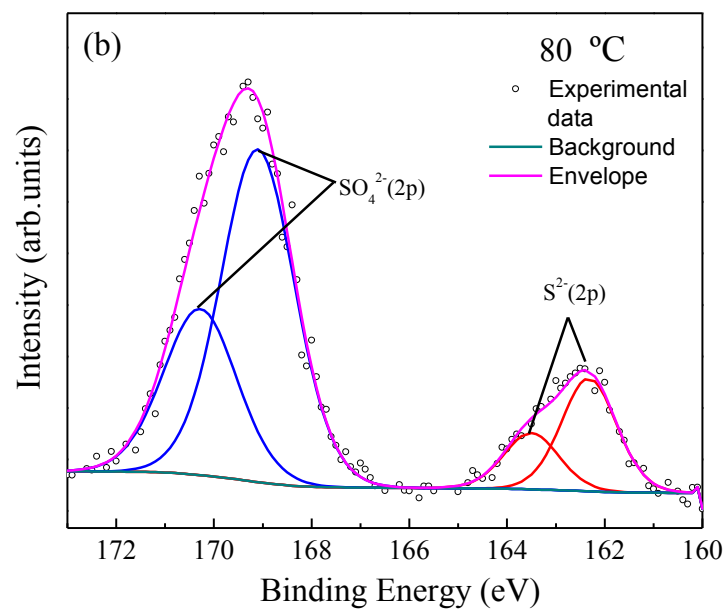
valence of sulphur species tends to decrease to reach S^{2-} . Also, the low-valence sulphur species (SO_3^{2-} , $S_2O_3^{2-}$ and S^{2-}) tend to accelerate the entry of hydrogen into metals, thus enhancing the general and localized corrosion

Figures C-8 (a) to (c) show the XPS peaks of the major metal components in Alloy 800 after immersion in the test solution at various temperatures. The following phenomena are observed:

- (1) Figure C-8 (a) shows both Fe^0 and Fe^{2+}_{OX} were detected in Alloy 800 specimen after 7 days of immersion in the test solution at various temperatures. In room temperature, Fe^0 is dominant due to the XPS sputtering could penetrate the thickness of passive layer and detected some of the substrate. With an increase in temperature, especially under the boiling condition, the Fe^{2+}_{OX} spectroscopy became dominant attribute to the thickness of passive layer is increasing under higher temperature.
- (2) From Figure C-8 (b), it can be seen that Ni shows a similar behavior to that of Fe. Ni^0 and Ni^{2+}_{OH} can be detected under all conditions. Ni^0 is the dominant species at 20 °C, but its relative ratio to the other metals tested decreases with increasing of temperature. In the immersion test of the boiling solution, the peak intensity of Ni^{2+}_{OH} continues to increase and become the dominant valence.
- (3) Figure C-8 (c) shows that the intensity of Cr^0 is relatively low compared to that of Cr^{3+}_{OX} and Cr^{3+}_{OH} . All three peaks grow weaker as the temperature increases and under the boiling condition, where Cr^0 is remarkably decreased.

From the SIMS (Figs. C-5 and C-6) and XPS (Figs. C-7 and C-8) results, the passive film form under boiling condition shows more reduced S species incorporation, more metal ions and less metal elemental states than the passive film formed under 99 °C. Since the temperature between these two conditions is small, it can be concluded that the boiling bubbles caused more porosity, more Ni dissolution; the bubbles also lead to less Cr depletion but the Cr in the passive film exist as $\text{Cr}^{3+}_{\text{OH}}$ states. All of the above effect cause the reduce of pitting and corrosion resistance with the effect of boiling bubbles.





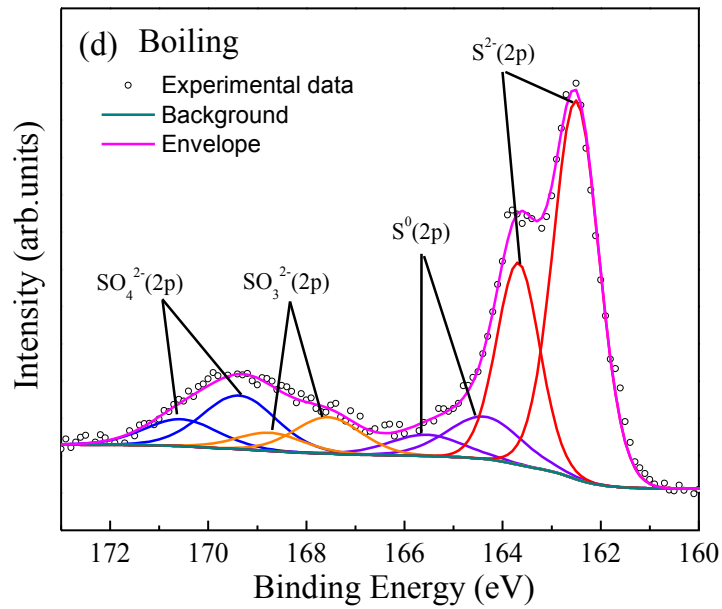
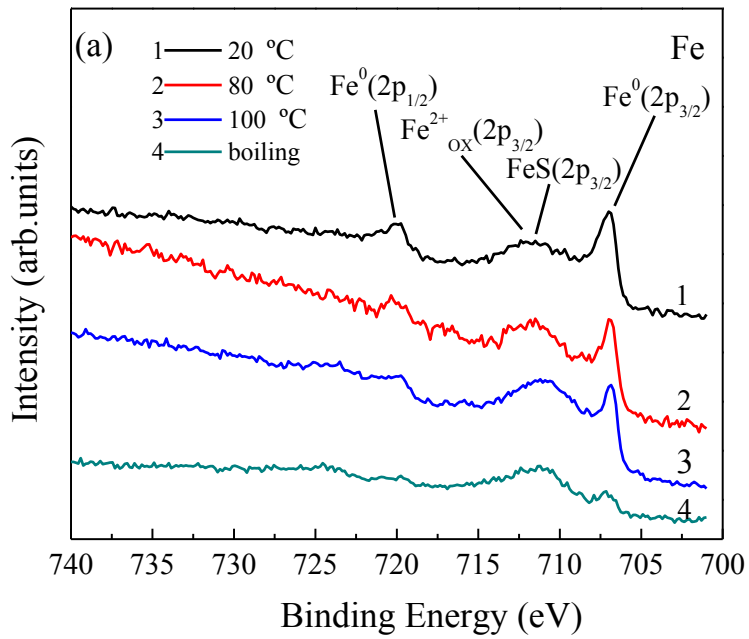


Figure C-7. XPS analysis of S in the Alloy 800 specimen after immersion in the test solution at various temperatures.



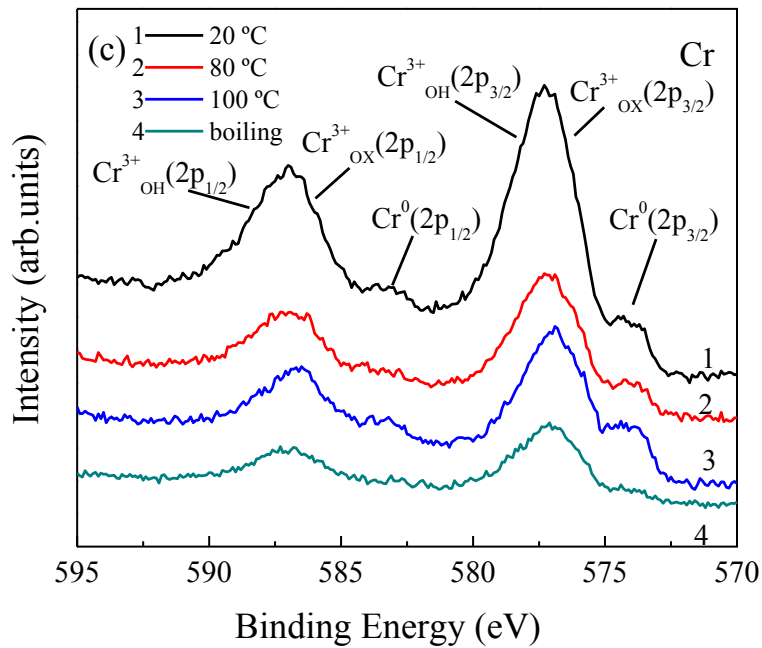
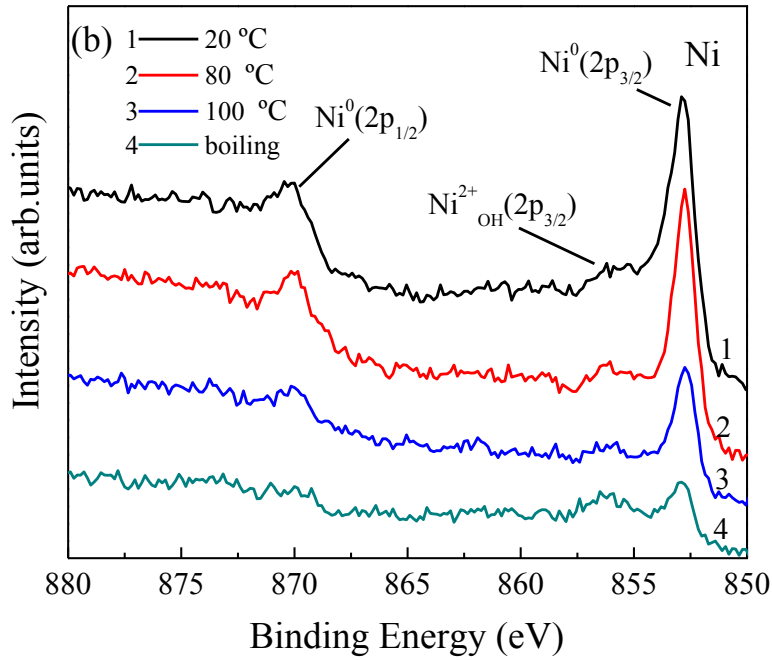


Figure C-8. XPS analyses of Fe, Ni and Cr in the Alloy 800 specimen after immersion in the test solution at various temperatures.

C.3.6 Effect of boiling bubbles on passivation degradation

Figure C-9 shows the phonological representation of the degradation of anodic film at different solution temperatures and boiling condition. Our experimental results show that boiling bubbles affected the degradation of Alloy 800 in the following ways:

(1) Dissolution rate of anodic film:

As shown in Figure C-9, the dissolution of the passive film can be represented by:



where M represents the metal in the passive film, i.e., Fe^{3+} , Ni^{2+} and Cr^{3+} . Under steady state conditions, the dissolution rate of the passive film, K, is equal to the rate of passive film formation. Before any localized corrosion begins, the dissolution rate of the passive film indicates the corrosion rate. The anodic polarization curves shown in Figure C-2 indicate that dissolution rate of passive film increased not only with a temperature increase but also further increased with the movement of bubbles. As shown in Figure C-9, when solution temperature increases from 20 °C to 99 °C, the oxygen and cation vacancies in the anodic film increases, leading to a more defective structure of anodic film and a faster dissolution rate [48, 49]. When boiling occurred, the movement of boiling bubbles increases the electrolyte convection and the transport of corrosion product on the surface of the passive film. All of these effects would

increase the defects in the anodic film, making it easier for the aggressive ions (Cl^- and $\text{S}_2\text{O}_3^{2-}$) to penetrate the inner layer of the anodic film, and resulting in an enhanced dissolution rate of the anodic film as shown in Figure C-9, $K_3 > K_2 > K_1$.

(2) Thickness of anodic film:

Figures C-5 (a) and (b) show the depth profiles of elements O and S, which represents the thickness of anodic films form on the surface of Alloy 800. It can be seen that the thickness of anodic film increases from the solution temperature of 20 °C to 99 °C. At the boiling condition, the thickness of anodic film increase further with the existence of boiling bubbles ($\delta_3 > \delta_2 > \delta_1$) as shown in Figure C-9. As the temperature increased, film growth was enhanced and the thickness of hydroxide and oxide layers increased [50]. When boiling began, the bubble enhanced movement of the electrolyte further increased the oxygen vacancy and anion vacancy diffusion rate so that the passivation reaction penetrate deeper into the matrix metal. Therefore, under boiling condition, the anodic film thickness was greater than that in other conditions.

(3) Sulphur incorporation in the anodic film:

Thiosulphate and chloride have been found to have a synergistic effect on anodic film breakdown when the concentration ratio of chloride to thiosulphate is high [51, 52]. It has been reported [53] that the addition of sulphate increased the corrosion rate of Alloy 600 and Alloy 800 at high temperature due to impairment of the passive layer caused by sulphate reduction. Sulphur species in the anodic film were identified using SIMS, most sulphur species being in the

outer 60 nm of the film as shown in Figure C-5 (b). Increases in temperature and boiling bubbles increased the depth of sulphur incorporation leading to an increase in anodic film thickness. The XPS results shown in Figure C-5 (a) to (d) indicate that the valence of the sulfur species in the anodic film decreased with an increase in electrolyte temperature and the occurrence of boiling bubbles. As shown in Figure C-9, when the temperature increased, the tendency of sulphur species to be reduced increased. Associated with chloride, sulphur with a lower valence would lower the pitting potential and increase the passive current [54]. Under the boiling condition, S^{2-} is more dominant than the other conditions, which means that the anodic film formed in this condition is more vulnerable to the aggressive environment, leading a decrease of pitting potential as shown in Figure C-3.

(4) Composition of anodic film:

Passive layers on alloys normally have bilayer structure with the outside layer predominantly composed of hydroxides and inner layer predominantly composed of oxides [55-57]. Huang et al. found that the passive film on Alloy 690 in a high temperature aqueous environment showed a complex composition with varying portions of Cr_2O_4 , $FeCr_2O_4$ and $NiFe_2O_4$ depending on the potential [58]. In the present work, the anodic layer is consisted of Cr_2O_3 , $Cr_2(OH)_3$, Fe_2O_3 , NiO and possibly FeS and NiS as these valence of metals is detected by XPS shown in Figures C-6 (a) to (c). When the temperature increased, the XPS signal of elemental metal (Fe^0 , Ni^0 and Cr^0) decreased and the content of high valence of metals ($Fe^{2+/3+}$, Ni^{2+} and Cr^{3+}) increased. One possible reason is that matrix metals cannot be detected due to an increase in the thickness of the

anodic layer; also sulphur was incorporated deep and reacted with metals, which reduced the relative content of elemental metal.

Nickchi et al. [59] stated that the mass transfer coefficient of the oxidant increased and the content of metal decreased at the outermost layer of the film with the increase of temperature in corrosion test of Alloy 800. When boiling occurred, the forced convection further increased the mass transfer coefficient of the oxidant [38], which lead to further corrosion of the anodic layer. SIMS results shown in Figure C-8 (b) indicates that the boiling bubbles increased the preferential dissolution of Ni, possibly because the corrosion product NiS was removed from the outer layer of the anodic film by movement of the bubbles, exposing more Ni/NiO to react with sulphur species.

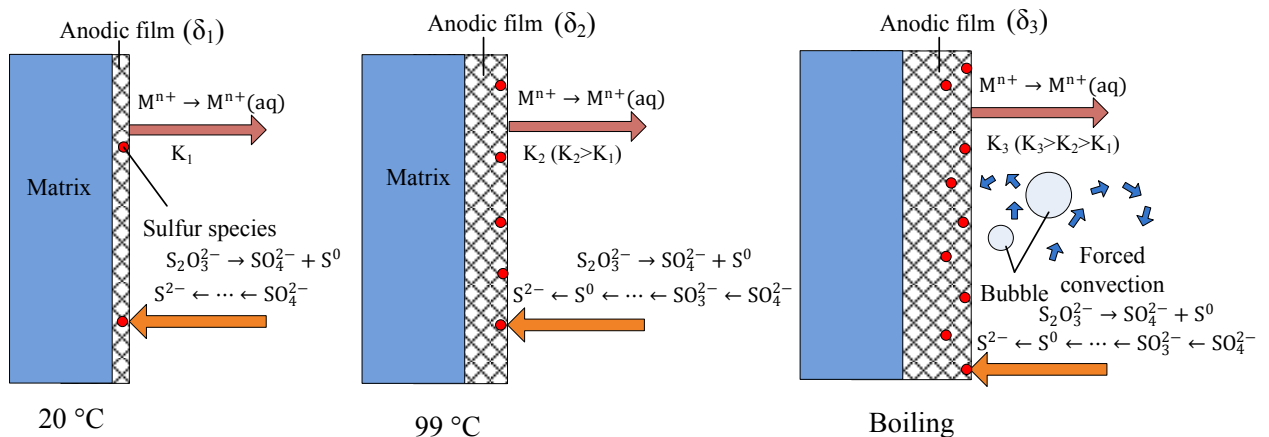


Figure C-9. Effect of boiling bubble on the degradation of anodic film on Alloy 800 after immersion in the test solution at various temperatures.

C.4 Conclusions

In the present study, the effect of boiling bubbles on the passivity degradation of Alloy 800 in the presence of thiosulphate was investigated and the following conclusions were obtained:

- (1) In aqueous solution, the corrosion potential for Alloy 800 decreased with an increasing the solution temperature from room temperature to 99 °C. In boiling electrolyte condition, the increased in the corrosion potential was due to an increase in cathodic reactions, which caused by bubble-enhanced convection.
- (2) The critical pitting potential of Alloy 800 decreased and the corrosion current increased in the presence of boiling bubbles. The dissolution rate of the anodic film increased due to the bubble-enhanced forced convection.
- (3) The presence of boiling bubbles increased the thickness of anodic film on Alloy 800, and enhances sulphur incorporation into the passive film. More lower valance sulphur species and metal ions were detected under the boiling condition. The lower valance sulphur further accelerated the passive film degradation under boiling condition.

C.5 References

- [1] Kilian, R., N. Wieling and L. Stieding, "Corrosion resistance of SG tubing material Incoloy 800 mod. and Inconel 690 TT," *Materials and Corrosion*, 42 (1991): pp. 490-496.
- [2] Lu, Y., S. Ramamurthy and G. Goszczynski, "An aging assessment on ex-service Alloy 800 steam generator tubing," *Nuclear engineering and design*, 242 (2012): pp. 91-99.
- [3] Tapping, R., Y. Lu and M. Pandey. *Alloy 800 SG tubing: current status and future challenges*. in *Proceedings of the 13th International Conference on Environmental Degradation of Materials in Nuclear Power Systems-Water Reactors*. 2007.
- [4] Staehle, R. and J. Gorman, "Quantitative assessment of submodes of stress corrosion cracking on the secondary side of steam generator tubing in pressurized water reactors: Part 2," *Corrosion*, 60 (2004): pp. 5-63.
- [5] Staehle, R. and J. Gorman, "Quantitative assessment of submodes of stress corrosion cracking on the secondary side of steam generator tubing in pressurized water reactors: Part 1," *Corrosion*, 59 (2003): pp. 931-994.
- [6] Staehle, R. and J. Gorman, "Quantitative assessment of submodes of stress corrosion cracking on the secondary side of steam generator tubing in pressurized water reactors: Part 3," *Corrosion*, 60 (2004): pp. 115-180.
- [7] Xia, D.-H., R.-K. Zhu, Y. Behnamian, C. Shen, J.-L. Luo, Y.-C. Lu and S. Klimas, "pH Effect on Sulfur-Induced Passivity Degradation of Alloy 800 in Simulated Crevice Chemistries," *Journal of The Electrochemical Society*, 161 (2014): pp. C201-C214.
- [8] Tsai, W.-T. and T.-F. Wu, "Pitting corrosion of alloy 690 in thiosulfate-containing chloride solutions," *Journal of Nuclear Materials*, 277 (2000): pp. 169-174.
- [9] Newman, R., H. Isaacs and B. Alman, "Effects of sulfur compounds on the pitting behavior of type 304 stainless steel in near-neutral chloride solutions," *Corrosion*, 38 (1982): pp. 261-265.
- [10] Ho, J. and G. Yu, "Pitting corrosion of Inconel 600 in chloride and thiosulfate anion solutions at low temperature," *Corrosion*, 48 (1992): pp. 147-158.
- [11] Park, Y., J. Galvele, A. Agrawal and R. Staehle, "Stress corrosion cracking and anodic behavior of AISI 304 stainless steel, Inconel 600, and Incoloy 800 straining in boiling NaOH solutions," *Corrosion*, 34 (1978): pp. 413-418.
- [12] Roberge, R., "Effect of the nickel content in the pitting of stainless steels in low chloride and thiosulfate solutions," *Corrosion*, 44 (1988): pp. 274-280.

- [13] Lu, Y., G. Goszczynski and S. Ramamurthy, "Degradation of alloy 800 under steam generator secondary side crevice conditions," 17th International Conference on Nuclear Engineering, (2009): pp. 1-9.
- [14] Williams, D., R. Möller and H. Grabke, "The high-temperature corrosion of alloy 800 in carburizing, oxidizing, and sulfidizing environments," *Oxidation of Metals*, 16 (1981): pp. 253-266.
- [15] Stellwag, B., "Pitting Resistance of Alloy 800 as a Function of Temperature and Prefilming in High-Temperature Water," *Corrosion*, 53 (1997): pp. 120-128.
- [16] Luo, B., "Characterization of pH Effect on Corrosion Resistance of Nuclear Steam Generator Tubing Alloy by In-situ Scanning Electrochemical Microscopy," *Acta Physico-Chimica Sinica*, 30 (2014): pp. 59-66.
- [17] Geringer, J. and D.D. Macdonald, "Modeling fretting-corrosion wear of 316L SS against poly(methyl methacrylate) with the Point Defect Model: Fundamental theory, assessment, and outlook," *Electrochimica Acta*, 79 (2012): pp. 17-30.
- [18] Sloppy, J.D., Z. Lu, E.C. Dickey and D.D. Macdonald, "Growth mechanism of anodic tantalum pentoxide formed in phosphoric acid," *Electrochimica Acta*, 87 (2013): pp. 82-91.
- [19] Xia, D.H., S.Z. Song, J.H. Wang and H.C. Bi, "Corrosion detection of metal cans for beverage packaging," *CIESC Journal*, 63 (2012): pp. 1797-1802.
- [20] Xia, D.H., S.Z. Song, J.H. Wang, H.C. Bi and Z.W. Han, "Corrosion behavior of tinplate in NaCl solution," *Transactions of Nonferrous Metals Society of China* 22 (2012): pp. 717-724.
- [21] Boden, P., "Corrosion of Cu and Cu-base alloys under conditions of boiling heat transfer-I. Corrosion of Cu," *Corrosion Science*, 11 (1971): pp. 353-362.
- [22] Cowan, R. and A. Kaznoff, "Electrochemical measurements of corrosion processes in a boiling water nuclear reactor," *Corrosion*, 29 (1973): pp. 123-132.
- [23] Olmedo, A., M. Villegas and M. Alvarez, "Corrosion behaviour of Alloy 800 in high temperature aqueous solutions: Electrochemical studies," *Journal of Nuclear Materials*, 229 (1996): pp. 102-114.
- [24] Macdonald, D.D., A.C. Scott and P. Wentreck, "External reference electrodes for use in high temperature aqueous systems," *Journal of The Electrochemical Society*, 126 (1979): pp. 908-911.

- [25] Neal, A.L., S. Techkarnjanaruk, A. Dohnalkova, D. McCready, B.M. Peyton and G.G. Geesey, "Iron sulfides and sulfur species produced at hematite surfaces in the presence of sulfate-reducing bacteria," *Geochimica et Cosmochimica Acta*, 65 (2001): pp. 223-235.
- [26] Lindberg, B., K. Hamrin, G. Johansson, U. Gelius, A. Fahlman, C. Nordling and K. Siegbahn, "Molecular spectroscopy by means of ESCA II. Sulfur compounds. Correlation of electron binding energy with structure," *Physica Scripta*, 1 (1970): pp. 286.
- [27] Yuan, S., B. Liang, Y. Zhao and S.O. Pehkonen, "Surface chemistry and corrosion behaviour of 304 stainless steel in simulated seawater containing inorganic sulphide and sulphate-reducing bacteria," *Corrosion Science*, 74 (2013): pp. 353-366.
- [28] Siriwardane, R.V. and J.M. Cook, "Interactions of SO₂ with sodium deposited on CaO," *Journal of colloid and interface science*, 114 (1986): pp. 525-535.
- [29] Pratt, A.R., I.J. Muir and H.W. Nesbitt, "X-ray photoelectron and Auger electron spectroscopic studies of pyrrhotite and mechanism of air oxidation," *Geochimica et Cosmochimica Acta*, 58 (1994): pp. 827-841.
- [30] Mycroft, J.R., G.M. Bancroft, N.S. McIntyre, J.W. Lorimer and I.R. Hill, "Detection of sulphur and polysulphides on electrochemically oxidized pyrite surfaces by X-ray photoelectron spectroscopy and Raman spectroscopy," *Journal of Electroanalytical Chemistry and Interfacial Electrochemistry*, 292 (1990): pp. 139-152.
- [31] Lu, B., J. Luo and Y. Lu, "Effects of pH on lead-induced passivity degradation of nuclear steam generator tubing alloy in high temperature crevice chemistries," *Electrochimica Acta*, 87 (2013): pp. 824-838.
- [32] Naumkin, A.V., A. Kraut-Vass, S.W. Gaarenstroom and C.J. Powell, "NIST X-ray Photoelectron Spectroscopy Database," NIST Standard Reference Database 20, Version 4.1, (2000).
- [33] Smestad, G., A. Ennaoui, S. Fiechter, H. Tributsch, W. Hofmann, M. Birkholz and W. Kautek, "Photoactive thin film semiconducting iron pyrite prepared by sulfurization of iron oxides," *Solar Energy Materials*, 20 (1990): pp. 149-165.
- [34] Tabet, N., I. Allam and R.C. Yin, "X-ray photoelectron spectroscopy study of the carburization of the nickel-based alloy Haynes 214," *Applied Surface Science*, 195 (2002): pp. 166-174.
- [35] Macdonald, D.D. and S. Sharifi-Asl, "Volt Equivalent diagrams as a means of displaying the electrochemical thermodynamics of the sulfur–water system," *Corrosion Science*, 81 (2014): pp. 102-109.
- [36] Li, X., J. Wang, E.-H. Han and W. Ke, "Corrosion behavior for Alloy 690 and Alloy 800 tubes in simulated primary water," *Corrosion Science*, 67 (2013): pp. 169-178.

- [37] Sun, H., X. Wu and E.-H. Han, "Effects of temperature on the protective property, structure and composition of the oxide film on Alloy 625," *Corrosion Science*, 51 (2009): pp. 2565-2572.
- [38] Shen, C., A. Afacan, J. Luo and S.J. Klimas, "Mass transfer of dissolved oxygen using rotating cylinder electrode under bulk boiling conditions," *International Journal of Heat and Mass Transfer*, 70 (2014): pp. 162-168.
- [39] Xia, D., S. Song, R. Zhu, Y. Behnamian, C. Shen, J. Wang, J. Luo, Y. Lu and S. Klimas, "A Mechanistic Study on Thiosulfate-enhanced Passivity Degradation of Alloy 800 in Chloride Solutions," *Electrochimica Acta*, (2013).
- [40] Sato, N., "Anodic Breakdown of Passive Films on Metals," *Journal of The Electrochemical Society*, 129 (1982): pp. 255-260.
- [41] Azumi, K., T. Ohtsuka and N. Sato, "Impedance of Iron Electrode Passivated in Borate and Phosphate Solutions," *J. Jpn. Inst. Met.*, 49 (1985): pp. 729-736.
- [42] Yin, Q., G. Kelsall, D. Vaughan and N. Brandon, "Mathematical models for time-dependent impedance of passive electrodes," *Journal of The Electrochemical Society*, 148 (2001): pp. A200-A208.
- [43] Rondelli, G., P. Torricelli, M. Fini and R. Giardino, "In vitro corrosion study by EIS of a nickel-free stainless steel for orthopaedic applications," *Biomaterials*, 26 (2005): pp. 739-744.
- [44] Ge, H.-H., G.-D. Zhou and W.-Q. Wu, "Passivation model of 316 stainless steel in simulated cooling water and the effect of sulfide on the passive film," *Applied Surface Science*, 211 (2003): pp. 321-334.
- [45] Huang, J., X. Wu and E.-H. Han, "Electrochemical properties and growth mechanism of passive films on Alloy 690 in high-temperature alkaline environments," *Corrosion Science*, 52 (2010): pp. 3444-3452.
- [46] Chao, C., L. Lin and D. Macdonald, "A point defect model for anodic passive films I. Film growth kinetics," *Journal of The Electrochemical Society*, 128 (1981): pp. 1187-1194.
- [47] Horvath, J. and H. Uhlig, "Critical Potentials for Pitting Corrosion of Ni, Cr, Ni, Cr, Fe, and Related Stainless Steels," *Journal of The Electrochemical Society*, 115 (1968): pp. 791-795.
- [48] Carranza, R.M. and M.G. Alvarez, "The effect of temperature on the passive film properties and pitting behaviour of a Fe-Cr-Ni alloy," *Corrosion Science*, 38 (1996): pp. 909-925.

- [49] Cardoso, M.V., S.T. Amaral and E.M.A. Martini, "Temperature effect in the corrosion resistance of Ni-Fe-Cr alloy in chloride medium," *Corrosion Science*, 50 (2008): pp. 2429-2436.
- [50] Zhang, X. and D.W. Shoesmith, "Influence of temperature on passive film properties on Ni-Cr-Mo Alloy C-2000," *Corrosion Science*, 76 (2013): pp. 424-431.
- [51] Zanotto, F., V. Grassi, A. Balbo, C. Monticelli and F. Zucchi, "Stress corrosion cracking of LDX 2101® duplex stainless steel in chloride solutions in the presence of thiosulphate," *Corrosion Science*, 80 (2014): pp. 205-212.
- [52] Laitinen, T., "Localized corrosion of stainless steel in chloride, sulfate and thiosulfate containing environments," *Corrosion Science*, 42 (2000): pp. 421-441.
- [53] Persaud, S.Y., A.G. Carcea and R.C. Newman, "Electrochemical aspects of stress corrosion cracking of Ni-Cr-Fe alloys in acid sulfate solutions relevant to nuclear steam generators," *ECS Transactions*, 53 (2013): pp. 3-14.
- [54] Chiba, A., I. Muto, Y. Sugawara and N. Hara, "Pit Initiation Mechanism at MnS Inclusions in Stainless Steel: Synergistic Effect of Elemental Sulfur and Chloride Ions," *Journal of The Electrochemical Society*, 160 (2013): pp. C511-C520.
- [55] Bastidas, J.M., C.L. Torres, E. Cano and J.L. Polo, "Influence of molybdenum on passivation of polarised stainless steels in a chloride environment," *Corrosion Science*, 44 (2002): pp. 625-633.
- [56] Dutta, R.S., R. Purandare, A. Lobo, S.K. Kulkarni and G.K. Dey, "Microstructural aspects of the corrosion of Alloy 800," *Corrosion Science*, 46 (2004): pp. 2937-2953.
- [57] Oh, K., S. Ahn, K. Eom, K. Jung and H. Kwon, "Observation of passive films on Fe-20Cr-xNi (x=0, 10, 20 wt.%) alloys using TEM and Cs-corrected STEM-EELS," *Corrosion Science*, 79 (2014): pp. 34-40.
- [58] Huang, J., X. Wu and E.-H. Han, "Influence of pH on electrochemical properties of passive films formed on Alloy 690 in high temperature aqueous environments," *Corrosion Science*, 51 (2009): pp. 2976-2982.
- [59] Nickchi, T. and A. Alfantazi, "Corrosion characteristics of alloy 800 in aqueous solutions up to 200 C," *Journal of The Electrochemical Society*, 160 (2013): pp. C64-C76.

